Separation and Purification Technology 316 (2023) 123764

Contents lists available at ScienceDirect

Separation and Purification Technology

journal homepage: www.elsevier.com/locate/seppur

Review

Advances in the decontamination of wastewaters with synthetic organic dyes by electrochemical Fenton-based processes

Fengxia Deng [a,b,*], Enric Brillas [b,*]

[a] State Key Laboratory of Urban Water Resource and Environment, School of Environment, Harbin Institute of Technology, Harbin 150090, PR China
[b] Laboratori d'Electroquímica dels Materials i del Medi Ambient, Secció de Química Física, Facultat de Química, Universitat de Barcelona, Martí i Franquès 1-11, Barcelona, Spain

ARTICLE INFO

Keywords:
Carbonaceous cathodes
Heterogeneous electro-Fenton
Homogeneous electro-Fenton
Microbial fuel cells
Photoelectro-Fenton
Wastewater treatment

ABSTRACT

Large amounts of diverse colored synthetic organic dyes are discharged from industrial effluents in the environment causing non-esthetic pollution and serious health-risk problems. Dyes are very stable upon solar irradiation, temperature, and biological treatment, then being non-removed in conventional wastewater treatment plants. The decontamination of dyeing effluents by potent methods has received increasing attention over the last years, showing a marked relevance in the electrochemical Fenton-based processes consisting of H_2O_2 electrogeneration and its catalytic decomposition with Fe^{2+} to form $^{\bullet}OH$. This paper presents a comprehensive review of these processes in the period 2018–2022 dealing with the discoloration and mineralization of synthetic solutions and real wastewaters with single or mixed synthetic organic dyes. Homogeneous electro-Fenton (EF), heterogeneous EF with solid catalysts or functionalized cathodes, photoelectro-Fenton (PEF), microbial fuel cells, other hybrid processes with adsorption, nanofiltration, electro-peroxone, or photoelectrocatalysis, and sequential processes with electrocoagulation or sonication are summarized. The principles of methods are explained to understand the role of the oxidizing agents generated. The H_2O_2 accumulation at pH 3.0 is described with cathodes of raw and modified carbonaceous materials as well as gas-diffusion electrodes, and the effect of the anode, the electrolyte composition, the applied current density or cathodic potential, and the Fe^{2+} and dye contents on the homogeneous EF performance are discussed. Rapid discoloration and much slower mineralization were found by homogeneous EF. Similar behavior was obtained for heterogeneous EF, although allowed operating at a more neutral pH without sludge precipitation. The dye removal was more improved in PEF and solar PEF (SPEF) due to the positive photolysis of Fe(III) species by UVA light and sunlight, respectively. SPEF can be envisaged as the best and more cost-effective electrochemical Fenton-based treatment for dyes destruction.

1. Introduction

About 10,000 synthetic organic dyes are available worldwide for an annual production larger than 10^6 tons, with the United Kingdom, Germany, the United States, Brazil, India, and China being the dominant producers. These compounds are highly soluble in water and extensively used to impart color to food, biological stains, pharmaceutical and cosmetic products, photographs, paper, paints, and textiles. Synthetic organic dyes are also used for the control of activated sludge for groundwater and of sewage and wastewater treatment [1].

The chromophore group determines the classification of dyes. About 70% of these compounds at the industrial scale are azo dyes containing one or various -N = N- groups linked to aromatic moieties (benzene, naphthalene, etc.) with hydroxyl (–OH) or sulfonate ($-SO_3^-$) groups to improve their solubility. Other dyes belong to families like anthraquinone, thiazine, triphenylmethyl, indigoide, and xanthene [1]. Fig. 1 illustrates several examples of typical dyes treated in this review, showing their chemical structure along with their common and/or color index (C.I.) name. The C.I. nomenclature consists of the name of a general characteristic property of the dye, followed by the name of its color and an order number. The most common first names are Acid or Basic, indicating that they are negatively or positively charged, respectively. Other names can be Vat for derives from natural indigo, disperse in the case of non-ionic dyes used in aqueous dispersion, etc.

The dye industries generate high quantities of various wastewater

* Corresponding authors at: State Key Laboratory of Urban Water Resource and Environment, School of Environment, Harbin Institute of Technology, Harbin, 150090, PR China (F. Deng).
E-mail addresses: dengfx_hit@163.com (F. Deng), brillas@ub.edu (E. Brillas).

https://doi.org/10.1016/j.seppur.2023.123764
Received 22 January 2023; Received in revised form 1 April 2023; Accepted 1 April 2023
Available online 5 April 2023
1383-5866/© 2023 The Authors. Published by Elsevier B.V. This is an open access article under the CC BY license (http://creativecommons.org/licenses/by/4.0/).

Nomenclature

λ	Wavelength (nm)
A	Absorbance
ACE	Average current efficiency
ACF	Activated carbon fiber
BDD	Boron-doped diamond
COD	Chemical oxygen demand (mg O_2 L^{-1})
CPC	Compound parabolic collector
DSA	Dimensionally stable anode
EC	Energy consumption per unit volume (kWh m^{-3})
E_{cat}	Cathodic potential (V)
EC_{COD}	Energy consumption per unit COD mass (kWh (kg COD)$^{-1}$)
EC_{TOC}	Energy consumption per unit TOC mass (kWh (kg TOC)$^{-1}$)
EF	Electro-Fenton
EO	Electrochemical oxidation
EO-H_2O_2	Electrochemical oxidation with electrogenerated H_2O_2
GDE	Air-diffusion electrode, usually of carbon-polytetrafluoroethylene (PTFE) (for H_2O_2 generation)
Hetero –PEF	Heterogeneous photoelectro-Fenton
Hetero –SPEF	Heterogeneous solar photoelectro-Fenton
Hetero-EF	Heterogeneous electro-Fenton
Homo-EF	Homogeneous electro-Fenton
Homo-PEF	Homogeneous photoelectro-Fenton
Homo-SPEF	Homogeneous solar photoelectro-Fenton
I	Current (mA or A)
J	Current density (mA cm^{-2})
k_1	Pseudo-first-order rate constant for the target compound decay (min^{-1})
k_{dis}	Pseudo-first-order rate constant for decolorization (min^{-1})
MCE	Mineralization current efficiency (%)
PEC	Photoelectrocatalysis
PEF	Photoelectro-Fenton (with UV light)
ROS	Reactive oxygen species
SCE	Saturated calomel electrode (reference electrode)
SPEC	Solar photoelectrocatalysis
SPEF	Solar photoelectro-Fenton
TOC	Total organic carbon (mg C L^{-1})
US	Ultrasound
UVA	Ultraviolet A (315–400 nm)
UVB	Ultraviolet B (280–315 nm)
UVC	Ultraviolet C (100–280 nm)

containing hazardous chemicals discharged into the aquatic environment [2,3]. The waters contaminated with dyes present a visible colorization causing non-esthetic pollution and serious health risks. The esthetic quality of water is degraded by enhancing its biochemical and chemical oxygen demands and inhibiting plant growth by impairing photosynthesis [3]. The recalcitrance and bioaccumulation of dyes can promote toxicity, mutagenicity, and carcinogenicity over aquatic beings and even humans, although their knowledge is incomplete owing to their large variety. It causes public concern and legislation problems are a big challenge to environmental scientists [1].

Most synthetic organic dyes are not degradable in conventional wastewater treatment plants (WWTPs) because of their high stability upon solar irradiation and temperature coupled with high resistance to biological attack [1,2]. For this reason, over the past three decades, practical and powerful methods have been developed to decolorize and destroy the organic components of dyeing wastewater to avoid their dangerous environmental impact. Different techniques have been extensively checked, including adsorption, membrane filtration, microbial treatments, ozonation, and pre-eminently advanced oxidation process (AOPs). The most powerful treatments are the chemical and photochemical AOPs such as photocatalysis, Fenton, and photo-Fenton [4,5] and the electrochemical AOPs (EAOPs) such as electrocoagulation (EC), electrochemical oxidation (EO), electrochemical reduction, electro-Fenton (EF), photoelectro-Fenton (PEF), and solar PEF (SPEF) [1,6–9]. A hybrid combination of these processes like bio-EF [10] and sequential processes has been proposed as well. The main feature of all these AOPs is the in situ production of strong oxidizing radicals like hydroxyl radical ($^{\bullet}OH$), which is the second strongest oxidant known with a standard reduction potential (E°) of 2.8 V/SHE and with the ability to mineralize most organic pollutants in waters. In previous work, one of us has published two reviews in 2009 [1] and 2015 [6] on the general destruction of synthetic organic dyes by EAOPs. These processes have been extensively investigated in the following 5 y, making it necessary to review the methodology and data reported to analyze the novel trends of the EAOPs to remove dyes. Among them, single and combined electrochemical Fenton-based processes are simple and efficient methods with potential viability for application to industrial scale and are considered the most potent EAOPs. The analysis of the recent results of these techniques can foresee their future development.

This review aims to present a general and critical study over the removal of single and mixed synthetic organic dyes from synthetic waters and real wastewaters by electrochemical Fenton-based technologies. They include homo-EF, hetero-EF, PEF, SPEF, and other combined (hybrid and sequential) methods. The principles of each technology, the role of the oxidizing agents formed, the systems used, and the effect of the operating variables on the process performance are examined and discussed to better understand their advantages and limitations for the environmental prevention of pollution from synthetic organic dyes. A final section of Conclusions and Prospects designs the future trends of these procedures.

2. Bibliometric analysis

The keywords “Electro-Fenton and Dyes” and “Photoelectro-Fenton and Dyes” were introduced in the Scopus database to retrieve the peer-reviewed literature related to the treatment of dyes employing electrochemical Fenton-based processes up to November 2022. Only the publications (reviews and scientific papers) in English covering the later 5 years (period 2018–2022) were individually selected after a careful analysis. Communications and conferences in congresses and book chapters were excluded. The criteria used to include a publication in the present review were;

(i) The correct application of electrochemical Fenton-based treatments to the remediation of synthetic and real wastewaters contaminated with a single or a mixture of dyes,
(ii) a detailed description of the experimental set-up and materials used, including the synthesis of new catalysts, the experimental conditions used, the theoretical calculations made, and the equipment required for analyses, and
(iii) an appropriate discussion of the results obtained, mainly related to the discoloration of the treated dye solutions and their kinetic analysis, the influence of the different experimental variables on dye removal, the clarification and identification of the oxidizing agents generated, and the measurement of mineralization parameters such as total organic carbon (TOC) and/or chemical oxygen demand (COD) and energetic parameters as well as the identification of by-products generated, The present review includes 23 figures and 5 tables that have been designed to characterize the above parameters.

The above analysis identified the destruction of dyes by different

homo- and hetero-EF treatments and PEF and SPEF processes. Other works reported the application of microbial fuel cells (MFCs) and other hybrid and sequential processes with other technologies. The review briefly outlines the principles of all these methods to further analyze in more detail the degradation and mineralization of synthetic organic dyes from synthetic and real wastewaters. Emphasis on the systems used, the effect of operating parameters, and the role of generated oxidants have concluded.

The above criteria detected 11 reviews dealing with some information on the destruction of dyes by single and hybrid EAOPs. While the review by Nidheehs et al. [11] considered the destruction of organic pollutants by BDD anodes, four other reviews reported the general treatment of organic contaminants including dyes by Fenton and EAOPs [4,5,8,9]. Metal-organic frameworks (MOFs) [12] and graphene-modified composites [13] as electrodes in EF are also described. Other reviews described the application of bio-EF [10] and MFCs [14,15] to destroy dyes and emerging pollutants. One of us has presented a review with a small description of the PEF process for dyes [7]. However, any of the previously published reviews considered a general treatment of dyes by electrochemical Fenton-based methods, covering the period from

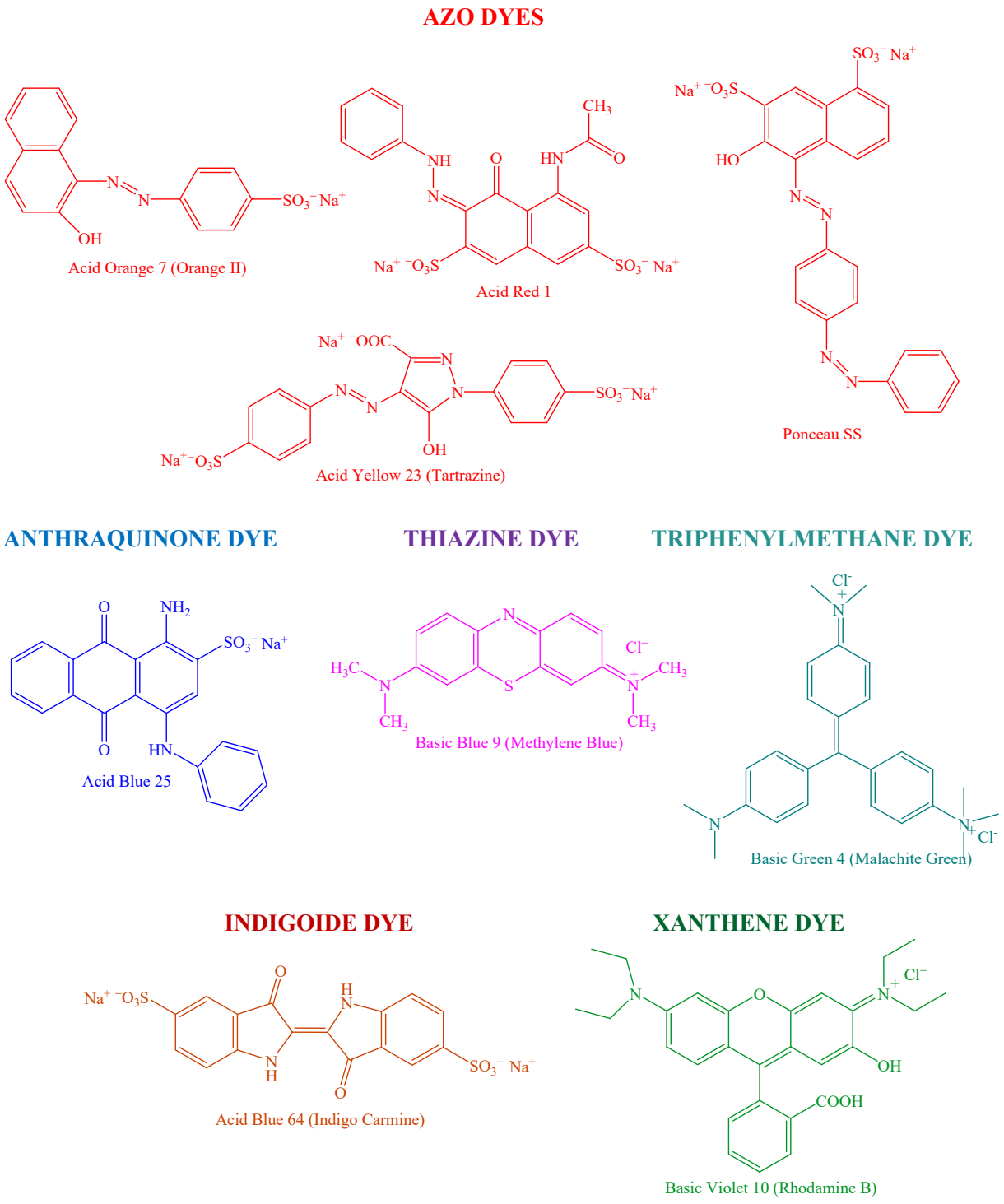

Fig. 1. Chemical structure of typical synthetic organic dyes treated in this review, classified by their chromophore group. The color index and/or common (between parentheses) name of each dye is given.

2018 to 2022, as presented in this review article.

The bibliometric analysis was completed by identifying 148 scientific articles on the destruction of synthetic organic dyes by diverse electrochemical Fenton-based treatments. Fig. 2a presents the annual distribution of such articles from 2018 to 2022. An enhancement from 26 articles in 2018 to 35 articles in 2022 can be observed, demonstrating the increasing interest in applying these technologies to dyes abatement. Fig. 2b highlights the superiority of homo-EF studies with 52 articles (35.1%) followed by hetero-EF ones with 45 articles (30.4%). While the former method used raw and modified carbonaceous materials and GDE as cathodes, different solid catalysts and functionalized cathodes were tested in the second one. Fewer 25 articles (16.9%) were devoted to PEF, related to homo- and hetero-processes with different artificial lamps, even SPEF with sunlight. Only 6 (3.4%) articles developed MFCs, whereas 13 articles (8.8%) considered other hybrid processes involving adsorption, nanofiltration, O_3 in electro-peroxone, and photo-electrocatalysis (PEC). Finally, 8 articles (5.4%) proposed sequential processes with EC or sonication (ultrasound (US) among others.

3. Homogeneous electro-Fenton process of dyes

The homo-EF process has been the most studied treatment of dyes in waters, as can be seen in Fig. 2b. After a brief description of its principles, this section will analyze the scientific papers published based on the kind of cathode tested, including raw carbonaceous, gas-diffusion, and modified carbonaceous materials.

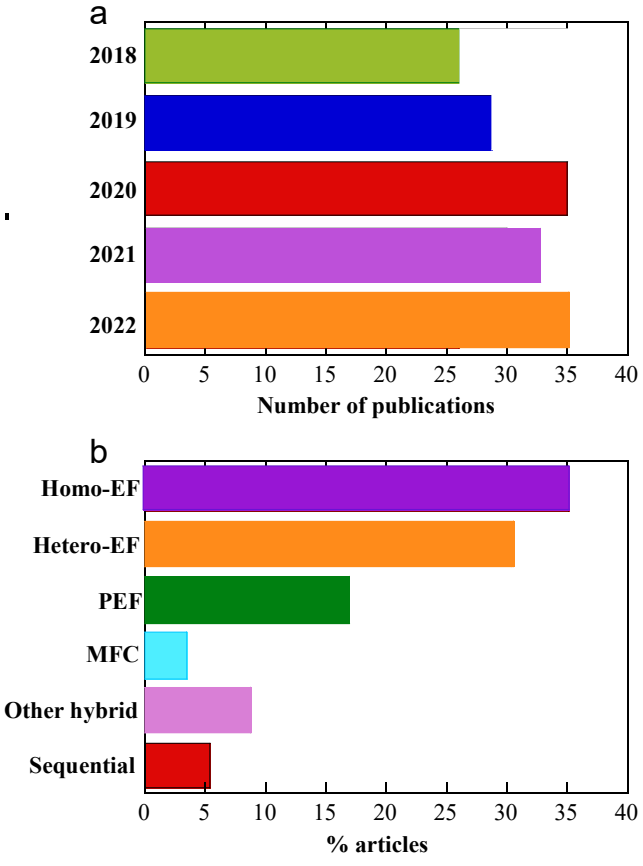

Fig. 2. Bibliometric analysis of the literature. (a) Number of publications by year. (b) Percentage of articles for homo-electro-Fenton (homo-EF), hetero-electro-Fenton (hetero-EF), photoelectro-Fenton (PEF), microbial fuel cells (MFC), other hybrid processes, and sequential processes.

3.1. Principles

The homo-EF process is an electrochemical alternative to the homo-Fenton treatment, in which a mixture of H_2O_2 and Fe^{2+} (so-called Fenton's reagent) is added to the contaminated water to originate homogeneous $^{\bullet}OH$ from the well-known homogeneous Fenton's reaction (1) with a relatively high second-order rate constant $k_2 = 63\ M^{-1}\ s^{-1}$ at optimum pH = 3.0 [16,17]:

$$Fe^{2+} + H_2O_2 \rightarrow Fe^{3+} + {}^{\bullet}OH + OH^- \quad (1)$$

The Fe^{3+} ion formed from reaction (1) can attack H_2O_2 and regenerate Fe^{2+} via the Fenton-like reaction (2) with a very small $k_2 \sim 2 \times 10^{-3}\ M^{-1}\ s^{-1}$. This reaction produces another reactive oxygen species (ROS), the hydroperoxyl radical ($HO_2^{\bullet}$), with lower oxidation power ($E^{\circ} = 1.65$ V/SHE) than $^{\bullet}OH$ [17]. Despite this, $HO_2^{\bullet}$ can also reduce Fe^{3+} to Fe^{2+} from reaction (3). It is noteworthy that the very low rates of reactions (2) and (3) as compared to reaction (1) are reflected by a stop of the process after consumption of one of the reactants (H_2O_2 and/or Fe^{2+}).

$$Fe^{3+} + H_2O_2 \rightarrow Fe^{2+} + HO_2^{\bullet} + H^{+\ -} \quad (2)$$

$$Fe^{3+} + HO_2^{\bullet} \rightarrow Fe^{2+} + O_2 + H^+ \quad (3)$$

The industrial implementation of homo-Fenton is rather limited to acidic effluents where the generated Fe^{3+} produces small quantities of $Fe(OH)_3$ sludge. Its application to typical real wastewaters of pH between 6.5 and 8.5 requires two additional processes, the acidification of the effluent down to pH ~ 3.0 before treatment and its neutralization at the end of the treatment with the consequent precipitation of large amounts of $Fe(OH)_3$ that needs subsequent depuration. This pH treatment train enhances enormously the operating cost of the homo-Fenton process. These drawbacks have been tried to be solved by means of EF technology.

Homo-EF is an EAOP consisting of the continuous production of H_2O_2 by the two-electron reduction of O_2 as pure gas or air injection, usually at a carbonaceous cathode via reaction (4) with $E^{\circ} = +0.68$ V/SHE [7,8,18]. Although H_2O_2 is almost completely accumulated in the cathodic compartment of a divided cell, its concentration decreases sharply in an undivided cell because of its anodic oxidation to the weak oxidant $HO_2^{\bullet}$ by reaction (5) [17]. Then, low levels of Fe^{2+} are added to the contaminated solution to generate Fe^{3+} and homogeneous $^{\bullet}OH$ from Fenton's reaction (1). In an undivided cell, organic pollutants are destroyed by a competitive reaction between homogeneous $^{\bullet}OH$ and heterogeneous $^{\bullet}OH$, so-called M($^{\bullet}OH$), formed from water discharge at the anode M of the cell by reaction (6) [11,19].

$$O_2 + 2H^+ + 2e^- \rightarrow H_2O_2 \quad (4)$$

$$H_2O_2 \rightarrow HO_2^{\bullet} + H^+ + e^- \quad (5)$$

$$M + H_2O \rightarrow M({}^{\bullet}OH) + H^+ + e^- \quad (6)$$

Boron-doped diamond (BDD) electrode is recognized as a more powerful anode than conventional ones like Pt and metal mixed oxides (MMO) or dimensionally stable anodes (DSA) due to its greater generation of BDD($^{\bullet}OH$) [11]. Homo-EF outperforms simpler EAOPs like electrochemical oxidation (EO), where no H_2O_2 is formed on a metallic cathode (usually stainless steel or Ti) or EO with electrogenerated H_2O_2 (EO-H_2O_2) without Fe^{2+} present in the medium. In the latter two treatments, only M($^{\bullet}OH$) is the main oxidant of organics [11,19].

Several advantages of homo-EF over homo-Fenton are: (i) no need for handling and hazardous storage due to its explosive thermal decomposition, and (ii) no limitation of catalytic iron as a reactant because of the continuous Fe^{2+} regeneration from Fe^{3+} reduction at the cathode from reaction (7) with $E^{\circ} = +0.77$ V/SHE to maintain the activity of the Fe^{3+}/Fe^{2+} cycle with minimum $Fe(OH)_3$ sludge precipitation [17]. Nevertheless, homo-EF and homo-Fenton have similar

drawbacks such as an optimum pH close to 3.0, loss of performance due to $Fe(OH)_3$ precipitation at pH > 4.0, and accumulation of final persistent Fe(III)-carboxylate complexes. The EF technology overcomes these drawbacks by applying hetero-EF and PEF among other methods.

$$Fe^{3+} + e^- \rightarrow Fe^{2+} \quad (7)$$

To know the ability of H_2O_2 accumulation in the solution from a given cathode, tests are performed without any organic pollutants to avoid their reaction. The H_2O_2 concentration can be typically determined by titration methods such as permanganometry or iodometry, and then, it can be calculated the percentage of current efficiency (% CE) from Eq. (8) and the energy consumption per unit volume (EC) from Eq. (9), as shows Table 1 [7,20–22]. When the solution contains a given dye, the most common parameter to follow is discoloration is the spectrophotometric measurement of the evolution of its absorbance (A) at the maximum wavelength (λ_{max}) of the dye. As shown in Table 1, the discoloration process is quantified by the normalized absorbance (A / A_0) from Eq. (10), the percentage of color removal from Eq. (11), and the pseudo-first-order rate constant for discoloration (k_{dis}) calculated as the slope of the linear ln (A / A_0) vs, time plot from Eq. (12). The mineralization process is characterized by determining the time course of COD and/or TOC. Table 1 highlights that these parameters are given as the normalized COD (COD / COD_0) from Eq. (13) and/or the normalized TOC (TOC / TOC_0) from Eq. (14), or alternatively as the corresponding percentages of COD and TOC removals from Eq. (15) and (16). From these data, it is feasible to determine the percentage of average current efficiency (ACE) by Eq. (17) or the percentage of mineralization current efficiency (MCE) by Eq. (18). Several energetic parameters such as EC from Eq. (9), the energy consumption per unit COD mass (EC_{COD}) from Eq. (20), and the energy consumption per unit TOC mass (EC_{TOC}) from Eq. (21) can be calculated as well. Apart from these characteristic parameters valid for all EF treatments, other particular energetic parameters like the energy consumption total per unit volume (EC_{total}) from Eq. (19) and the energy consumption total per unit TOC mass ($EC_{TOC,\ total}$) from Eq. (22) can also be provided for the PEF process to account for the additional energy supplied by the artificial lamp illuminating the solution.

The reusability of the cathode is assessed by comparing the discoloration achieved in successive treatment cycles, which is an important indicator to understand its stability for practical application. Many EF works identify generated oxidants by specific scavengers, although in some cases, they are detected by electron paramagnetic resonance (EPR) using solutions of 5,5-dimethyl-1-pyrroline-N-oxide (DMPO) or 2,2,6,6-tetramethylpiperidine (TEMP). Organic by-products formed during the discoloration and/or mineralization processes can be identified by gas chromatography-mass spectrometry (GC–MS), high-performance liquid chromatography (HPLC), and/or liquid chromatography-mass spectrometry (LC-MS). Inorganic ions released from the heteroatoms contained in the target dye are quantified by ion chromatography.

3.2. Raw carbonaceous cathodes

BDD [22], graphite [23–33], carbon felt (CF) [21,34–39], carbon fiber [40], and reticulated vitreous carbon (RVC) [40,41] have been applied as pristine carbonaceous cathodes in homo-EF for dyeing wastewaters treatment. Table 2 collects relevant results reported in selected scientific papers using such cathodes, whereas Fig. 3 shows the sketches of several undivided electrolytic cells used in these assays. A typical two-electrode tank reactor with a BDD anode and a CF cathode is presented in Fig. 3a [37]. Fig. 3b depicts a three-electrode tank reactor equipped with an anode, a cathode, and an SCE reference electrode [29]. A more complex flow-by plant with liquid recirculation and a filter-press cell equipped with a BDD anode and a BDD cathode is given in Fig. 3c [22], whereas Fig. 3d schematizes the cylindrical glass reactor with horizontal anode and cathode proposed by Elbatea et al. [31].

Table 1
Main operating and energetic parameters used to quantify the accumulation of H_2O_2 and the discoloration and mineralization performance of the electro-Fenton-based processes of dyes in aqueous matrices [7,20–22].

Symbol (units)	Equation	Symbol meaning	Number
H_2O_2 accumulation			
Percentage of current efficiency			
% CE	$\frac{100zF[H_2O_2]V}{M(H_2O_2)It}$	z: number of electrons for O_2 reduction (=2) F: Faraday constant $[H_2O_2]$: H_2O_2 concentration V: Solution volume (L) $M(H_2O_2)$: Molecular mass of H_2O_2 I: Current (A) t: Electrolysis time (h)	(8)
Energy consumption per unit volume			
EC (kWh m^{-3})	$\frac{E_{cell}It}{V}$	E_{cell}: Cell voltage (V)	(9)
Discoloration			
Normalized absorbance			
A/A_0		A: Dye absorbance at λ_{max} for time t A_0: Initial dye absorbance at λ_{max}	(10)
Percentage of discoloration or color removal			
% Color removal	$\frac{100(A_0 - A)}{A_0}$		(11)
Pseudo-first-order rate constant for discoloration			
k_{dis} (s^{-1}, min^{-1})	$\ln(A_0/A) = k_{dis}t$	t: Electrolysis time (s, min)	(12)
Mineralization			
Normalized chemical oxygen demand (COD)			
COD/COD_0		COD: COD concentration at time t (mg O_2 L^{-1}) COD_0: Initial COD concentration (mg O_2 L^{-1})	(13)
Normalized total organic carbon (TOC)			
TOC/TOC_0		TOC: TOC concentration at time t (mg C L^{-1}) TOC_0: Initial TOC concentration (mg C L^{-1})	(14)
Percentage of COD removal			
% COD removal	$\frac{100\,(COD_0 - COD)}{COD_0}$		(15)
Percentage of TOC removal			
% TOC removal	$\frac{100\,(TOC_0 - TOC)}{TOC_0}$		(16)
Percentage of average current efficiency			
% ACE	$\frac{100\,FV\,(COD_0 - COD)}{8It}$	8: Equivalent of oxygen (mg) t: Electrolysis time (s)	(17)
Percentage of mineralization current efficiency			
% MCE	$\frac{nFV\,(TOC_0 - TOC)}{4.32 \times 10^5 mIt}$	n: Number of electrons exchanged for total theoretical mineralization m: Number of carbon atoms of target dye t: Electrolysis time (h)	(18)
Energy consumption per unit volume			
EC (kWh m^{-3})	$\frac{E_{cell}It}{V}$	t: Electrolysis time (h)	(9)
Energy consumption total per unit volume			
EC_{total} (kWh m^{-3})	$\frac{(E_{cell}I + U)t}{V}$	U: Electrical power of the lamp (V)	(19)

(continued on next page)

Table 1 (*continued*)

Symbol (units)	Equation	Symbol meaning	Number
Energy consumption per unit COD mass EC_{COD} (kWh (g COD)$^{-1}$)	$\frac{E_{cell}It}{V(COD_0 - COD)}$		(20)
Energy consumption per unit TOC mass EC_{TOC} (kWh (g TOC)$^{-1}$)	$\frac{E_{cell}It}{V(TOC_0 - TOC)}$		(21)
Energy consumption total per unit TOC mass $EC_{TOC,total}$ (kWh (g TOC)$^{-1}$)	$\frac{(E_{cell}I + U)t}{V(TOC_0 - TOC)}$		(22)

Results in Table 2 allow inferring that the homo-EF tests were carried out at pH 3.0 related to the optimum efficiency of Fenton's reaction (1) to generate homogeneous $^{\bullet}OH$ as the main oxidant. The discoloration and mineralization processes of treated solutions enhanced with increasing *j* as a result of a greater $^{\bullet}OH$ production from reaction (1) by the acceleration of reaction (4) yielding higher H_2O_2 generation, and M($^{\bullet}OH$) from the rise in the rate of reaction (6). As mentioned above, the production of BDD($^{\bullet}OH$) is higher than that of Pt($^{\bullet}OH$), which indicates that the role of the anode is also evident and BDD is more advantageous than Pt. Na_2SO_4 is the ubiquitous electrolyte used in synthetic solutions despite it can generate oxidants like persulfate ($S_2O_8^{2-}$) and sulfate radical anion ($SO_4^{\bullet-}$), which compete with $^{\bullet}OH$ to destroy the dye and its by-products [6]. The effect of Cl^- in the electrolyte is much more significant and has been investigated by Titchou et al. [21] since this ion can form homogeneous active chlorine (HClO with $E^{\circ} = 1.39$ V/SHE) by anodic oxidation reactions (23) and (24) at pH 3.0:

$$2Cl^- \rightarrow Cl_2 + 2e^- \quad (23)$$

$$Cl_2 + H_2O \rightarrow HClO + Cl^- + H^+ \quad (24)$$

These authors used a two-electrode tank reactor like Fig. 3a, equipped with a BDD anode and a CF cathode to treat 230 mL of 60 mg L^{-1} the diazo dye Direct Red 23 in 12.5 mM Na_2SO_4 and/or 25 mM NaCl with 0.05–0.50 mM Fe^{2+}at pH 3.0 upon an air flow rate = 1 L min^{-1} and by applying *j* between 2.5 and 15 mA cm^{-2}. They found that a mixture of 75% Na_2SO_4 + 25% NaCl with 0.1 mM Fe^{2+} at $j = 2.5$ mA cm^{-2} gave the best performance because of the preferable competitive attack of homogeneous HClO and $^{\bullet}OH$ alongside heterogeneous M($^{\bullet}OH$). After 360 min of electrolysis, 84% of TOC was removed with an MCE = 5.4%, EC_{TOC} = 1.08 kWh (g TOC)$^{-1}$, and cost = 1.54 US$ m^{-3}. Generated radicals were identified with scavengers and the overall release of SO_4^{2-} from the -SO_3^- groups of the dye was confirmed (see Table 2). Based on this study, Hien et al. [39] used the same equipment to treat 230 mL of real textile wastewater with 0.45 g L^{-1} TOC, 0.18 g L^{-1} SO_4^{2-}, and 0.44 g $L^{-1}Cl^-$. Operating with a BDD anode at pH 3.0, air flow rate = 1 L min^{-1}, and $I = 500$ mA, they obtained a 93% discoloration after 120 min of EO-H_2O_2 with HClO and BDD($^{\bullet}OH$) as main oxidants. In contrast, 95% of loss of color was more rapidly attained, in only 24 min, by homo-EF after the addition of 0.10 mM Fe^{2+}, demonstrating the larger oxidation power of homogeneous $^{\bullet}OH$ formed from Fenton's reaction (1). This was reflected at 360 min where TOC reductions of 95% by EO-H_2O_2 with EC_{TOC} = 275 kWh (g TOC)$^{-1}$ and 100% by homo-EF with smaller EC_{TOC} = 215 kWh (g TOC)$^{-1}$(see Table 2) were achieved. An important drawback of these technologies was related to the formation of toxic and undesirable ClO_3^- and ClO_4^- ions from the oxidation of HClO at the BDD anode, which can be mitigated with much lower *I* but with lower oxidation power. However, the absence of techno-economic study does not allow benchmarking the feasible better viability of homo-EF with other available technologies.

Fig. 4 exemplifies the behavior obtained for the mineralization of the diazo dye Black NT2 (chemical structure given in Fig. 4a) by homo-EF in 0.050 M Na_2SO_4 [22]. The flow-by reactor with a BDD/BDD pair of electrodes of Fig. 3c was tested under recirculation of 4 L of pure water at pH = 3.0 under liquid flow rate = 12 L min^{-1} and air flow rate = 1 L h^{-1}. In the absence of the dye and Fe^{2+}, Fig. 4b makes evident the increase of accumulated H_2O_2 by raising *j* from 7 to 30 mA cm^{-2} due to the increase in the rate of reaction (4). Increasing steady H_2O_2 contents of 1.46, 1.56, and 1.75 mM were reached after 40 min of electrolysis of 7, 15, and 30 mA cm^{-2}, just when the rate of generation and destruction of this compound from reactions (4) and (5), respectively, became equal. The CE of the process at $j = 30$ mA cm^{-2} was 12% at 60 min (see Table 2). The higher H_2O_2 accumulation explains the quicker TOC removal (see Fig. 4c), smaller MCE by the greater E_{cell} value (see Fig. 4d), and higher EC_{TOC} (see Fig. 4e) determined for the mineralization of 250 mg L^{-1} of the dye with 0.30 mM Fe^{2+} upon the rise of *j* from 7 to 30 mA cm^{-2}. For the higher *j*, 99% of TOC removal, 95% of MCE, and 0.11 kWh (g TOC)$^{-1}$ of EC_{TOC} were found at 120 min (see also Table 2). However, the increase of *j* causes efficiency loss owing to the removal of homogeneous $^{\bullet}OH$ from the parasitic reactions (25) and (26) [1]:

$$H_2O_2 + {}^{\bullet}OH \rightarrow HO_2^{\bullet} + H_2O \quad (25)$$

$$2{}^{\bullet}OH \rightarrow H_2O_2 \quad (26)$$

Several final carboxylic acids like maleic, fumaric, malic, glyoxylic, oxalic, and formic were detected by ion-exclusion HPLC. These products are derived from the cleavage of the dye aromatics and form hardly oxidizable Fe(III) complexes, making the mineralization process more difficult [1,6].

Matyszczak et al. [26–29] reported the catalytic behavior of different metallic $M^{(n+1)+}/M^{n+}$ pairs capable of triggering Fenton-like reactions similar to Fenton's reaction (1) with the production of homogeneous $^{\bullet}OH$ in the bulk. Fig. 5a depicts the chemical structure of the triphenylmethane dye Bromocresol Green, which was selected for the operation of the three-electrode tank reactor of Fig. 3b with a Pt anode and a graphite cathode. 800 mL of 0.030 mM dye were decolorized with 0.050 M Na_2SO_4 and 0.15 mM catalyst in pure water at pH 2.5 under an O_2 flow rate = 3.88 L min^{-1} [29]. Fig. 5b illustrates that the normalized absorbance at E_{cat} = -0.50 V/SCE decayed more slowly in the sequence: $Co^{2+} > Ce^{3+} > Ni^{2+} > Mn^{2+} > Fe^{2+}$, attaining percentages of color removal of 78.3% > 71.8% >70.8% > 68.7% > 41.8% after 110 min of electrolysis (see Fig. 5c). These authors showed more relevant results when treated 16 mg of Bromocresol Green or 8 mg of Mehanil Yellow upon the same conditions, but using Sn^{2+}, Bi^{3+}, or Fe^{2+} as catalyst [28]. The color removal obtained increased sequentially: $Sn^{2+} < Bi^{3+} < Fe^{2+}$for the former dye, while for the latter, the opposite trend was observed (see Table 2). The strange behavior of the metallic $M^{(n+1)+}/M^{n+}$ pairs failed to justify in these studies, but it can be presupposed that it can be related to the ability of the ions to form $M^{(n+1)+}$ complexes with the target dye, hindering its oxidation with homogeneous $^{\bullet}OH$ and heterogeneous Pt($^{\bullet}OH$). However, the above catalytic information is only of academic value, since the toxicity of such metallic ions avoids their application in practice, except Fe^{2+} that is compatible with all living beings, the reason why the electrochemical Fenton-based processes are being developed for the remediation of dyeing effluents.

3.3. Gas-diffusion electrodes

Less information is known about the use of GDE cathodes in the homo-EF process for treating synthetic organics dyes. Only Lacasa et al. [42] and Soto et al. [43] mentioned such cathodes, as can be seen in Table 2. The three-electrode reactor with an anode (Pt, Ni, or RVC), a GDE cathode fed with O_2, and an Ag|AgCl reference electrode developed by the former authors is shown in Fig. 3e. Fig. 6a depicts an irregular

Table 2
Selected results obtained for the homogeneous electro-Fenton (homo-EF) treatment of synthetic organic dyes from wastewaters using undivided cells.

Dye	System (anode/cathode)	Experimental remarks	Best results	Ref.
Raw carbonaceous cathodes				
Black NT2	Flow-by two-electrode reactor (BDD/BDD)	4 L of 250 mg L^{-1} dye in pure water, 0.050 M Na_2SO_4, 0.30 mM Fe^{2+}, pH 3.0, liquid flow rate = 12 L min^{-1}, air flow rate = 1 L h^{-1}, j = 7–30 mA cm^{-2}, 120 min	Greater H_2O_2 accumulation at higher j: 1.75 mM with EC = 12% at 30 mA cm^{-2} in 60 min. TOC removal, MCE, and EC_{TOC} (kWh (g TOC)$^{-1}$) in 120 min: 93%, 270%, and 0.005 at 7 mA cm^{-2}, 95%, 160% and 0.027 at 15 mA cm^{-2}, and 99%, 95%, and 0.11 at 30 mA cm^{-2}. Final carboxylic acids detected by ion-exclusion HPLC	[22]
Bromocresol Green	Three-electrode tank reactor (Pt/graphite)	800 mL of 0.030 mM dye in pure water, 0.050 M Na_2SO_4, 0.15 mM catalyst, pH 2.5, O_2 flow rate = 3.88 L min^{-1}, E_{cat} = -0.50 V/SCE, 110 min	Discoloration: 78.3% with Co^{2+} > 71.8% with Ce^{3+} >70.8% with Ni^{2+} > 68.7% with Mn^{2+} > 41.8% with Fe^{2+}	[26]
Bromocresol Green Methanil Yellow	Three-electrode tank reactor (Pt/graphite)	800 mL of 16 or 8 mg of dye in pure water, 0.050 M Na_2SO_4, 0.15 mM catalyst, pH 2.5, O_2 flow rate = 3.88 L min^{-1}, E_{cat} = -0.50 V/SCE, 80 min	Discoloration for Bromocresol Green: 63.0% with Sn^{2+}< 72.6% with Bi^{3+} < 82.7% with Fe^{2+}. Discoloration for Methanil Yellow: 56.6% with Sn^{2+}> 56.1% with Bi^{3+} > 51.6% with Fe^{2+}	[28]
Carmoisine Red	Two-electrode tank reactor (Pt/graphite)	Solutions of 1 g L^{-1} dye in pure water, 1 M Na_2SO_4, 0.05–0.60 mM Fe^{2+}, pH 3.0, air bubbling, j = 40–300 mA cm^{-2}, 300 min	Maximum 92% discoloration in 60 min for the best conditions: 0.20 mM Fe^{2+} and $j \geq$ 200 mA cm^{-2}. Detection of aromatic by-products and final carboxylic acids by LC-MS/MS. Quantification of released SO_4^{2-} by ion chromatography	[29]
Naphtol Blue Black	Two-electrode tank reactor (Pt or BDD/CF [d])	175 mL of 0.25 mM dye in pure water, 0.050 M Na_2SO_4, 0.10 mM Fe^{2+}, pH 3.0, 25 °C, air bubbling, I = 60–300 mA, 360 min	At 60 mA, 100% discoloration in 15 min using BDD (k_{dis} = 0.343 min^{-1}) and Pt (k_{dis} = 0.283 min^{-1}). With BDD at 240 min: 80% TOC removal and MCE = 27%. Detection of by-products by GC–MS and NO_3^-, NH_4^+, and SO_4^{2-} by ion chromatography	[35]
Direct Red 23	Two-electrode tank reactor (BDD/CF)	230 mL of 60 mg L^{-1} dye in pure water, 12.5 mM Na_2SO_4 and/or 25 mM NaCl, 0.05–0.50 mM Fe^{2+}, pH 3.0, air flow rate = 1 L min^{-1}, j = 2.5–15 mA cm^{-2}, 360 min	Best conditions for a mixture with 75% Na_2SO_4 + 25% NaCl and 0.1 mM Fe^{2+} at 2.5 mA cm^{-2}: 84% TOC removal, MCE = 5.4%, EC_{TOC} = 1.08 kWh (g TOC)$^{-1}$, and cost = 1.54 US$ m^{-3}. Identification of generated radicals with scavengers. SO_4^{2-} completely removed from the electrolyte	[21]
Textile wastewater	Two-electrode tank reactor (Pt or BDD/CF)	230 mL of dye wastewater (0.45 g L^{-1} TOC, 0.18 g L^{-1} SO_4^{2-}, 0.44 g $L^{-1}Cl^-$), 0.10 mM Fe^{2+}, pH 3.0, air flow rate = 1 L min^{-1}, I = 200 and 500 mA, 360 min	Discoloration and TOC removal higher for BDD than Pt. For BDD at 500 mA, discoloration: 93% for EO-H_2O_2 in 120 min and 95% in 24 min by homo-EF. TOC removal: 95% by EO-H_2O_2 and 100% by homo-EF. EC_{TOC} = 275 and 215 kWh (g TOC)$^{-1}$, respectively. Quantification of ClO_3^- and ClO_4^- using BDD by ion chromatography	[39]
Gas-diffusion electrodes				
Methylene Blue	Three-electrode glass reactor (Pt, Ni, or RVC [b] /carbon-PTFE GDE [c])	Solution of 100 mg L^{-1} dye in pure water, 0.050 M Na_2SO_4, 0.10 mM Fe^{2+}, pH 3.0, 25 °C, O_2 flow rate = 0.15 mL min^{-1}, E_{cat} from −0.5 to −1.3 V/Ag|AgCl, 480 min	More H_2O_2 accumulation at higher $E_{cat.}$. With Pt at −0.13 V, total discoloration in 240 min (k_{dis} = 0.052 min^{-1}). TOC decay at this potential and 480 min: 66% (RVC) < 78% (Ni) < 81% (Pt). For all the electrodes, MCE drops similarly up to a 1.3%	[42]
Methylene Blue	Two-electrode tank reactor (DSA [d] /carbon-PTFE GDE)	500 mL of 20 mg L^{-1} dye in pure water, 0.10 M Na_2SO_4, 0.50 mM Fe^{2+}, pH 3.0–6.0, 25 °C, air flow rate = 150 mL min^{-1}, j = 16.67 mA cm^{-2}, 10 min	Similar discoloration rate for all pH values. At pH 3.0, total discoloration in 8 min with k_{dis} = 0.56 min^{-1}. At pH 6.0, k_{dis} = 0.39 min^{-1}	[43]
Modified carbonaceous cathodes				
Acid Orange 7	Three-electrode tank reactor (Pt/GF [e] |polypyrrole| lignine)	200 mL of 10 mg L^{-1} of dye in pure water, 0.050 M Na_2SO_4, 0.50 mM Fe^{2+}, pH 3.0, O_2 flow rate = 0.25 L min^{-1}, E_{cat} from −0.20 to −0.80 V/SCE	Greater H_2O_2 accumulation at −0.50 V: 205 mg L^{-1} with EC = 96% in 360 min (in a divided cell). Discoloration and TOC decay in the undivided cell: 93% (k_{dis} = 0.513 min^{-1}) in 20 min and 77% in 13 h.Good reusability (<8% lost) after 10 consecutive cycles of 20 min	[44]
Acid Orange 7	Two-electrode tank reactor (Ni|Ti/carbon nanotube fiber|carbon fiber)	100 mL of 0.1 mM of dye in pure water, 0.050 M Na_2SO_4, 0.20 mM Fe^{2+}, pH 3.0, 25 °C, O_2 bubbling, I = 25 mA, 360 min	TOC removal; 12% with carbon fiber < 64% with the modified cathode. Low reusability: only 42% TOC abatement after 10 consecutive cycles	[47]
Acid Orange 7	Three-electrode tank reactor (Pt/Au|N-carbon)	200 mL of 1 mM of dye in pure water, 0.050 M Na_2SO_4, 1.0 mM Fe^{2+}, pH 3.0, O_2 bubbling, E_{cat} = -0.30 V/Ag|AgCl, 180 min	95% TOC removal	[49]
Acid Orange 7	Three-electrode tank reactor (Pt/ACF [f])	600 mL of 0.1 mM of dye in pure water, 0.050 M Na_2SO_4, 0.20–1.0 mM Fe^{2+}, pH 3.0, air bubbling, E_{cat} from −0.50 to −2.50 V/SCE, 120 min	Higher H_2O_2 accumulation of 37.8 mg L^{-1} with CE = 65% and EC = 0.266 kWh m^{-3} at −0.80 V in 120 min. Under these conditions with 0.30 mM Fe^{2+}: 92% discoloration, 75% TOC decay, and MCE = 52%. Low reusability: discoloration decay dropped down to 80% in 60 h	[20]
Acid Orange 7	Three-electrode tank reactor (DSA/ACF)	400 mL of 0.1 mM of dye in pure water, 0.010–0.50 M Na_2SO_4, 0.20–1.0 mM Fe^{2+}, pH 3.0, 25 °C, air bubbling, E_{cat} from −0.80 to −3.0 V/SCE, 120 min	Higher H_2O_2 accumulation of 70.3 mg L^{-1} with CE = 79% and EC = 0.40 kWh m^{-3} at −0.80 V in 120 min. Under these conditions with 0.050 M Na_2SO_4 and 0.30 mM Fe^{2+}: 95% discoloration, 75% TOC decay, and MCE = 22.0%	[54]
Acid Orange 7	Flow-through two-electrode reactor (DSA/ACF|carbon black-PTFE)	300 mL of 100 mg L^{-1} dye in pure water, 0.050 M Na_2SO_4, 0.30 mM Fe^{2+}, pH 3.0, liquid flow rate = 3.5–10.5 mL min^{-1}, I = 50–200 mA, 120 min	H_2O_2 accumulated: 50 mg L^{-1} at 50 mA < 180 mg L^{-1} at 200 mA for 7 L min^{-1}. Similar CE = 24% for all liquid flow rates. Discoloration: 87% at 50 mA and 100% at higher I for the best liquid flow rate of 7 mL min^{-1}. Rapid loss of color removal at 100 mA with isopropanol as scavenger. Good reusability after 5 consecutive steps.	[55]

(*continued on next page*)

Table 2 (*continued*)

Dye	System (anode/cathode)	Experimental remarks	Best results	Ref.
Reactive Black 5	Three-electrode tank reactor (Pt/CF|CNTs [g] or CF|graphene)	250 mL of 40 mg L^{-1} of dye in pure water, 0.1 M KNO_3, 20 mg L^{-1} $FeSO_4{\cdot}7H_2O$, pH 3.0, air bubbling, E_{cat} = -0.65 V/Ag|AgCl, 30 min	H_2O_2 accumulation: 0.10 mM with CF < 0.14 mM with CNTs < 0.26 mM with CF|graphene. Discoloration and TOC decay: 46% and 11% with CF < 55% and 50% with CNTs < 76% and 56% with CF|graphene	[57]
Rhodamine B	Three-electrode with a floating cathode (Pt/oxidized carbon black)	Solutions of 0.1 mM of dye in pure water, 0.10 M Na_2SO_4, 1.0 mM Fe^{2+}, pH 5.13, E_{cat} from −0.20 to −3.0 V/Ag|AgCl, 32 min	Maximum H_2O_2 accumulation of 510 mg L^{-1} with CE = 61% at −1.0 V. Under these conditions, 95% discoloration and 78% TOC abatement. For raw carbon black, 80% discoloration and 20% TOC decay	[59]
Rhodamine B	Three-electrode tank reactor (DSA/degreasing cotton|graphite-PTFE)	100 mL of 30–90 mg L^{-1} of dye in pure water, 0.10 M Na_2SO_4, 0–1.0 mM Fe^{2+}, pH 2.5–4.0, 20 °C, air flow rate = 2.0 L min^{-1}, E_{cat} = -1.10 V/SCE	Faster discoloration and TOC decay for 50 mg L^{-1} dye, 0.70 mM Fe^{2+}, and pH 2.5. Under these conditions: 15 min for total discoloration with k_{dis} = 0.411 min^{-1} and 90% TOC removal in 120 min. Generated oxidant radicals detected with scavengers. By-products identified by GC–MS.	[65]
Acid Red 18	Two-electrode tank reactor (Ti|RuO_2-IrO_2/NPC [h] |GF)	200 mL of 100 mg L^{-1} of dye in pure water, 0.050 M Na_2SO_4, 0–0.56 mM Fe^{2+}, pH 7.0, 25 °C, air flow rate = 0.6 L min^{-1}, j = 17.5 mA cm^{-2}, 120 min	Maximum H_2O_2 accumulation: 517 mg L^{-1} with EC = 0.0054 kWh m^{-3}. Discoloration: 48% in the absence of Fe^{2+} and > 98% for Fe^{2+} ≥ 0.36 mM. Excellent reusability after 8 successive cycles.	[66]

[a] CF: Carbon felt.
[b] RVC: Reticulated vitreous carbon.
[c] GDE: Gas-diffusion electrode.
[d] DSA: Dimensionally stable anode.
[e] GF: Graphite felt.
[f] ACF: Activated carbon fiber.
[g] CNTs: Carbon nanotubes,
[h] NPC: Nanoporous carbon.

H_2O_2 accumulation in a 0.050 M Na_2SO_4 solution in pure water at pH 3.0 and 25 °C contained in this system with a Pt mesh anode by varying the E_{cat} value for 480 min. While a similar H_2O_2 content could be observed at the end of the trials at −0.5 and −0.7 V/Ag|AgCl, the concentration of this species grew progressively at higher E_{cat} values of −1.0 and −1.3 V/Ag|AgCl. In the latter case, no quasi-steady state was reached and H_2O_2 content continued to rise with electrolysis time, indicating a high ability for its electrogeneration from reaction (4), always faster than its removal from reaction (5) that differs from the behavior observed for raw carbonaceous materials (see Fig. 4a). These cathodic potentials were applied to the discoloration of 100 mg L^{-1} of the thiazine dye Methylene Blue (see chemical structure in Fig. 1) by homo-EF with 0.10 mM Fe^{2+} and Fig. 6b shows a gradual higher loss of color with raising E_{cat} from −0.5 to −1.3 V/Ag|AgCl, related to k_{dis} values changing between 0.0081 and 0.052 min^{-1}, according to a progressive greater $^{\bullet}OH$ and Pt($^{\bullet}OH$) production. However, Fig. 6c shows that the higher TOC removal was achieved at E_{cat} = -1.0 V/Ag|AgCl, which can be considered optimal under these conditions, since the excess of homogeneous $^{\bullet}OH$ formed at higher cathodic potential was consumed by parasitic reactions like (25) and (26). The authors also highlighted the positive oxidative role of the physisorbed M($^{\bullet}OH$) formed from different anodes by reaction (6). Fig. 6d illustrates that after 480 min at E_{cat} = -1.3 V/Ag|AgCl with similar homogeneous $^{\bullet}OH$ generation from Fenton's reaction (1), more percentage of TOC was removed in the order: RVC (66%) < Ni (78%) < Pt (81%). This is indicative of a higher oxidation power of Pt($^{\bullet}OH$) over the other generated M($^{\bullet}OH$) species. Nevertheless, the application of the more powerful BDD anode to facilite the rapid mineralization of the dye was not checked.

Soto et al. [43] treated the same dye solutions in a two-electrode tank reactor like Fig. 3a with a DSA anode and a carbon-PTFE GDE cathode fed with an air flow rate = 150 mL min^{-1}. The runs were made with 500 mL of 20 mg L^{-1} Methylene Blue, 0.10 M Na_2SO_4, and 0.50 mM Fe^{2+} in pure water at pH 3.0–6.0 and 25 °C that were discolored by homo-EF at j = 16.67 mA cm^{-2}. At pH = 3.0, the solution became colorless in only 8 min with k_{dis} = 0.56 min^{-1}, increasing slightly up to pH = 6.0 with k_{dis} = 0.39 min^{-1}, due to the progressive deceleration of Fenton's reaction (1) to generate homogeneous $^{\bullet}OH$ (see Table 2). The k_{dis}-values for this system are much higher compared to those pointed out in Fig. 6b. This can be associated with the use of a much greater Fe^{2+} concentration as catalyst (0.50 vs. 0.10 mM) that largely accelerated Fenton's reaction (1).

3.4. 3.4. Modified carbonaceous cathodes

A large variety of modified carbonaceous cathodes have been synthesized aiming to enhance the yield of H_2O_2 in the homo-EF treatment. They include graphite felt (GF)|polypyrrole|lignine [44], anodized GF [45], Janus GF [46], carbon nanotube fiber|carbon fiber [47], TiO_2|reduced graphene oxide (rGO) [48], N-carbon|Au [49], carbon|N, P or S [50–52], activated carbon fiber (ACF) [20,53,54], ACF|carbon black-PTFE [55], carbon black-PTFE|PdAu [56], CF|carbon nanotubes (CNTs) or CF|graphene [57], N-CNTs|$CoSe_2$ [58], oxidized carbon black [59], activated graphite [60], graphite|agroindustrial residue activated carbon [61], GF|CNTs [62], CNTs|rGO [63], carbon black|polyphenylene sulfide film [64], degreasing cotton|graphite-PTFE [65], and nanoporous carbon (NPC)|GF [66]. Selected results for these works are listed in Table 2.

The as-synthesized modified carbonaceous cathodes in the above works were characterized by several technologies. Their surface structure was typically analyzed by scanning electron microscopy (SEM), their crystallinity and structure were elucidated by X-ray diffraction (XRD) spectroscopy and sometimes by Raman spectroscopy. The chemical bond-functional groups were identified by Fourier-transform infrared (FT-IR) spectra and the elemental composition and state of oxidation of species on the electrocatalyst surface were elucidated by X-ray photoelectron spectroscopy (XPS). The electroactive area is also frequently determined by cyclic voltammetry (CV) and the interfacial properties by electrochemical impedance spectroscopy (EIS). In some cases, the surface area was measured by the Brunauer-Emmett-Teller (BET) method.

The main applicability of the modified carbonaceous cathodes is to produce more H_2O_2 than the pristine one at pH close to 3.0 in order to produce more amount of $^{\bullet}OH$ from Fenton's reaction (1). This behavior was usually confirmed in the published articles in the absence of dyes, and the best accumulations achieved for several modified cathodes under different conditions are given in Table 2. Thus, 205 mg L^{-1} of H_2O_2 with EC = 96% were accumulated after 360 min at E_{cat} = -0.50 V/

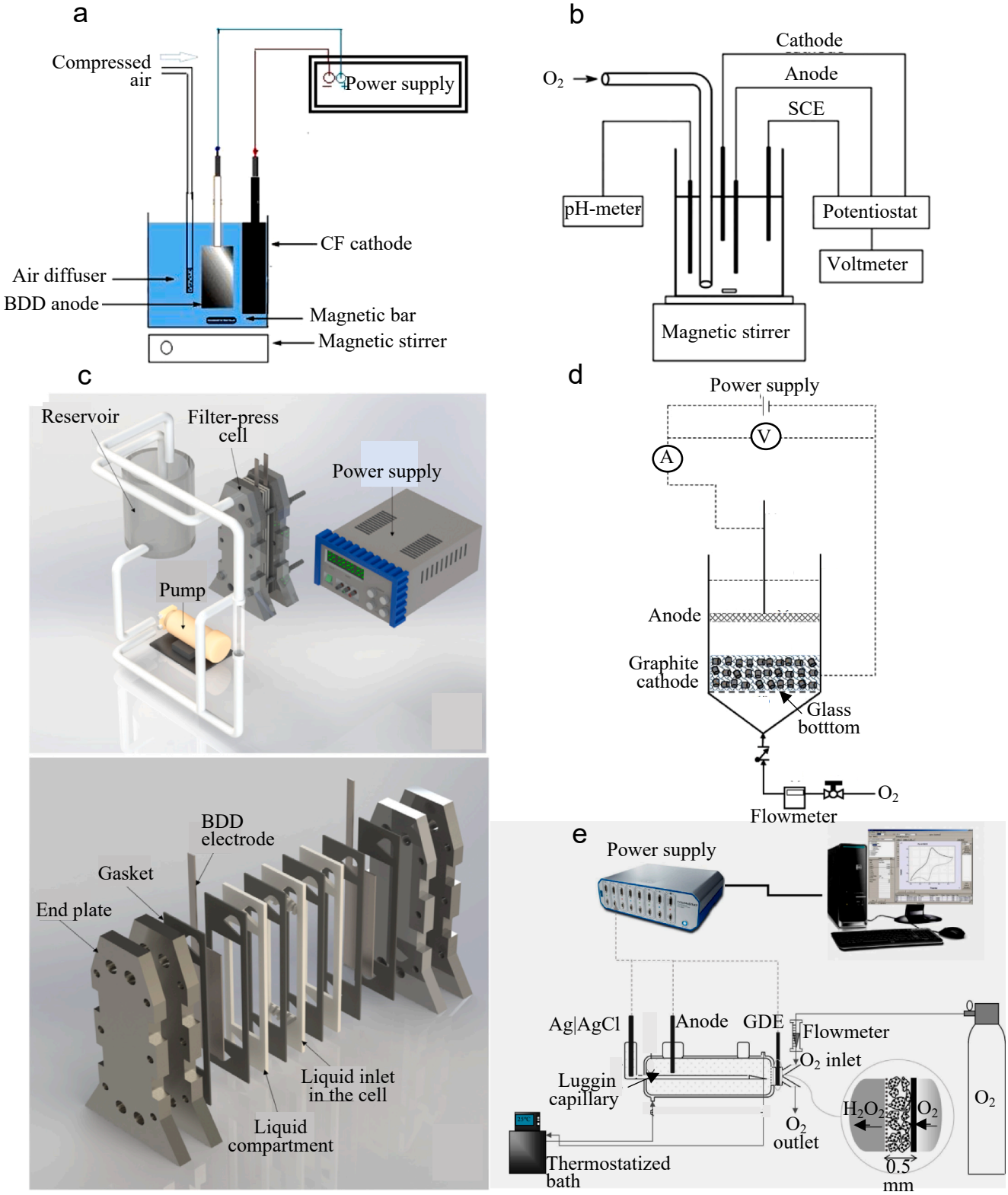

Fig. 3. Sketches of undivided electrolytic systems used for the homo-EF treatment of dyes. (a) Two-electrode tank reactor with a BDD anode and a carbon-felt (CF) cathode (adapted from [37]). (b) Three-electrode tank reactor with an anode, a cathode, and an SCE reference electrode (adapted from [29]). (c) Flow-by plant (up) with a filter-press cell (down) containing a BDD/BDD pair of electrodes (adapted from [22]). (d) Cylindrical glass reactor with horizontal anode and cathode (adapted from [30]). (e) Three-electrode reactor with an anode, a gas-diffusion electrode (GDE) as cathode, and an Ag|AgCl reference electrode (adapted from [42]).

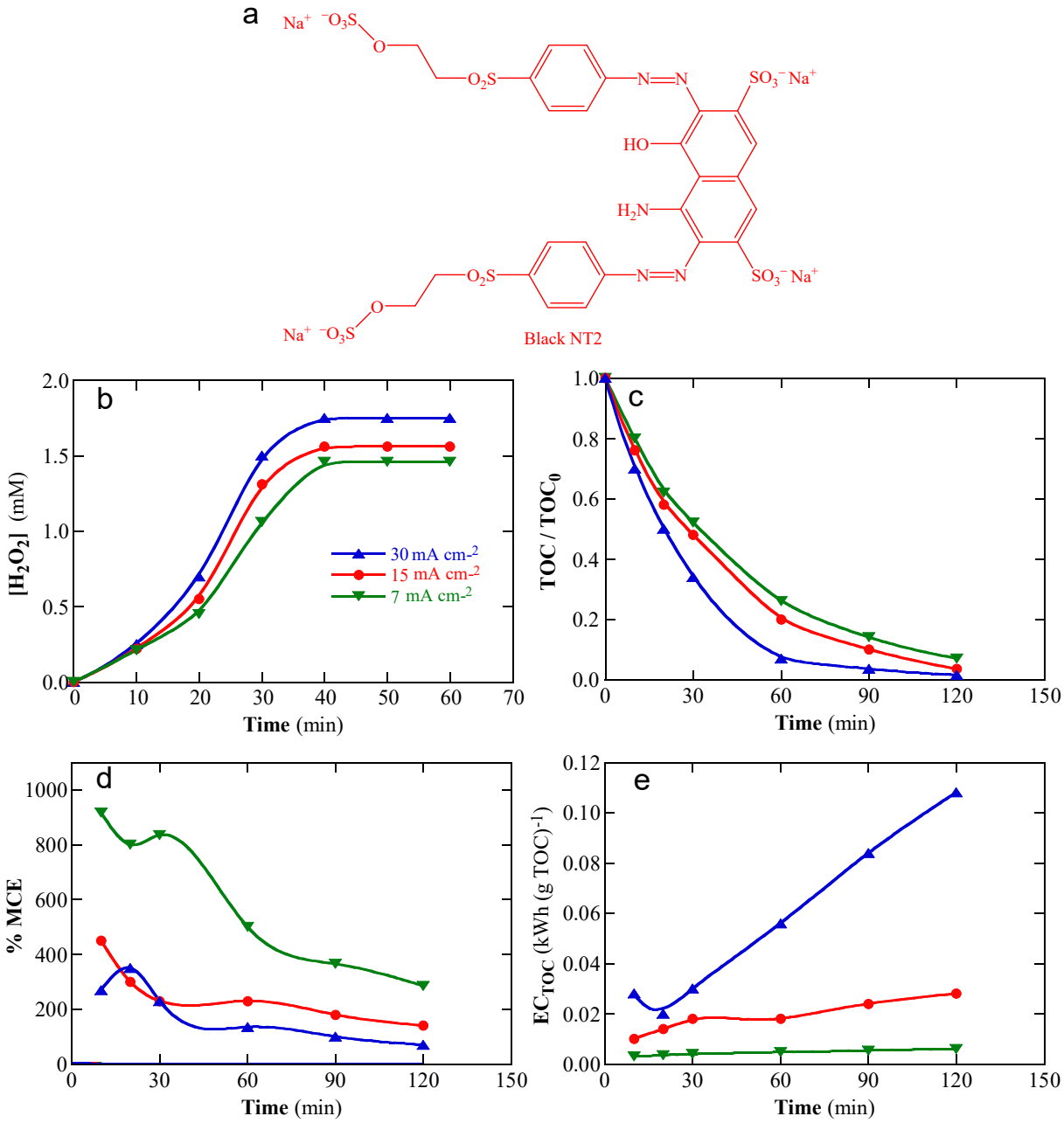

Fig. 4. (a) Chemical structure of the diazo dye Black NT2. (b) Effect of current density over the variation of the concentration of accumulated H_2O_2 with time for the electrolysis of 4 L of 0.050 M Na_2SO_4 at pH 3.0 with the flow-by plant of Fig. 3c equipped with a filter-press BDD/BDD cell under liquid flow rate = 12 L min^{-1} and air flow rate = 1 L h^{-1}. Effect of current density on the time course of (c) normalized TOC, (d) percentage of mineralization current efficiency, and (e) energy consumption per unit TOC mass for the homo-EF process upon the above conditions of the solution containing 250 mg L^{-1} of Black NT2 and 0.30 mM Fe^{2+}. Adapted from [22]

SCE in a divided cell containing a GF||polypyrrole|lignine cathode, outperforming the 10 mg L^{-1} obtained for the unmodified GF [44]. For an ACF cathode prepared by heating CF at 900 °C, the maximum accumulated H_2O_2 was 37.8 mg L^{-1} with CE = 65% and EC = 0.266 kWh m^{-3} at E_{cat} = -0.80 V/SCE (I = 99.6 mA) after 120 min in an undivided three-electrode cell with a Pt anode [20]. These authors demonstrated by CV a smaller electroactivity of the raw CF as compared to ACF. Better results of 70.3 mg L^{-1} of accumulated H_2O_2 with CE = 79% and EC = 0.40 kWh m^{-3} have been reported by Temur-Ergan et al. [54] operating under similar conditions with a DSA anode and the same ACF cathode, suggesting a slower removal of H_2O_2 on DSA than Pt from reaction (5). Table 2 also shows excellent H_2O_2 accumulation of other modified cathodes like ACF|carbon black-PTFE [55], CF|CNTs or CF|graphene [57], oxidized carbon black [59], and NPC|GF [66].

Faster discoloration and mineralization were attained by homo-EF with modified carbonaceous cathodes with respect to the corresponding raw ones as a result of the greater generation of H_2O_2 and •OH, as pointed out above. For the azo dye Acid Orange 7 (see chemical structure in Fig. 1), high TOC removal of 95% was obtained by treating 200 mL of 1 mM of dye in 0.050 M Na_2SO_4 and 1.0 mM Fe^{2+} in pure water at pH 3.0 with a three-electrode tank reactor like of Fig. 3b with a Pt anode and an Au|N-carbon cathode at E_{cat} = -0.30 V/Ag|AgCl lasting 180 min (see Table 2) [49]. Huong Le et al. [47] studied the homo-EF of 100 mL of 0.1 mM of the same dye with 0.050 M Na_2SO_4 and 0.20 mM Fe^{2+} in pure water at pH 3.0 and 25 °C using a three-electrode tank reactor like of Fig. 3b with a Ni|Ti anode and a modified carbon nanotube fiber|

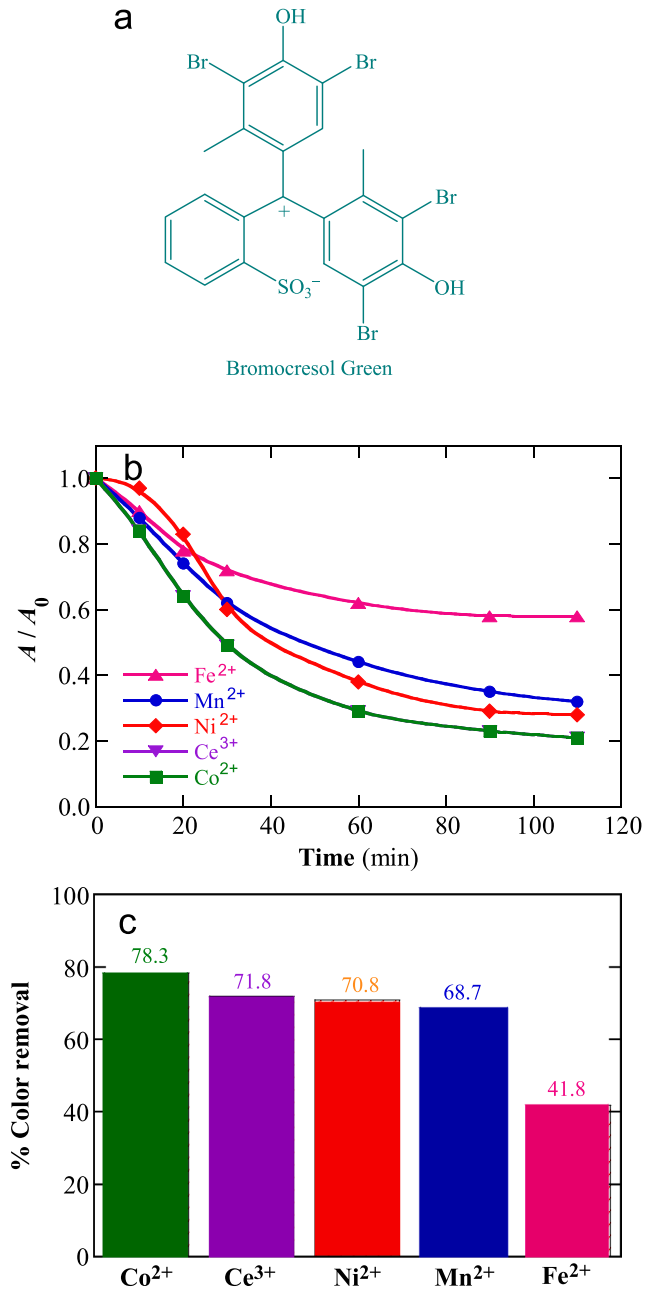

Fig. 5. (a) Chemical structure of the triphenylmethane dye Bromocresol Green. (b) Change of normalized absorbance with time for the homo-EF and homo-EF-like with different cations treatments of 800 mL of 0.030 mM of the above dye with 0.050 M Na_2SO_4 and 0.15 mM of each catalyst in pure water at pH 2.5 using the three-electrode cell of Fig. 3b with a Pt anode and a graphite cathode upon an O_2 flow rate = 3.88 L min^{-1} and at E_{cat} = -0.50 V/SCE. (c) Percentage of color removal after 110 min of the above assays.
Adapted from [29]

carbon fiber cathode by applying an $I = 25$ mA for 360 min. They found a low TOC removal of 12% with the raw carbon fiber, which grew up to 64% with the modified cathode (see Table 2). Despite this excellent result, the modified cathode showed low reusability only giving 42% TOC abatement after 10 consecutive cycles, preventing its further use in practice. In contrast, GF|polypyrrole|lignine [44], ACF|carbon black-PTFE [55], and NPC|GF [66] cathodes showed good reusability and were more useful for practical applications. Table 2 also shows that Pt or DSA were pre-eminently tested as anodes in homo-EF, being preferred to BDD by their lower cost despite their lower oxidation ability. Note that the former anodes originate much smaller contents of ClO_3^- and ClO_4^- than BDD in real effluents with Cl^- ion, then being more environment friendly [6].

Several works have explored the application of homo-EF at near-neutral or neutral pH. Zhang et al. [59] treated a solution of 0.1 mM of the xanthene dye Rhodamine B (see chemical structure in Fig. 1) in pure water with 0.10 M Na_2SO_4 and 1.0 mM Fe^{2+} at pH 5.13. The cell was a three-electrode tank reactor like Fig. 3b with a Pt anode and a floating oxidized carbon black cathode, being applied an E_{cat} from −0.20 to −3.0 V/Ag|AgCl for a short time of 32 min. At the optimum E_{cat} = -1.0 V/Ag|AgCl, the solution was rapidly discolored up to 95% with 78% TOC abatement. Less potent was the raw carbon black that yielded 80% color removal and 20% TOC decay (see Table 2). Surprising results have been described by Liu et al. [66] when decolorized 200 mL of 100 mg L^{-1} of the azo dye Acid Red 18 (so-called Ponceau 4R) with 0.050 M Na_2SO_4 and 0–0.56 mM Fe^{2+}at pH 7.0 and 25 °C under an air flow rate = 0.6 L min^{-1} using a two-electrode tank reactor like of Fig. 3a with a Ti|RuO_2-IrO_2 (DSA) anode and a NPC|GF cathode at $j = 17.5$ mA cm^{-2} lasting 120 min. While 48% of color removal was reached by EO-H_2O_2 (without Fe^{2+}), > 98% discoloration was achieved by homo-EF by adding ≥ 0.36 mM Fe^{2+}. Under these neutral pH conditions, a large amount of $Fe(OH)_3$ sludge precipitation is expected that could yield a similar discoloration at high Fe^{2+} contents, although this point was not confirmed by the authors.

Apart from the electrolytic conditions (anode, cathode, applied j or E_{cat}, and electrolyte composition), the solution pH, the contents of Fe^{2+} and dye determine the performance of the homo-EF process as well and need to be optimized for achieving the best operating conditions. As an example, Fig. 7 depicts the behavior of 100 mL of 30–90 mg L^{-1} of Rhodamine B with 0.10 M Na_2SO_4 and 0–1.0 mM Fe^{2+} in pure water at pH 2.5–4.0 and 20 °C upon an air flow rate = 2.0 L min^{-1} [65]. The runs were carried out with a three-electrode tank reactor like of Fig. 3b with a DSA anode and a degreasing cotton|graphite-PTFE cathode at E_{cat} = -1.10 V/SCE. Fig. 7a highlights the quicker discoloration at pH = 2.5 for 50 mg L^{-1} dye and 0.7 mM Fe^{2+}, being completely colorless in 15 min. In fact, a similar rate was obtained at pH 3.0, confirming that homogeneous $^{\bullet}OH$ from Fenton's reaction (1) was the main oxidant in comparison to the M($^{\bullet}OH$) formed from reaction (6). The influence of Fe^{2+} concentration at pH = 2.50 and 50 mg L^{-1} dye on k_{dis} and the percentage of TOC removal at 120 min is presented in Fig. 7b and c, respectively. In both cases, maximum k_{dis} = 0.411 min^{-1} and 90% TOC decay were obtained for 0.7 mM Fe^{2+}. The increase of both parameters with increasing Fe^{2+} up to 0.7 mM can be ascribed to the gradual acceleration of Fenton's reaction (1), whereupon they dropped down by the concomitant loss of homogeneous $^{\bullet}OH$ from the attack of the excess of Fe^{2+} by the parasitic reaction (27) [16]:

$$Fe^{2+} + {}^{\bullet}OH \rightarrow Fe^{3+} + OH^- \quad (27)$$

When the effect of dye concentration was analyzed at the optimum pH = 2.50 and 0.7 mM Fe^{2+}, the maximum k_{dis} was determined at 50 mg L^{-1} dye (see Fig. 7d), whereas a similar TOC removal of 90–91% was found for 50–90 mg L^{-1} dye (see Fig. 7e). These results suggest that color removal is slower with increasing dye content at shorter electrolysis times, as higher amounts of dye are destroyed more slowly with similar amounts of homogeneous $^{\bullet}OH$ generated. Conversely, the analogous TOC removal found between 50 and 90 mg L^{-1} dye makes evident the large oxidation power of the homo-EF treatment for high dye contents. This suggests that the solutions were mineralized up to the formation of a similar percentage of hardly oxidizable by-products such as Fe(III)-carboxylate complexes, so that, the non-reactant homogeneous $^{\bullet}OH$ was destroyed through their parasitic reactions, e.g., reactions (25)-(27).

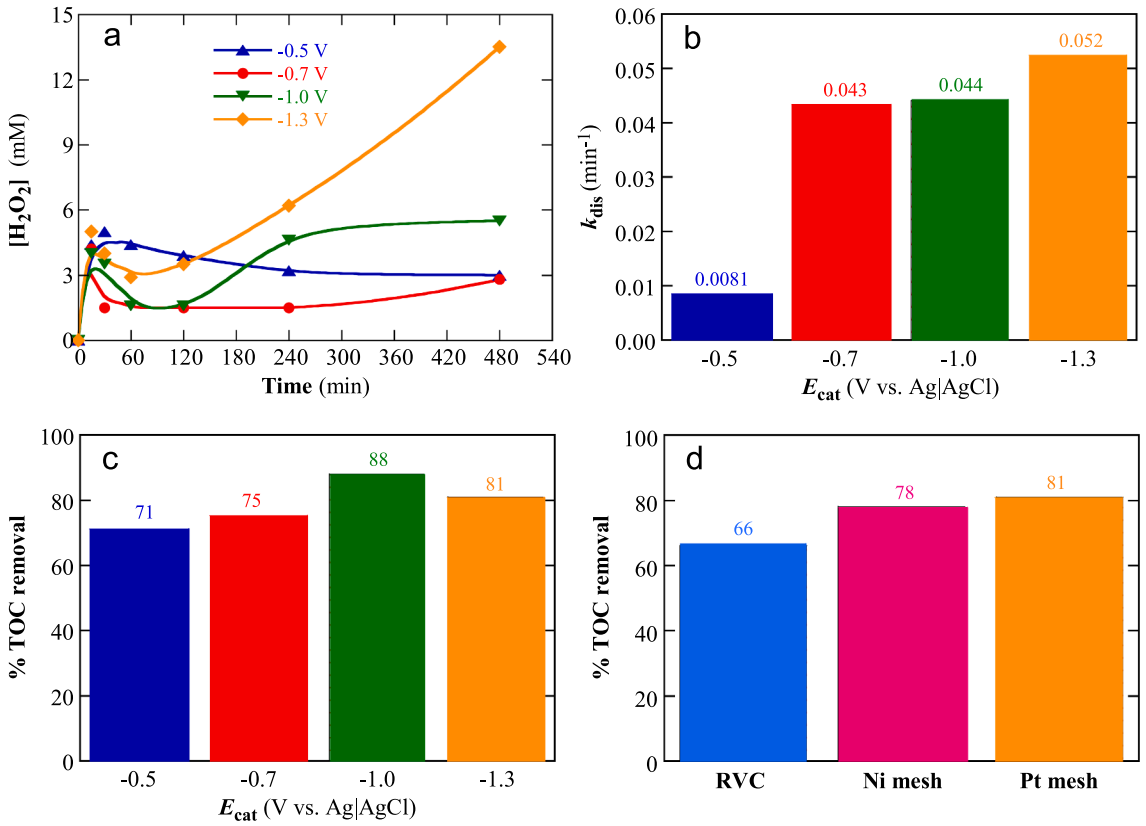

Fig. 6. (a) Effect of the applied cathodic potential vs. Ag|AgCl on the change of the concentration of accumulated H_2O_2 with time for the electrolysis of a 0.050 M Na_2SO_4 solution in pure water at pH 3.0 and 25 °C with the three-electrode reactor of Fig. 3e with a Pt mesh anode and a carbon-PTFE GDE cathode fed with an O_2 flow rate = 0.15 mL min^{-1}. Influence of the applied cathodic potential over (b) the rate constant for discoloration and (c) percentage of TOC removal at 480 min for the homo-EF process of a solution with 100 mg L^{-1} of Methylene Blue and 0.10 mM Fe^{2+} upon the above conditions. (d) Percentage of TOC removal after 480 min of the same treatment with reticulated vitreous carbon (RVC), Ni mesh, or Pt mesh anode at E_{cat} = -1.3 V/Ag|AgCl.
Adapted from [42]

4. Heterogeneous electro-Fenton process of dyes

As discussed above, iron ions tend to precipitate as $Fe(OH)_3$ at pH > 4.0 along with the accumulation of persistent Fe(III)-carboxylate complexes. This propitiates the drop of dye discoloration in the homo-Fenton and homo-EF processes that operate at optimum pH = 3.0. Another concern is the difficulty of reusing iron ions as a catalyst. To overcome these limitations related to Fenton's reaction (1), the hetero-EF process has been proposed, where H_2O_2 is transformed into $^{\bullet}OH$ on the surface of a solid catalyst or functional cathode and hence, much fewer amounts of this oxidant radical are produced as compared to the counterpart homo-EF. Despite this, hetero-EF allows working to near neutral pH conditions without significant iron precipitation [16]. When this treatment is considered with iron solid catalysts or functionalized cathodes, the same heterogeneous reactions as in homo-EF are proposed but with the participation of surface Fe^{2+} and Fe^{3+}, designed as $\equiv Fe^{2+}$ and $\equiv Fe^{3+}$. Some authors consider that these surface iron ions are rather hydroxylated, i.e., linked to a –OH group. The heterogeneous Fenton's reaction with the production of heterogeneous $^{\bullet}OH$ can be expressed as follows [16]:

$$\equiv Fe^{2+} + H_2O_2 \rightarrow \equiv Fe^{3+} + {}^{\bullet}OH + OH^- \quad (28)$$

This subsection describes the characteristics of hetero-EF applied to dye remediation and Table 3 lists relevant results reported in selected articles.

4.1. Solid catalysts

In the hetero-EF process with solid catalysts, iron ions/other metals/metal oxides have been checked in their initial form, as minerals like magnetite or hematite, or deposited on diverse supports. The commonly used supports can be divided into two categories: inorganic supports and polymeric materials. Table 3 shows several examples of inorganic supports such as silica, clays, activated carbon, graphene oxide (GO), CeO_2, zeolite, and amorphous ribbon, as well as polymeric materials like alginate beads and polyacrylamide hydrogels. Three types of heterogeneous catalysts have been tested in the hetero-EF process for dye wastewater treatment [67]:

(i) Natural Fe-containing minerals such as chalcopyrite and pyrite [68], pyrite waste slag [69], hematite and magnetite [70], and Fe-rich laterite [71],
(ii) iron or multivalent transition metals, including sponge iron [69], $LaCu_{0.5}Mn_{0.5}O_3$ perovskite [72], iron-coated nickel foam [73], $FeSe_2$ nanoparticles [74], and Fe-based amorphous alloys ($Fe_{80}Si_{10}B_{10}$ and $Fe_{83}Si_5B_8P_4$) [75], and
(iii) iron-bearing materials deposited on supports like rGO|Fe_3O_4 [76], Fe-zeolite [77–79], $CoFe_2O_4$|NOM [80,81], iron-doped mesoporous silica [82], perovskite ($La_{1-x}Nd_xFeO_3$)|AC [83], $CuFeO_2$|CeO_2 [84], Fe-C [85], sepiolite|pyrite [86], $FeVO_4$|CeO_2 [87], Cu|C loaded on rGO [88], and Fe_3O_4|CS|GA NPs [89].

4.1.1. Natural Fe-containing minerals

Due to their abundance in the earth's crust, several minerals have been successfully used as catalysts for dye discoloration in hetero-EF such as pyrite (FeS_2), hematite (α-Fe_2O_3), magnetite (Fe_3O_4), and chalcopyrite ($CuFeS_2$). Among these, pyrite and chalcopyrite offer new

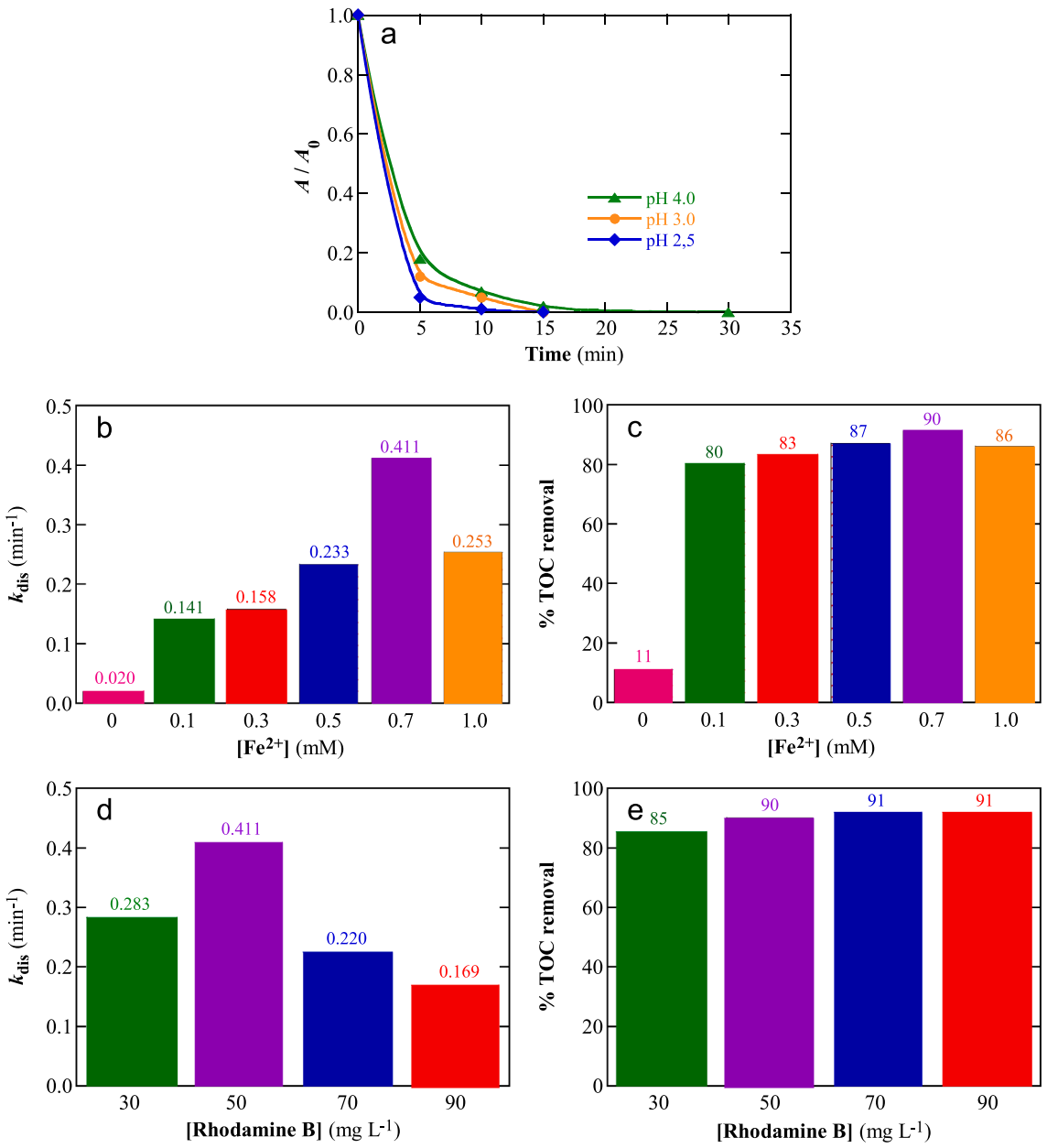

Fig. 7. (a) Effect of pH on the normalized absorbance vs. time for the homo-EF treatment of 100 mL of 50 mg L^{-1} of the xanthene dye Rhodamine B with 0.10 M Na_2SO_4 and 0.7 mM Fe^{2+} in pure water at 20 °C using a three-electrode tank reactor like of Fig. 3b with a DSA anode and a degreasing cotton|graphite-PTFE cathode by applying an E_{cat} = -1.10 V/SCE. Effect of Fe^{2+} concentration over (b) the rate constant for discoloration and (c) percentage of TOC removal at 120 min upon the above conditions at pH 2.5 and 50 mg L^{-1} dye. Influence of Rhodamine B concentration on (d) the rate constant for discoloration and (e) percentage of TOC removal at 120 min under the above conditions with 0.7 mM Fe^{2+} at pH 2.5.
Adapted from [65]

possibilities for boosting the hetero-EF performance due to (i) their ability to regulate solubilized iron ions in the presence of O_2 to operate partially in homo-EF and (ii) the self-adjustment into acidic pH required for Fenton's reaction from reactions (29)-(34) [69,90]:

$$2FeS_2 + 7O_2 + 2H_2O \rightarrow 2Fe^{2+} + 4SO_4^{2-} + 4H^+ \quad (29)$$

$$2FeS_2 + 15H_2O_2 \rightarrow 2Fe^{3+} + 14H_2O + 4SO_4^{2-} + 2H^+ \quad (30)$$

$$FeS_2 + 14\ Fe^{3+} + 8H_2O \rightarrow 15Fe^{2+} + 2SO_4^{2-} + 16H^+ \quad (31)$$

$$CuFeS_2 + 4O_2 \rightarrow Cu^{2+} + Fe^{2+} + 2SO_4^{2-} \quad (32)$$

$$CuFeS_2 + 4H^+ + O_2 \rightarrow Cu^{2+} + Fe^{2+} + 2S^0 + 2H_2O \quad (33)$$

$$CuFeS_2 + 16Fe^{3+} + 8H_2O \rightarrow Cu^{2+} + 17Fe^{2+} + 2SO_4^{2-} + 16H^+ \quad (34)$$

Yao et al. [68] studied the behavior of these catalysts to destroy the azo dye Reactive Red X-3B, whose chemical structure is shown in Fig. 8a. These authors treated 400 mL of 1.10 g L^{-1} of the dye in 0.050 M Na_2SO_4 and 10 g L^{-1} of each hetero-catalyst at pH = 6.0 using a graphite/graphite cell like of Fig. 3a by applying a j = 20 mA cm^{-2}. Fig. 8b and c highlight that the percent of color and COD removal increased in the order: pyrite ≈ chalcopyrite < sponge-Fe < Fe-carbon composite, whereas Fig. 8d makes evident the expected decay of EC_{COD} in the same order. For the more powerful process, 99.6% discoloration and 80% COD removal were achieved in 180 min, with EC_{COD} = 0.31 kWh (g COD)$^{-1}$ at 80 min (see Table 3). Good stability and reusability of the Fe-carbon composite were found after 5 consecutive runs. For the pyrite and chalcopyrite assays, the pH dropped from 6.0 to 2.9 and 3.2 and the iron ion gradually increased to 7.12 and 13.06 mg L^{-1},

Table 3
Selected results reported for the heterogeneous electro-Fenton (hetero-EF) treatment of synthetic organic dyes from wastewaters using undivided cells.

Dye	System (anode/cathode)	Experimental remarks	Best results	Ref,
Solid catalysts				
Natural Fe-containing minerals				
Reactive Red X-3B	Two-electrode reactor (graphite/graphite). Catalysts: chalcopyrite, pyrite, sponge iron, and iron-carbon composite	400 mL of 1.10 g L^{-1} of dye in pure water, 0.050 M Na_2SO_4, catalyst dosage = 10 g L^{-1}, pH = 6.0, j = 20 mA cm^{-2}, 180 min	99.6% discoloration and 80% COD removal for iron-carbon composite. Good stability and reusability after 5 consecutive runs. EC_{COD} (kWh (g COD)$^{-1}$): 0.84 in the absence of catalyst > 0.50 with pyrite > 0.46 with chalcopyrite > 0.31 with iron-carbon composite	[68]
Malachite Green	Two-electrode reactor (Ti|PbO_2/CF). Catalyst: industrial pyrite waste slag	250 mL of 50 mg L^{-1} dye in pure water, Na_2SO_4 supporting electrolyte, catalyst dosage: 0.04–0.20 g L^{-1}, pH = 3.0–11.0, j = 3–7 mA cm^{-2}, air flow rate = 3 L min^{-1}, 240 min	For pH = 5.0, 0.12 g L^{-1} catalyst and j = 5 mA cm^{-2}: 98% discoloration after 50 min (k_{dis} = 0.082 min^{-1}), 97.7% TOC removal, MCE = 0.392%, and EC = 1.942 kWh m^{-3}. Easy to separate and good reuse after 5 consecutive runs. Fukui function, dual descriptor (DD), and GC–MS were adopted to explore the degradation pathway	[69]
Methylene Blue	Two-electrode reactor with rotating cathode (Ti mesh|DSA/graphite) . Catalyst: $LaCu_{0.5}Mn_{0.5}O_3$	130 mL of 10 mg L^{-1} of dye in pure water, 0.050 M Na_2SO_4, catalyst dosage = 0–2.5 g L^{-1}, pH = 3.0–8.5, 22 °C. air flow rate = 10–30 mL min^{-1}, E_{cell} = 1–3 V, 240 min	100% discoloration at circumneutral (6.5) and basic (8.5) pH and 26 % of TOC reduction under optimum conditions: 1.8 g L^{-1} of $LaCu_{0.5}Mn_{0.5}O_3$, 20 mL min^{-1} of air flow, and E_{cell} = 3 V (2.6 mA cm^{-2}). Successive 5 runs proved a good durability and stability of solid catalysts, with only a slight reduction of performance due to the fouling of the electrode surface	[72]
Iron or multivalent transition metals				
Methyl Blue Rhodamine B	Two-electrode reactor (Pt mesh/graphite). Catalysts: $Fe_{80}Si_{10}B_{10}$ amorphous ribbon and $Fe_{83}Si_5B_8P_4$ ribbon	150 mL of 20 mg L^{-1} of dye in pure water, 0.10 M Na_2SO_4, pH = 3.0, 25 °C, catalyst dosage = 0.2 g L^{-1}, O_2 content = 0–10 mM, I = 50 mA, 20 min	100% discoloration: with k_{dis} (min^{-1}) and TOC removal: 0.376 and 50% for Methyl Blue and 0.233 and 17% for Rhodamine B with $Fe_{83}Si_5B_{10}$, and 0.514 and 61% for Methyl Blue and 0.364 and 28% for Rhodamine B with $Fe_{83}Si_5B_8$ P_4. $Fe_{83}Si_5B_8P_4$ maintained good reusability after 26 discoloration cycles of Methyl Blue	[75]
Iron-bearing materials deposited on supports				
Reactive Red 195	Two-electrode reactor(stainless steel /stainless steel) . Catalyst: rGO|Fe_3O_4	Solutions with 100–300 mg L^{-1} of dye in pure water, 0.050 M Na_2SO_4, catalyst dosage = 0.5–2.5 mg, pH = 1.0–9.0, air flow rate = 400 mL min^{-1}, I = 50–250 mA, 60 min	93.3% discoloration and 75% COD removal with EC_{COD} = 0.33 kWh (g COD)$^{-1}$ for 186.43 mg L^{-1} dye, 2.0 mg catalyst, pH 3.04, and I = 194.96 mA, The catalyst almost remained efficient after 6 consecutive cycles. Only 2.4% of iron from the catalyst was dissolved.	[76]
Reactive Red 120	Two-electrode reactor (graphite/graphite). Catalyst: Fe-ZSM-5 nanocatalyst	200 mL of 10 mg L^{-1} of dye in pure water, 0.050 M Na_2SO_4, catalyst dosage = 0–0.1 g with Fe loading = 0.1%-1.0%, pH = 1.0–7.0, 25 °C, I = 100 mA (around E_{cell} = 15 V), 25 °C, 30 min	98% discoloration with 1.0% Fe loading at pH = 3.0. The catalyst was reusable because it recovered the active sites through regeneration process and then, it provided > 95% in 3 successive runs	[77]
Acid Blue 25	Two-electrode cylindrical rotating reactor (graphite/graphite).Catalysts: Fe|Cu-ZSM-5 (7–3), Fe|Co-ZSM-5(7–3), Fe||Cr-ZSM-5 (7–3)	750 mL of 200 mg L^{-1} of dye in pure water, 0.010–0.050 M Na_2SO_4, catalyst dosage = 100 mg L^{-1}, pH = 3.0, 25 °C, j = 3.57 mA cm^{-2}, 90 min	Best performance with Fe|Cu-ZSM-5(7–3). For 0.010 M Na_2SO_4, 97% of discoloration, 79% of COD decay, and 65% of TOC removal. 5 consecutive cycles did not fall considerably the removal efficiency, indicating a good reusability of the catalyst, which was cost-effective	[78]
Acid Black 210	Two-electrode reactor with rotating cathode(BDD/carbon-PTFE GDE) . Catalyst: $CoFe_2O_4$|NOM magnetic hybrid catalyst (Hb200)	140 mL of 14–55 mg L^{-1} of dye in pure water and in real tannery wastewater, 0.050 M Na_2SO_4, catalyst dosage = 30 and 100 mg, pH = 3.0, 25 °C, air flow rate = 1.2 L min^{-1}, j = 14.1–42.2 mA cm^{-2}, 420 min	Production rate of H_2O_2 of 12.2 mM $cm^{-2}h^{-1}$ with CE = 45.7% after 120 min at 28.2 mA cm^{-2}. After 30 min at this j, discoloration for 14 and 55 mg L^{-1} dye in pure water were 79.5% and 77.9% respectively, using 30 mg of catalyst, whereas 88.3% and 88.6% of loss of color using 100 mg of catalyst. For the real tannery wastewater with 55 mg L^{-1} dye and 30 mg catalyst at 420 min: k_{dis} = 0.0087 min^{-1}, 95% TOC removal, and EC_{TOC} = 0.34 kWh (g TOC)$^{-1}$. Excellent catalytic activity during 3 cycles, (10% lower mineralization in the last cycle). By-products identified by GC–MS	[80]
Acid Blue 29	Two-electrode reactor (BDD/carbon-PTFE GDE). Catalysts: hybrid sludge (HbLM) extracted from iron mining wastes	130 mL of 25 mg L^{-1} of dye in pure water, 0.050 M Na_2SO_4, catalyst dosage = 1.0 g L^{-1}, pH = 3.0 or 7.0, 25 °C, air flow rate = 300 mL min^{-1}, j = 33.3–66.7 mA cm^{-2}, 60 min	100% discoloration after 20 min at pH = 3.0 and j = 33.3 mA cm^{-2}, For EO-H_2O_2, only 62% discoloration, No acidification was needed and the process was efficient over the wide pH range checked	[81]
Acid Blue 25	Two-electrode reactor with rotating cathode (graphite/graphite).Catalyst: glutaraldehyde cross-linked magnetic chitosan nanoparticles (Fe_3O_4|CS|GA NPs)	750 mL of 25–250 mg L^{-1} dye in pure water, 0.050 M Na_2SO_4, iron content of the catalyst = 5–20 mmol Fe/g chitosan, catalyst dosage = 0.1–0.4 g L^{-1}, pH = 3.0–9.0, rotational speed = 0–150 rpm, I = 0.3–0.9 A, air flow rate = 3 L min^{-1}, 120 min	Discoloration: 94.8% after 90 min for 150 mg L^{-1} dye with 15 mmol Fe/g chitosan and catalyst dosage = 0.3 g L^{-1} at natural pH of dye (6.8), rotational speed = 100 rpm, and I = 0.7 A. 74% COD and 61% TOC removals after 120 min. Good reusability after 5	[89]

(*continued on next page*)

Table 3 (*continued*)

Dye	System (anode/cathode)	Experimental remarks	Best results	Ref,
			successive cycles. Free and surface •OH determined by radical scavengers such as TBA, KI, and p-BQ	
Functionalized cathodes				
Rhodamine B	Two-electrode tank reactor (DSA/Fe-NCCC [a])	300 mL of 83.3 mg L^{-1} of dye in pure water and real wastewater, 10 mg L^{-1} Na_2SO_4, pH = 3.0; O_2 flow rate = 1 L min^{-1}, E_{cell} = 5 V, 80 min	In pure water, 100% discoloration and 82% COD removal with EC_{COD} = 0.194 kWh (g COD)$^{-1}$. Excellent reusability after 20 runs. Generated •OH radical detected by scavengers (isopropanol). By-products identified by GC–MS. For wastewater from the comprehensive conditioning tank of the wastewater treatment station in Anshan Hifichem Co., Ltd with COD, pH, and color of the wastewater: 3175 mg L^{-1} COD, pH = 6.89, and color = 50 folds. 80% COD removal after 360 min of treatment	[95]
Methylene Blue	Two-electrode reactor (Pt sheet/n-Fe_3O_4|ACF)	200 mL of 100 mg L^{-1} of dye in pure water, Na_2SO_4 supporting electrolyte pH = 5.7, air flow rate = 200 mL min^{-1}, j = 5–50 mA cm^{-2}, 120 min	At 30 mA cm^{-2}, 90% discoloration with good reusability and stability after 5 successive runs. 98% COD removal	[96]
Acid Orange 7	Two-electrode single reactor (Pt/ferrocene-graphite|CNTs)	10 mL of 0.01–1 mM dye in pure water, 0.050 M Na_2SO_4, pH = 3.0 and 6.0, air bubbling, 25 °C, I = 20 mA, 180 min	TOC removal: 90%, 96%, 98%, and 2% for KS44-(15)/CNT, KS44-(25)/CNT, KS44-(20)/CNT, KS44-0[b]. For the best KS44-20 cathode, 98% TOC removal. Good reusability after 5 cycles of use	[97]
Congo Red	Three-electrode divided cell (Pt/Fe(H) ZSM-5)	Cathodic compartment filled with 50 mg L^{-1} of dye in pure water, 0.10 M NaCl, pH neutral, 25 °C, E_{cat} = 2.0 V/SCE, 60 min	74% discoloration in 10 min and almost 100% after 45 min. 64% TOC decay in 60 min. The pH of the system was controlled by the zeolite due to its strong acidic nature	[98]
Methyl Orange Methylene Blue	Two-electrode glass reactor (Pt/TFD|CF [c])	100 mL of 50 mg L^{-1} of dye in pure water, 0.050 M Na_2SO_4, pH = 3.0–9.0, air flow rate = 500 mL min^{-1}, j = 1–20 mA cm^{-2}, 120 min	Discoloration at pH = 7.0 and 50 min: 95% for Methyl Orange and 98% for Methylene Blue. TOC removal at 120 min: 45% and 40% for such dyes, respectively. EC_{COD} = 0.00298 kWh (g^{-} COD)$^{-1}$. Good reusability after 6 consecutive runs. Acidic groups continuously regenerated during electrolysis with release of H^+ to solution. •OH and $^1O_2$ as main ROS	[99]
Methyl Orange	Two-electrode reactor (PbO_2|SnO_2 /Ag|ZOF-SS, Ag|ZOF-CF, or Ag|ZOF-GAC [d]	Solutions of 20 and 25 mg L^{-1} of dye in pure water, 0.050 M Na_2SO_4, pH = 1.0–7.0, air flow rate = 200 mL min^{-1}, I = 3–12 mA, 180 min	100% discoloration with k_{dis} = 0.013 min^{-1} for Ag|ZOF-SS at pH 4.0 and I = 9 mA, •OH, $O_2^{\bullet-}$, and $HO_2^{\bullet}$ as main ROS. Degradation pathway proposed from LC-MS analysis	[100]
Methyl Orange	Two-electrode reactor (Pt /G|HEC [e])	200 mL of 10 mg L^{-1} of dye in pure water, 0.050 M Na_2SO_4 and 2 mM $FeCl_2{\cdot}4H_2O$, pH 3.0, O_2 bubbling, I = 30 mA, 90 min	99% discoloration. G|HEC belongs to a spinel structure revealed by XANES spectra	[101]
Tartrazine	Two-electrode reactor (Ti|Pt/$CoFe_2O_4$|CF)	250 mL of 10–100 mg L^{-1} of dye in pure water, 0.050 M of Cl^-, NO_3^-, SO_4^{2-}, HCO_3^-, or HPO_4^{2-}, pH = 2.0–9.0, air flow rate = 50 mL min^{-1}, j = 4.17–25.0 mA cm^{-2}, 40 min	97% discoloration and 47% of COD and 22.5% TOC removals for 50 mg L^{-1} dye, 0.050 M Na_2SO_4, pH 3.0, and j = 8.33 mA cm^{-2}. EC_{COD} = 0.00688 kWh (g COD)$^{-1}$. The BOD_5/COD of solution increased from 0.008 to 0.560 (40 min) and 0.794 (60 min). $O_2^{\bullet-}$, $^1O_2$, and •OH as key ROS	[102]
Remazol Black B	Three-electrode electrochemical cell (Pt/GDE-Fe ions)	150 mL of 17 mg L^{-1} of dye in pure water, 0.50 M Na_2SO_4, pH = 3.0, air flow rate = 0.1 L min^{-1}, E_{cat} = − 0.6 and −0.7 V/Hg/$HgSO_4$, 50 min	Better discoloration of 97% for − 0.6 V/Hg/$HgSO_4$. TOC removal, MCE, and EC_{TOC} (kWh (g TOC)$^{-1}$): 73%, 37%, and 0.080 for −0.6 V/Hg/$HgSO_4$ and 88%, 3%, and 0.157 at − 0.7 V/Hg/$HgSO_4$	[103]
Acid Orange 7 Methylene Blue	Two electrode tank reactor (DSA/N, S-EEGr.CF [f])	Solutions of 50 mg L^{-1} of dye in pure water, 0.050 M Na_2SO_4, pH = 3.0 or 7.0, air flow rate = 0.75 L min^{-1}, j = 6.25 mA cm^{-2}, 30 min	Good performance with a metal-free system avoiding iron ions addition. For Acid Orange 7, 100% and 90% discoloration after 60 min at pH 7.0 and 3.0, respectively. For Methylene Blue, 100% discoloration after 30 min at pH 7.0 and 40 min for pH 3.0. N,S-EEGr-CF not only accelerated electron transfer with improved H_2O_2 yield, but also activate H_2O_2 to form •OH. The low HOMO-LUMO gap of N, S-EEGr allowed maintaining its high chemical and catalytic activity	[104]
Acid Orange 7	Two electrode tank reactor (Pt/N-doped-CNF-Co|CoO_x [g])	Solutions of 0.1 mM of dye in pure water, 0.050 M Na_2SO_4, pH = 3.0 or 6.0, 25 °C, O_2 bubbling, j = 10 mA cm^{-2}, 40 min	For 10 wt% of Co|CoO_x NPs, 91% discoloration and 93% TOC removal at pH 3.0. 87–88% discoloration at pH 6.0 maintained during 10 consecutive cycles	[105]

[a] Fe-NCCC: iron-loaded needle coke composite cathode.
[b] KS44-0, KS44-(15)|CNT, KS44-(20)|CNT, and KS44-(25)|CNT represent an initial weight ratio of ferrocene of 0, 15, 20 and 25%, respectively.
[c] TFD|CF: tannic acid-Fe complex derivative-modified carbon felt.
[d] Ag|ZOF-SS, Ag|ZOF-CF, and Ag@ZOF-GAC represent silver doped zinc-based organic framework catalyst coted on the three substrates: stainless steel, carbon felt, and granular activated carbon.
[e] G|HEC: Graphene|(AlCrCuFeNi)O high-entropy ceramics.
[f] N,S-EEGr-CF: nitrogen and sulfur co-doped electrochemically exfoliated graphene carbon felt.
[g] N-doped-CNF-Co/CoO_x: nitrogen-doped carbon nanofiber (CNF) electrodes incorporating Co|CoO_x NPs.

respectively, but producing low contents of homogeneous $^{\bullet}OH$ from Fenton's reaction (1). The superior performance of the other two iron catalysts can be ascribed to the generation of higher quantity of heterogeneous $^{\bullet}OH$ from the presence of a much greater quantity of surface $\equiv Fe^{2+}$ by the heterogeneous Fenton's reaction (28).

Aside from pyrite and chalcopyrite, sulfuric acid refining produced at least 5 million tons of industrial pyrite waste slag every year, mainly composed of α-Fe_2O_3 alongside traces of Al, Cu, and Mn. Sun et al. [69] tested the iron catalyst of this waste in the hetero-EF treatment of the triphenylmethane dye Malachite Green. Fig. 9a schematizes the tank reactor like of Fig. 3a and reactions involved in these trials made with 250 mL of 50 mg L^{-1} this dye in Na_2SO_4 solution and 0.12 g L^{-1} of industrial pyrite waste slag at pH = 5.0 and j = 5 mA cm^{-2}. An excellent performance was obtained as compared to uncatalyzed assays (EO-H_2O_2 process). Fig. 9b-d show that the catalyst gave 98% discoloration in 50 min (k_{dis} = 0.082 min^{-1}), along with a high 97.7% TOC removal, MCE = 0.392%, and EC = 1.942 kWh m^{-3} at 240 min (see also Table 3).

4.1.2. Iron or multivalent transition metals

Inspired by its high mobility of oxygen and unusual redox properties, Cruz del Álamo et al. [72] considered $LaCu_{0.5}Mn_{0.5}O_3$ as heterogeneous catalyst in hetero-EF. They treated 130 mL of 10 mg L^{-1} of Methylene Blue with 0.050 M Na_2SO_4 and catalyst dosage = 0–2.5 g L^{-1} at pH = 3.0–8.5 and 22 °C using a two-electrode tank reactor with a Ti mesh|DSA anode and a rotating graphite cathode. They found an overall discoloration at circumneutral (6.5) and alkaline (8.5) pH and 26 % of TOC reduction at optimum conditions of 1.8 g L^{-1} of $LaCu_{0.5}Mn_{0.5}O_3$, 20 mL min^{-1} of air flow, and E_{cell} = 3 V (j = 2.6 mA cm^{-2}) (see Table 3). The low copper leaching (< 0.05 mg L^{-1}) along with its stability in 5 successive runs proved its feasible practical applicability as a hetero-catalyst in hetero-EF.

Taking advantage of its high conductivity and high porosity, sponge iron and iron-carbon composite catalysts have been confirmed as excellent hetero-catalysts for Reactive Red X-3B treatment, as pointed out above [68]. Iron diselenide ($FeSe_2$) catalyst with three morphologic forms (micro granular particles, nano-stick, and nanoflakes) have been prepared by controlling selenium precursors like selenium metal, selenious acid (H_2SeO_3), and selenium dioxide (SeO_2) [74]. Among them, the nano-stick $FeSe_2$ catalyst presented the best performance for the discoloration of Methylene Blue (93.3%) and Congo Red (90.4%) solutions owing to its narrow band gap (0.88 eV) and fast recycling of the $\equiv Fe^{3+}/\equiv Fe^{2+}$ pair. A series of Fe-based amorphous alloys such as $Fe_{80}Si_{10}B_{10}$ and $Fe_{83}Si_5B_8P_4$ has been synthesized as hetero-catalysts by Zou et al. [75]. They possessed large amounts of active sites attributed to their unique metastable structure and chemical homogeneity. The presence of Fe assured the active sites for heterogeneous Fenton's reaction (28), the introduction of P enhanced their catalytic effect, and Si was oxidized to SiO_2 to improve its stability. Hetero-EF treatments were carried out with 150 mL of 20 mg L^{-1} of Methly Blue or Rhodamine B dyes with 0.10 M Na_2SO_4 and 0.2 g L^{-1} of each hetero-catalyst in pure water at pH = 3.0 and 25 °C with a two-electrode reactor like Fig. 3a with a Pt mesh anode and a graphite cathode at I = 50 mA. Fig. 10a and b illustrate that both dye solutions were completely discolored in 20 min in the presence of $Fe_{83}Si_5B_8P_4$ based on UV–Vis spectroscopy. This behavior can be confirmed in Fig. 10c, related to high k_{dis}-value of 0.514 min^{-1} for Methyl Blue and 0.364 min^{-1} for Rhodamine B, as shown in Fig. 10d and Table 3. Lower performance can be observed for $Fe_{80}Si_{10}B_{10}$, more strongly diminishing for pure Fe powders. The superiority of $Fe_{83}Si_5B_8P_4$ as a hetero-catalyst was also reflected by a higher TOC removal of 60% for Methyl Blue (see Fig. 10e) and 30% for Rhodamine B (see Fig. 10f), as well a greater leaching of Fe. This suggests the presence of a larger removal by the homo-EF process in competence with the hetero-EF one. Despite this, it was found a good reusability of $Fe_{83}Si_5B_8P_4$ after 26 discoloration cycles of Methyl Blue, thus confirming its feasible applicability in practice.

4.1.3. Iron-bearing materials deposited on supports

More authors have considered the loading of iron-bearing materials on several supports aiming to expose more active sites of surface iron ions to the heterogeneous Fenton's reaction (28) and further enhance the chemical stability of the hetero-catalysts. Table 3 reflects the good performance of these materials in hetero-EF. For example, it has been reported approximately 100% of discoloration of Reactive Red 195 with rGO|Fe_3O_4 [76], Reactive Red 120 [77] and Acid Blue 25 [78,79] with-zeolites, and Acid Blue 25 with glutaraldehyde cross-linked magnetic chitosan [89]. Magnetic hetero-catalysts are promising since they endow easy separation and recovery nature using an external magnetic field. A hybrid magnetic nanostructured $CoFe_2O_4$|NOM catalyst (Hb200) with an average size of 4.85 nm was prepared by an economic sol–gel route, in which NOM served as a green solvent [80]. This preparation method was eco-friendly because hazardous organic polymers were replaced by NOM-rich water to serve as the polymerization agent, allowing faster destruction of the Acid Black 210 dye by hetero-EF than EO-H_2O_2, as can be seen in Fig. 11a and Table 3. As illustrated in the FTIR spectrum of Fig. 11b, the capacity of NOM for complexing metal species (Fe^{2+}, Fe^{3+}, and Co^{2+}) was confirmed by the presence of acidic functional groups such as carboxyl and phenolic hydroxyls [91]. This ferrite catalyst can then trigger a cyclic electron transfer to generate heterogeneous $^{\bullet}OH$ from the reaction of H_2O_2 with $\equiv Fe^{2+}$, $\equiv Fe^{3+}$, and $\equiv Co^{2+}$ in octahedral spinel structure as active sites [92]. Assays using 30 mg of Hb200 in the hetero-EF process were carried out with 140 mL of 55 mg L^{-1} of Acid Black 210 in real tannery wastewater with 0.050 M Na_2SO_4 at pH = 3.0 and 25 °C filling a BDD/carbon-PTFE GDE reactor with rotating cathode upon an air flow rate = 1.2 L min^{-1} and j = 28.2 mA cm^{-2}. Under these conditions, the wastewater was completely discolorized with k_{dis} = 0.0087 min^{-1} and reached an excellent 95% TOC removal in 420 min with EC_{TOC} = 0.34 kWh (g TOC)$^{-1}$ (see Table 3). In contrast, only 87.2% of color removal was found for EO-H_2O_2, demonstrating the high catalytic power of Hb200. A more sustainable sol–gel route has been proposed by dos Santos et al. [81] to prepare a magnetic hybrid HbLN hetero-catalyst from iron mining wastes, as schematized in Fig. 11c. The main component of this magnetic hybrid catalyst was $CoFe_2O_4$ with a high surface area of 167.9 m^2 g^{-1}, pointing to feasible reuse of mining wastes to update the preparation method of the Hb200 hetero-catalyst. For 130 mL of 25 mg L^{-1} of Acid Blue 29 in pure water with 0.050 M Na_2SO_4 and 1.0 g L^{-1}HbLN at 25 °C using a BDD/carbon-PTFE GDE reactor under an air flow rate = 300 mL min^{-1} by applying a j = 33.3 mA cm^{-2}, total discoloration was obtained after 20 min at pH = 3.0, which was prolonged to 60 min at pH 7.0. In contrast, only 62% of the color removal rate was found by EO-H_2O_2 at pH 3.0 (see Table 3). It is noticeable that for the magnetic hybrid catalyst, no prior acidification was needed and the k_{dis}-value increased 12-fold for a catalyst dosage of only 0.25 mg L^{-1} as compared to EO-H_2O_2. This suggests its feasible practical use for the dyeing wastewater remediation even under neutral pH.

To promote active sites uniformly dispersed on the support, inexpensive resins have been adapted with chelating and exchange properties for an in situ assembly strategy [93]. Fig. 11d shows that functional groups on the resins surface like –COOH and -SO_3H can react with the transition metallic ions to form spherical-like metal–organic composite hetero-catalysts. Among diverse transition metallic ions ($\equiv Fe^{2+}$, $\equiv Mn^{2+}$, $\equiv Co^{2+}$, $\equiv Ce^{3+}$, and $\equiv Cu^{2+}$), the $\equiv Mn^{2+}$-mediated hetero-catalyst showed the best performance to discolorize and mineralize Methylene Blue solutions [93]. One explanation of this behavior was its much higher accepting electron ability than others, leading to a faster speed in activating H_2O_2 for $^{\bullet}OH$ production via the recycling of $\equiv Mn^{2+}$ initiated by the heterogeneous Fenton-like reaction (35) and followed by reactions (36)-(38). The superiority of the functional resins was highlighted when compared to conventional materials such as Al_2O_3, alginate beads, clay spheres, and carbon particles. In this way, the highly efficient removal of Methylene Blue was due to the strong interaction (ionic cross-linking) between active sites and supports, which boosted

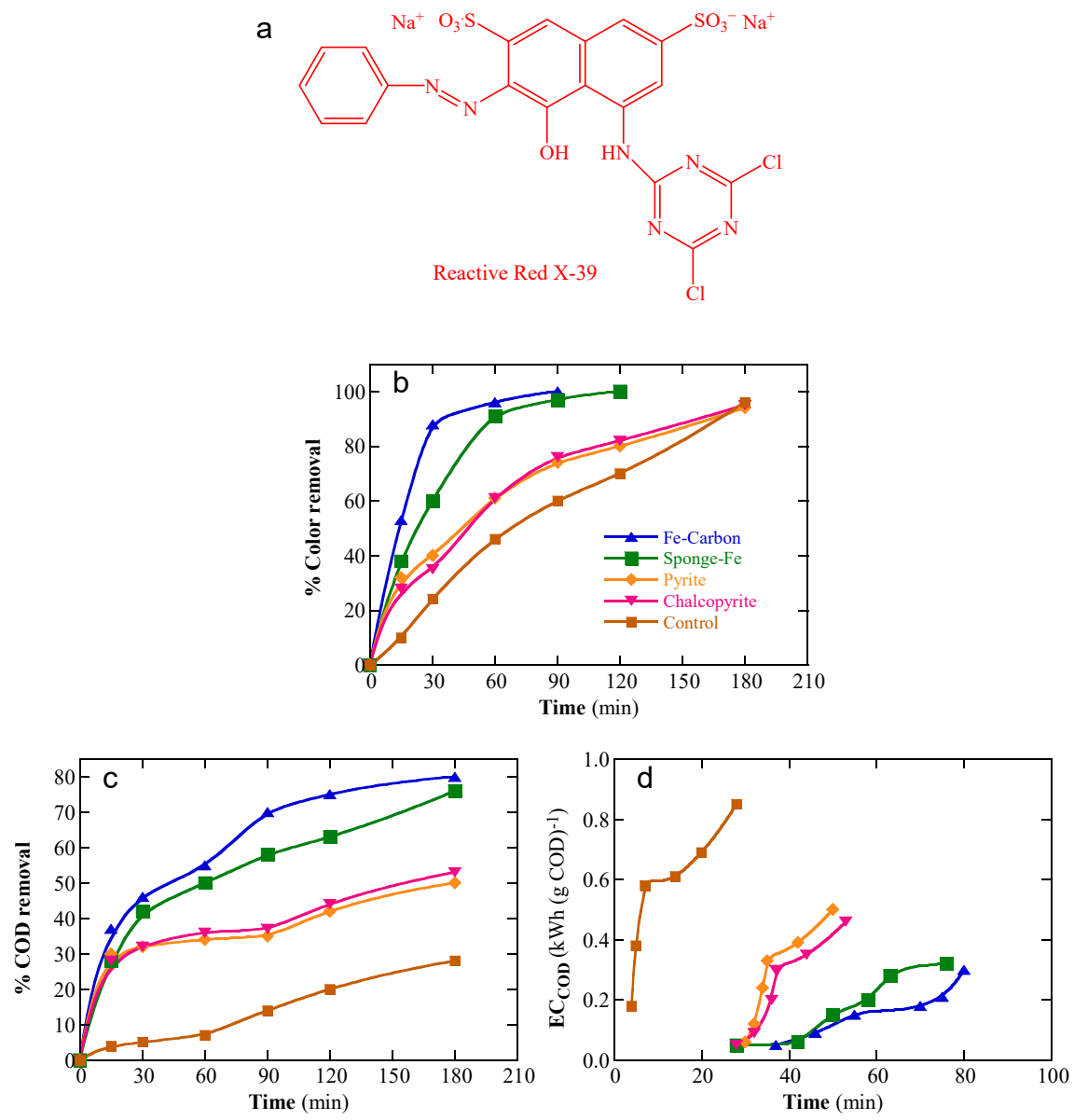

Fig. 8. (a) Chemical structure of the azo dye Reactive Red X-39. (b) Percentage of color removal, (c) percentage of COD removal, and (d) energy cost per unit COD mass for the hetero-EF process of 400 mL of 1.10 g L^{-1} of the above dye in pure water with 0.050 M Na_2SO_4, and 10 g L^{-1} of Fe-carbon composite, sponge-Fe, pyrite, and chalcopyrite as hetero-catalyst at pH = 6.0 using a two-electrode cell like of Fig. 3a with graphite anode and cathode by applying a j = 20 mA cm^{-2}. For the control treatment, no catalyst was added.
Adapted from [68]

the effective $\equiv Mn^{3+}/\equiv Mn^{2+}$ cycle. However, the formation of $\equiv MnO_2$ precipitate could cover the active sites, which results detrimental to dye discoloration in this hetero-EF process.

$$\equiv Mn^{2+} + H_2O_2 \rightarrow \equiv Mn^{3+} + {}^{\bullet}OH + OH^- \quad (35)$$

$$2\equiv Mn^{3+} + 2H_2O \rightarrow \equiv MnO_2 + Mn^{2+} + 4H^+ \quad (36)$$

$$\equiv MnO_2 + \text{Methylene Blue} \rightarrow \equiv Mn^{2+} + \text{Oxidation products} \quad (37)$$

$$\text{Methylene Blue or oxidation products} + {}^{\bullet}OH \rightarrow CO_2 + H_2O \quad (38)$$

Since the $\equiv Fe^{3+}/\equiv Fe^{2+}$ cycle limits the hetero-EF process with solid catalysts, transition metals coupled with iron ions have been introduced to trigger its recycle [94]. As an example, Zahrani and Ayati [79] developed Fe-based nanocatalysts derived from ZSM-5 nano zeolite where M denotes Cu, Co, or Cr ions (see Fig. 11e). The Fe-based nanocatalyst containing Cu ions showed the best performance for 750 mL of 200 mg L^{-1} of the anthraquinone dye Acid Blue 25 (see chemical structure in Fig. 1) in pure water with 0.010 M Na_2SO_4 and 100 mg L^{-1} of hetero-catalyst at pH = 3.0 and 25 °C using a graphite/graphite reactor at j = 3.57 mA cm^{-2} lasting 90 min. For this assay, 97% of discoloration, 79% of COD removal, and 65% of TOC abatement were found (see Table 3). No considerable change in the percent of color removal was found after 5 consecutive cycles, confirming the good reusability of the hetero-catalyst.

4.2. *Functionalized cathodes*

This sub-section conveys the application of hetero-EF with functionalized cathodes to boost homo-EF, allowing the enlargement of working pH because the occurrence of H_2O_2 formation and its activation mainly occur at the cathode surface. The functionalized cathodes tested include Fe-NCCC [95], Fe_3O_4|ACF [96], ferrocene-graphite|CNTs [97],

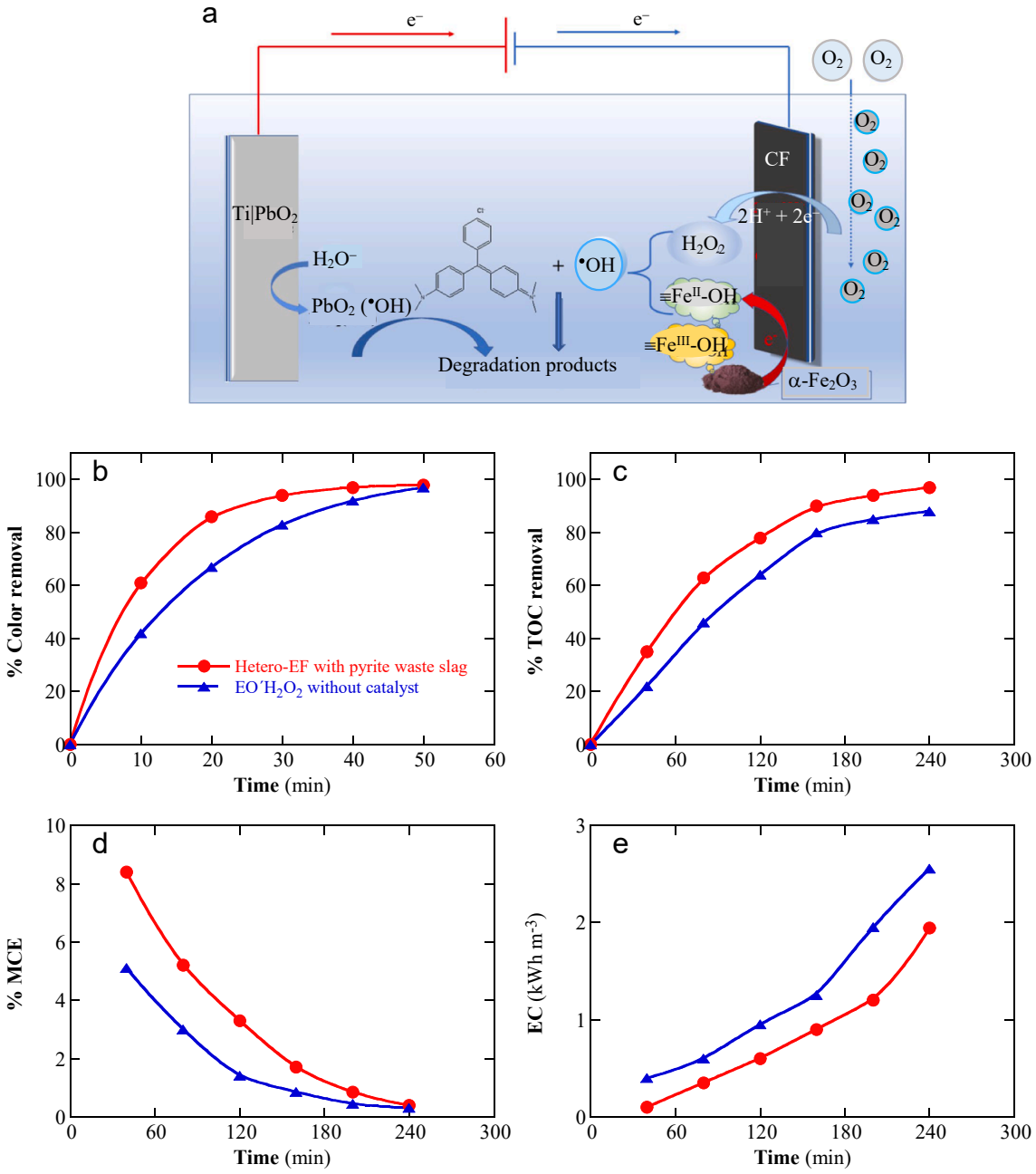

Fig. 9. (a) Scheme of the degradation mechanism of the triphenylmethane dye Malachite Green by hetero-EF with a two-electrode reactor like of Fig. 3a equipped with a Ti|PbO_2 anode and a CF cathode. The hetero-catalyst was an industrial pyrite waste slag mainly containing α-Fe_2O_3 alongside traces of Al, Cu, and Mn. Percentage of (b) color removal, (c) TOC removal, and (d) mineralization current efficiency, as well as (d) energy cost, for the treatment of 250 mL of 50 mg L^{-1} dye in pure water with Na_2SO_4 as supporting electrolyte and 0.12 g L^{-1} of catalyst or uncatalyzed (EO-H_2O_2 process) at pH = 5.0 and j = 5 mA cm^{-2}. Adapted from [69]

Fe(H)ZSM-5 [98], TFD|CF [99], Ag|ZOF-SS, Ag|ZOF-CF, or Ag|ZOF-GAC [100], G|HEC [101], $CoFe_2O_4$|CF [102], GDE-Fe ions [103], N, S-EEGr.CF [104], N-doped-CNF-Co|CoO_x [105], nano-titanium nitride-coated electrodes [106], single sheet iron oxide cathode [107], iron-rich MFI zeolite nanoseeds modified CF [108], MIL-53(Fe) coated porous CF [109], Fe(II)-based GDE [110], iron cathode from gas sludge [111], Fe_3O_4|MWCNTs composite [112], iron-zeolite [113], and $FeLaO_3$ entrapped cathode [114]. Selected results for these functionalized cathodes for dyes treatment in hetero-EF are listed in Table 3.

The selected iron-containing functionalized cathodes of Table 3 show a good performance on dye discoloration and mineralization [95–98,100,101,103]. The dominant role of ≡Fe^{2+} was the activation of the cathodic electrogenerated H_2O_2 into •OH through heterogeneous Fenton's reaction (28). However, this is confined by the narrow working pH and iron sludge production even in hetero-EF. Cleaner ways have been suggested to develop heterogeneous •OH production. Among such proposed functionalized cathodes, a metal-free material (N,S-EEGr-CF) was developed by Yang et al. [104] to broaden the pH range and avoid Fe^{2+} addition. They deduced that a novel three-electron oxygen reduction reaction (O_2 –H_2O_2 -•OH) was responsible for dyes destruction, where the N-EEGr onto CF catalyzed the electron transfer for H_2O_2 formation while the S-EEGr boosted H_2O_2 transformation into •OH.

The local atomic structure of the graphene|(AlCrCuFeNi)O high-entropy oxide cathode (G|HEC) has been deeply established by Chiu

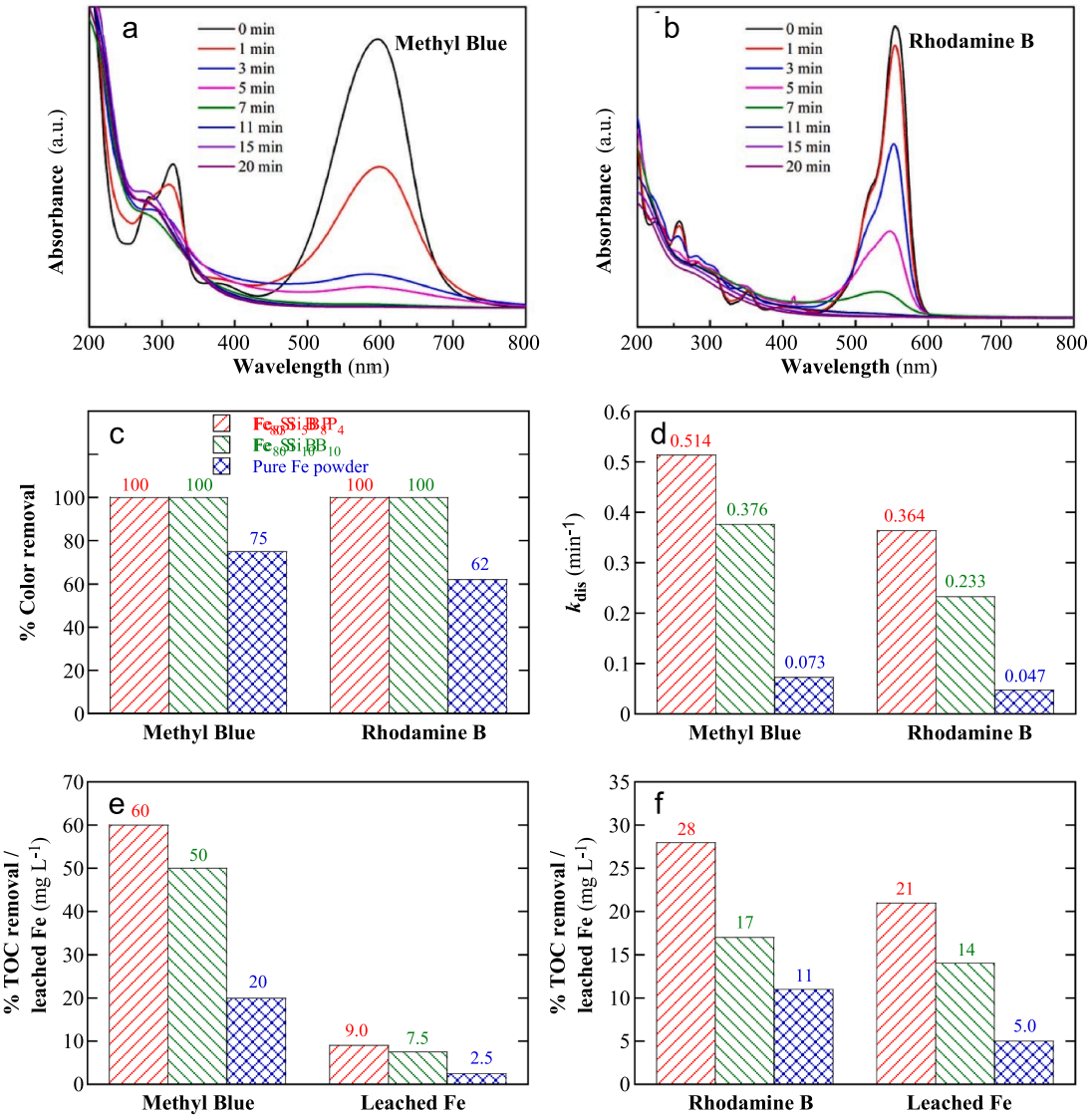

Fig. 10. Change of ultraviolet–visible (UV–Vis) absorbance spectra of 150 mL of 20 mg L^{-1} of (a) Methyl Blue and (b) Rhodamine B in pure water with 0.10 M Na_2SO_4 and 0.2 g L^{-1} of $Fe_{83}Si_5B_8P_4$ ribbons at pH = 3.0 and 25 °C during the hetero-EF treatment using a two-electrode reactor like Fig. 3a equipped with a Pt mesh anode and a graphite cathode at I = 50 mA. (c) Percent of color removal at 20 min and (d) rate constant for discoloration of the above processes of both dyes with $Fe_{83}Si_5B_8P_4$, $Fe_{80}Si_{10}B_{10}$, and pure Fe powder as hetero-catalysts. Percentage of TOC removal and leached Fe after 20 min of the same assays for (e) Methyl Blue and (f) Rhodamine B.
Adapted from [75]

et al. [101] through synchrotron X-ray scattering spectra. These authors found a fast discoloration, up to 99%, of 200 mL of 10 mg L^{-1} of the azo dye Methyl Orange in 0.050 M Na_2SO_4 and 2 mM $FeCl_2{\cdot}4H_2O$ at pH 3.0 using a two-electrode reactor like Fig. 3a with a Pt anode and the synthesized cathode by applying an I = 30 mA during 90 min (see Table 3). Further research and direct evidence are needed to confirm their proposal that graphene with adsorbed O_2 and high-entropy oxide were the active sites responsible for H_2O_2 formation/activation. Inspired by the concept of a pH regulator, just like FeS_2 that controls the solution pH via reactions (29)-(31), immobilizing pH regulators on the functionalized cathode is a wise design. An interesting work by Li et al. [99] designed a tannic acid-Fe complex cathode (TFD|CF) in which H^+ was released from tannic acid to acidify the bulk. Moreover, TFD|CF acted as a hetero-EF catalyst as well. This explained the high efficiency (discoloration > 95%, 83.2% of COD removal, and EC_{COD} = 0.00298 kWh (g COD^{-1}) for the hetero-EF treatment of Methyl Orange and Methylene Blue using this cathode at neutral and even alkaline pH (see Table 3). More research seems necessary to understand the properties of the TFD|CF cathode, particularly due to the lack of data on the potential oxidation of tannic acid on it.

A $CoFe_2O_4$|CF cathode has been synthesized by the solvothermal method, where both $\equiv Co^{3+}/\equiv Co^{2+}$ and $\equiv Fe^{3+}/\equiv Fe^{2+}$ couples could offer electrons to activate H_2O_2 and more importantly, to avoid the aggregation of spherical $CoFe_2O_4$ nanoparticles when coated on CF [102]. Fig. 12a presents a sketch of the degradation mechanism of the azo dye Tartrazine (see the chemical formula in Fig. 1) by hetero-EF with a two-electrode reactor like of Fig. 3a containing a Ti|Pt anode and such cathode, where the production of heterogeneous $^{\bullet}OH$ from the above two couples is illustrated. Fig. 12b depicts the influence of the anion over the discoloration of 250 mL of 50 mg L^{-1} of the dye in pure water with 0.050 M of each electrolyte at pH = 3.0 using the above system at j = 8.33 mA cm^{-2} for 40 min. As can be seen, the percentage of color removal decreased in the sequence: SO_4^{2-} (97%) > Cl^- (84%) > NO_3^- (78%, from NO_2^- formed at the cathode) > HCO_3^- (26%) > HPO_4^{2-} (4.9%), denoting the relative chelating power of the ions with both active redox couples. Another series of trials was made by adding

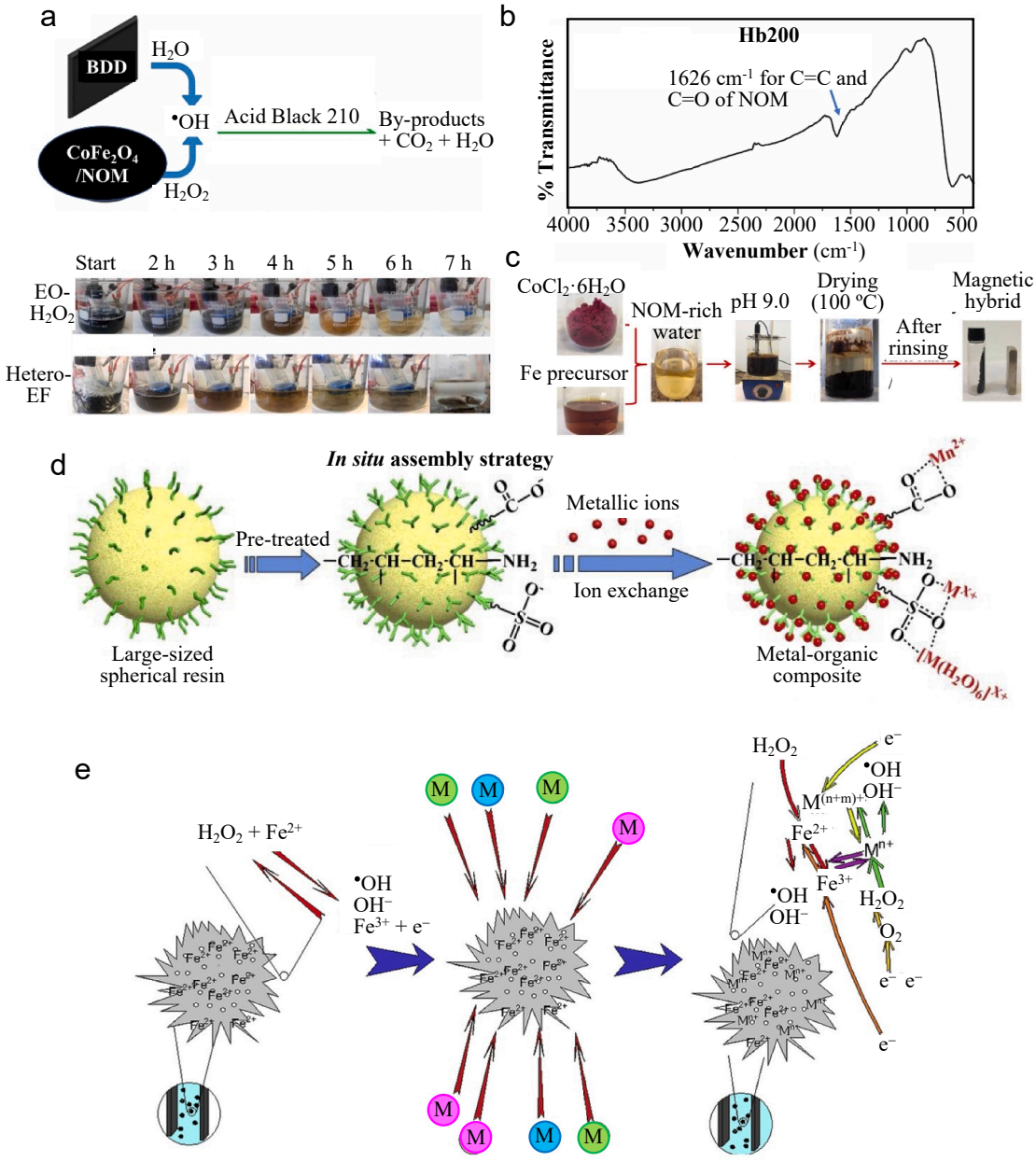

Fig. 11. (a) Electrochemical performance of Acid Black 210 solutions treated by EO-H_2O_2 and hetero-EF with an HB200 catalyst and (b) FTIR spectrum of the catalyst (adapted from [80]). (c) Diagram of the synthesis process of the magnetic hybrid material from iron mine wastes (adapted from [81)]). (d) Schematic illustration of in-situ assembling spherical Mn-based metal–organic composites prepared by ion exchange strategy (adapted from [93]). (e) Fe-based nanocatalysts preparation derived from ZSM-5 nanozeolite where M denotes Cu, Co, or Cr ions (adapted from [78]).

scavengers like of p-benzoquinone (p-BQ), furfuril alcohol (FFA), *tert*-butyl alcohol (TBA), and N_2 bubbling on the above solution with SO_4^{2-} electrolyte. From the data of Fig. 12c, apart from $^{\bullet}OH$, other species like $O_2^{\bullet-}$ and $^1O_2$ were inferred as reactive oxygen species in the degradation process (see Table 3). Under the attack of such oxidizing agents, both C-N and azo bonds of Tartrazine were broken down coupled with desulfonation reactions. Fig. 12d shows that the primary intermediates **2**–**4** were initially formed, which were subsequently oxidized to compounds **5**–**7** to be finally mineralized. They concluded that the degradation evolved at the surface catalysis confined to the solid–liquid surface and the lack of released Co and Fe excluded the involvement of homogenous reactions in the bulk. In fact, the absence of Co and Fe leaching from $CoFe_2O_4$ in an acid medium has been widely reported previously [115,116].

Barhoum et al. [105] reported the synthesis of a free-standing N-doped-carbon nanofiber (CNF)–Co|CoO_x cathode by the following steps: electrospinning of PAN/cobalt acetate solution, thermal peroxidation under air, and pyrolysis. The as-material was composed of (1 1 1) face-cantered cubic crystal structure of CoO_x (~15 nm), homogeneously distributed on the CNF surface, as deduced from the HR-TEM analysis, selected area electron diffraction (SAED) patterns, and elemental mapping images shown in Fig. 13a-d. Discoloration and mineralization trials were made with a solution with 0.1 mM Acid Orange 7 and 0.050 M Na_2SO_4 in pure water at pH = 3.0 and 25 °C filling a two-electrode tank reactor like of Fig. 3a with a Pt anode and the synthesized cathodes at j = 10 mA cm^{-2} lasting 40 min. Fig. 13e and f make evident that the best cathode contained a 10 wt% Co (CNF-Co10), yielding a high 94% of normalized absorbance decay and 92.4% of TOC removal, superior to a

homo-EF process with raw CNF and 0.2 mM Fe^{2+}. The system maintained good performance at pH = 6.0, demonstrating its viability to operate with dyeing effluents at neutral pH.

5. Photoelectro-Fenton process of dyes

PEF is a hybrid process that combines EF treatment and light irradiation. Depending on the homogeneous or heterogeneous catalyst checked, it can be classified as homo-PEF and hetero-PEF, respectively. The kind and intensity of irradiated light on the treated solution are key factors in this EAOP. Artificial lamps of ultraviolet C (UVC, λ = 100–280 nm) and ultraviolet A (UVA, λ = 215–400 nm) and light-emitting diodes (LED) are typically used. Alternatively, solar irradiation (λ > 300 nm) can be applied, directly as free and renewable sunlight or simulated with a Xe lamp with a similar radiation spectrum. In this case, the homo-SPEF and hetero-SPEF processes are tested.

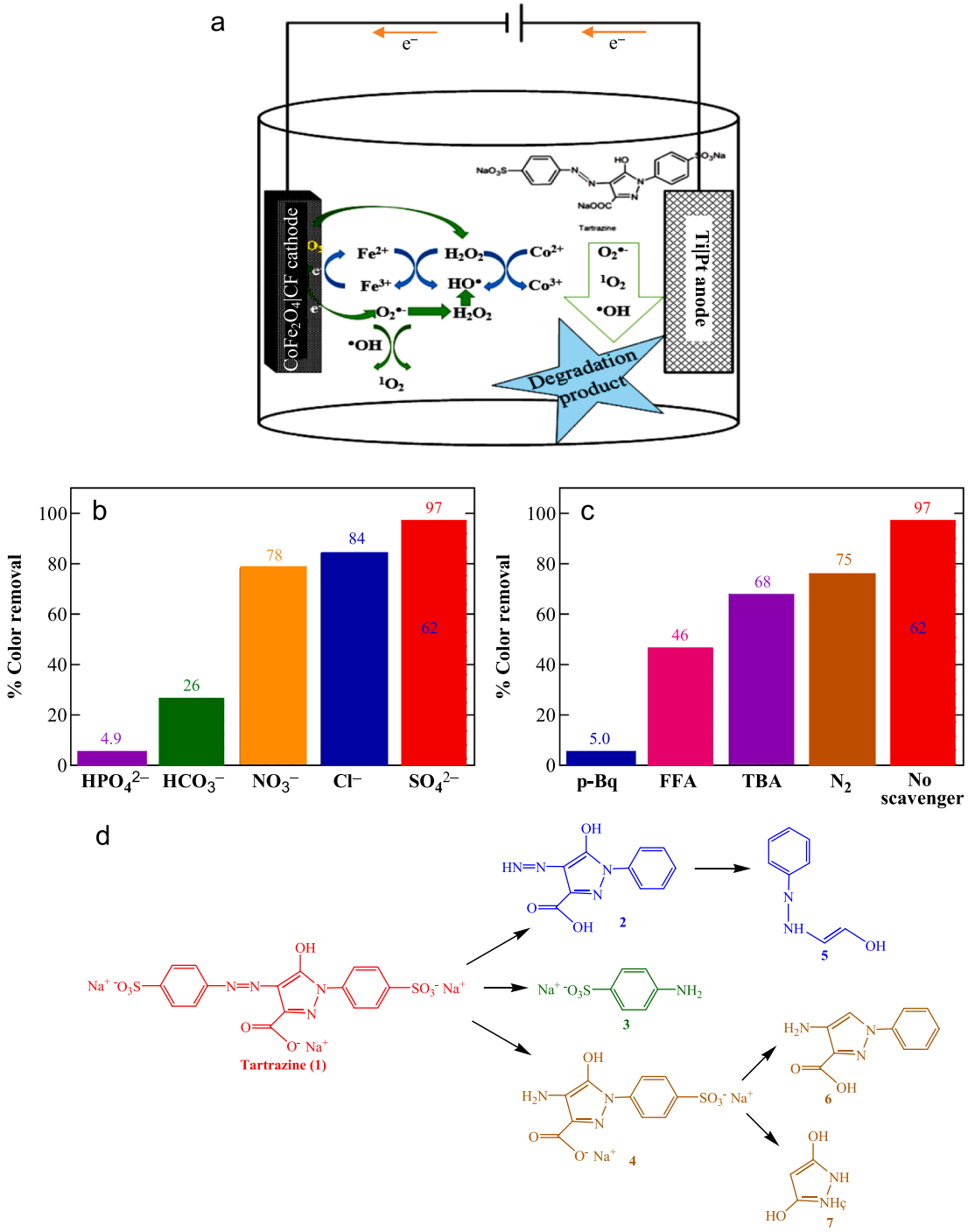

Fig. 12. (a) Sketch of the degradation mechanism of the azo dye Tartrazine by hetero-EF with a two-electrode reactor like of Fig. 3a equipped with a Ti|Pt anode and a $CoFe_2O_4$|CF cathode. (b) Percent of color removal after 40 min of electrolysis of 250 mL of 50 mg L^{-1} of this dye in pure water with 0.050 M of different electrolytes at pH = 3.0 using the above system at j = 8.33 mA cm^{-2}. (c) Effect of p-benzoquinone (p-BQ), furfuryl alcohol (FFA), *tert*-butyl alcohol (TBA), and N_2 bubbling on the percent of color removal of the assay with SO_4^{2-}electrolyte. (d) Proposed reaction sequence for the initial degradation of tartrazine (1).
Adapted from [102]

5.1. Homogeneous process

The greater number of articles dealing with dyes removal focus on homo-PEF with the treatment of solutions with the dyes Rhodamine B [117] with UVC light, as well as Blue BR, Violet SBL or Brown MF [118], Ponceau SS [119], Acid Orange 7 [120], Reactive Blue 4 [121], Chocolate Brown HT and Eriochrome Black [122], Reactive Black 5 [123], Methyl Orange [124,125], Bismark Brown G, Bismark Brown R, and Brown DGI [126], Brown HT [127], Direct Red 23 [128], and Acid Red 1 [129] with UVA light. Other articles considered the homo-SPEF process of the dyes Tartrazine, Ponceau SS, and Direct Blue 71 [130], Acid Blue 29 [131,132], Acid Orange 7 [133], and Erythrosine B [134]. The discoloration of a water machine effluent with dyes by homo-PEF has been reported by dos Santos et al. [135]. Table 4 summarizes the best results selected from the above publications.

A faster degradation and mineralization of dyes by homo-PEF or homo-SPEF than homo-EF is expected due to the acceleration of Fenton's reaction (1) by the extra Fe^{2+} regeneration from: (i) $Fe(OH)^{2+}$ photoreduction with additional $^{\bullet}OH$ production by photo-Fenton reaction (39) and (ii) photolysis of final Fe(III)-carboxylate complexes by the general reaction (40) [7,17]. The photodecarboxylation of these complexes also largely upgrades the mineralization process. When an UVC

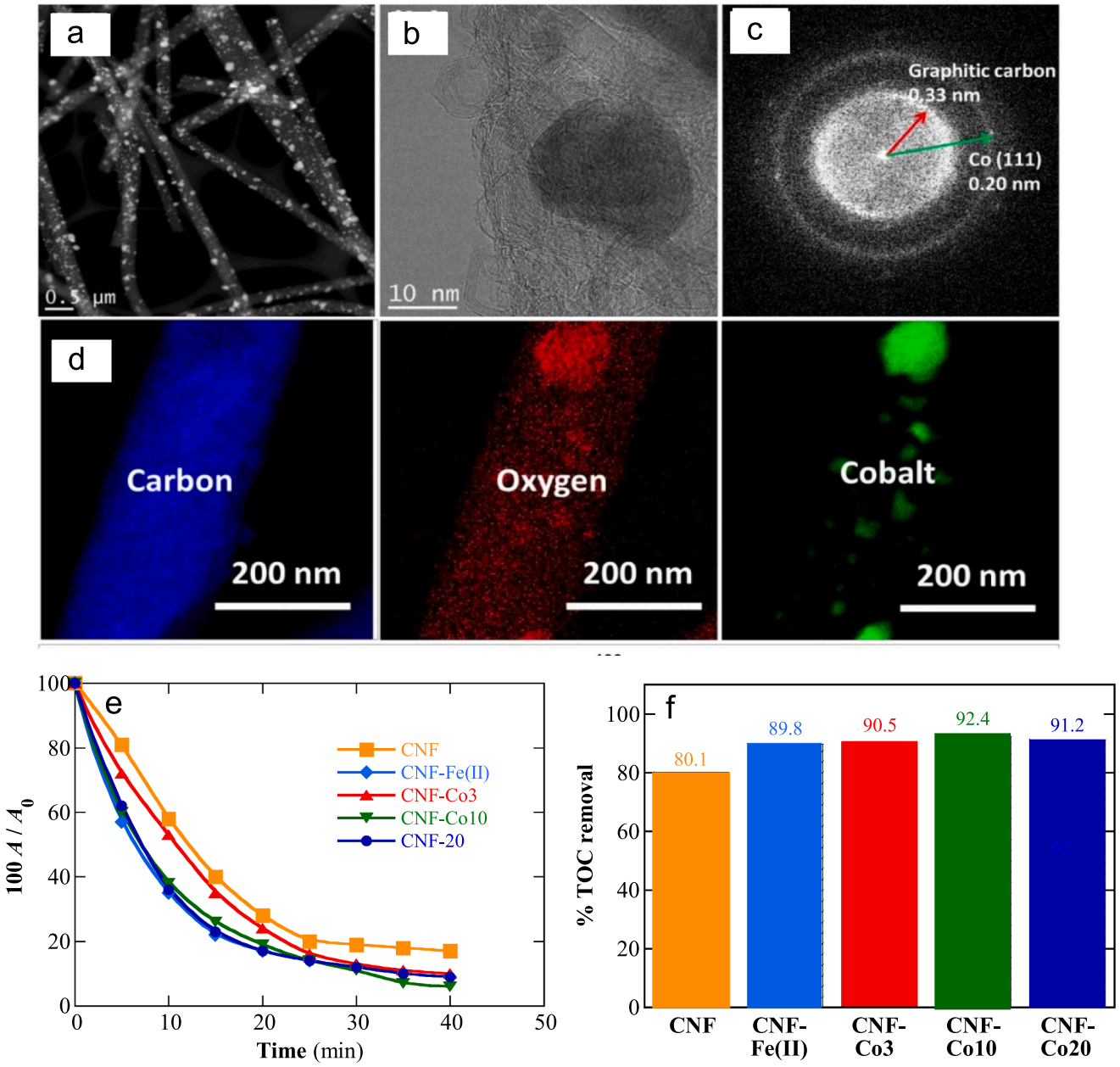

Fig. 13. High-resolution transmission electron microscopy (HR-TEM) analysis of the N-doped-CNF-Co|CoO_x (nitrogen-doped carbon nanofiber (CNF) electrodes incorporating Co|CoO_x NPs): (a) low magnification and (b) high magnification micrographs, (c) selected area electron diffraction (SAED) patterns, and (d) TEM with elemental mapping. Influence of the cathode material without and with 3%, 10%, and 20%wt%. of Co in the CNF electrode on the percentage of (e) normalized absorbance and (f) TOC removal after 40 min of electrolysis of a solution with 0.1 mM Acid Orange 7 and 0.050 M Na_2SO_4 in pure water at pH = 3.0 and 25 °C using a two-electrode tank reactor like of Fig. 3a with a Pt anode at j = 10 mA cm^{-2}. The CNF-Fe(II) treatment corresponds to a homo-EF process with raw CNF in the presence of 0.20 mM Fe^{2+}.
Adapted from [105]

Table 4
Selected results obtained for the photoelectro-Fenton (PEF) and solar PEF (SPEF) processes of synthetic organic dyes from wastewaters using undivided cells.

Dye	System (anode/cathode) light irradiation	Experimental remarks	Best results	Ref.
Homo-PEF				
Rhodamine B	Flow-through two-electrode reactor with a plane photoreactor (DSA/carbon-PTFE|GF) 5 W UVC light	500 mL of 0.02–0.16 mM of dye in pure water, 0.050 M Na_2SO_4, 0.10–0.40 mM Fe^{2+}, [EDTA]:[Fe^{2+}] from 0.5:1 to 4:1, pH 3.0–10–0, air flow rate = 20–80 mL min^{-1}, liquid flow rate = 7.0–35 mL min^{-1}, I = 20–100 mA, 60 min	At pH = 3.0 for 0.02 mM dye with 0.20 mM Fe^{2+}, [EDTA]:[Fe^{2+}] = 1:1, air flow rate = 20 mL min^{-1}, liquid flow rate = 7.0 mL min^{-1}, and 50 mA, 96% discoloration with k_{dis} = 0.083 min^{-1}. At pH = 7.0, 87% discoloration with k_{dis} = 0.033 min^{-1}. and in the absence of EDTA, 80% discoloration with k_{dis} = 0.025 min^{-1}. Large effect of isopropanol as radical scavenger. Overall removal of EDTA at pH 7.0	[117]
Blue BR Violet SBL Brown MF	Two-electrode tank reactor (BDD/BDD) 75 mW cm^{-2} UVA light	500 mL of 50 mg L^{-1} of each dye in pure water, 0.050 M Na_2SO_4, 0.50 mM Fe^{2+}, pH 3.0, air bubbling, j = 2–18 mA cm^{-2}, 60 min	Faster discoloration at higher j. For a mixture with the same dye content, discoloration at j = 18 mA cm^{-2}: 65% for EO-H_2O_2 < 100% in 50 min for homo-EF < 100% in 30 min for homo-PEF	[118]
Ponceau SS	Flow pre-pilot plant with a two-electrode reactor and a planar photoreactor (Pt or BDD/carbon-PTFE GDE) 160 W UVA light	2.5 L of 0.19 mM of dye in pure water, 0.050 M Na_2SO_4, 0.50 mM Fe^{2+}, pH 3.0, cathode fed with 400 mL min^{-1} of air, liquid flow rate = 200 L h^{-1}, 35 °C, j = 25–100 mA cm^{-2}, 360 min	Higher discoloration and mineralization for BDD than Pt, at higher j, and in the order: EO-H_2O_2 < homo-EF < homo-PEF. For the latter process with BDD at 100 mA cm^{-2}, k_{dis} = 0.087 min^{-1}, 98% TOC decay, MCE = 9.0%, and $EC_{TOC,total}$ = 10.4 kWh (g TOC)$^{-1}$. Five aromatic derivatives detected by GC–MS and four final carboxylic acids quantified by ion-exclusion HPLC	[119]
Methyl Orange	Flow plant with a two-electrode reactor and an acrylic reservoir photoreactor (DSA/carbon-PTFE|GF GDE) 15 W UVA light	2 L of 20–50 mg L^{-1} of TOC of the dye in pure water, 0.050 M Na_2SO_4, 0.50 mM Fe^{2+}, pH 3.0, cathode fed with air at 3 psi, liquid flow rate = 0.5–2.0 L min^{-1}, 25 °C, j = 10–25 mA cm^{-2}, 60 min	Greater discoloration and mineralization at higher j and liquid flow rate. For homo-PEF with 30 mg L^{-1} of TOC of the dye, 2.0 L min^{-1}, and 25 mA cm^{-2}, k_{dis} = 0.013 min^{-1}, 84% TOC decay, and $EC_{TOC,total}$ = 1.70 kWh (g TOC)$^{-1}$. Quantification of final carboxylic acids by ion-exclusion HPLC	[125]
Direct Red 23	Two-electrode tank reactor (BDD/CF) UVA LED 400 nm	230 mL of 80 mg L^{-1} of dye in pure water, 0.050 M Na_2SO_4 and/or 0.100 M NaCl, 0.10 mM Fe^{2+}, pH 3.0, 20 °C, cathode fed with air at 8.9 kPa, j = 20 mA cm^{-2}, 360 min	Better results for 75% Na_2SO_4 + 25% NaCl. For this mixture, k_{dis} (h^{-1}), TOC removal, MCE, and EC_{TOC} (kWh (g TOC)$^{-1}$): 0.72, 89%, 7.5%, and 2.05 for EO-H_2O_2, 0.84, 97%, 8.4%, and 1,46 for homo-EF, and 1.02, 100%, 17%, and 1.29 for homo-PEF	[128]
Homo-PEF-like				
Acid Red 1	Flow pre-pilot plant with a two-electrode FM01-LC reactor and a CPC photoreactor (DSA/stainless steel) 15 W UVA light or direct sunlight	6 L of 0.096–0.385 mM of dye in pure water, 0.025 M Na_2SO_4 + 0.035 M NaCl, 0–0.50 mM Fe^{2+}, pH 3.0, liquid flow rate = 3.2 L min^{-1}, j = 5–20 mA cm^{-2}, 480 min	Better performance with higher dye content and j, and using homo-SPEF-like < homo-SPEF-like < EO-HClO < homo-EF-like, For homo-SPEF-like with 0.196 mM dye and 0.40 mM Fe^{2+} at 15 mA cm^{-2}, total color removal in 180 min, 74% COD removal, ACE = 25%, EC_{COD} = 0.076 kWh (g COD)$^{-1}$. Detection of final carboxylic acids by ion-exclusion HPLC	[129]
Homo-SPEF				
Acid Blue 29	Two-electrode tank reactor (BDD, Pt, or Ti|RuO_2/carbon-PTFE GDE) direct sunlight	130 mL of 118 mg L^{-1} of dye in pure water, 0.050 M Na_2SO_4, 0.50 mM Fe^{2+}, pH 3.0, cathode fed with 300 mL min^{-1} of air, 35 °C, j = 33.3–100 mA cm^{-2}, 360 min	H_2O_2 accumulated in 180 min with increasing j: 432–875 mg L^{-1} for EO-H_2O_2, 152–317 mg L^{-1} for homo-EF, and 85–198 mg L^{-1} for homo-SPEF. Discoloration and COD decay increasing as EO-H_2O_2, < homo-EF < homo-SPEF. For the latter, k_{dis} (min^{-1}), COD removal, ACE, and EC_{COD} (kwh (g COD)$^{-1}$): 0.153, 100%, 22.1%, and 0.103 for BDD > 0.108, 96%, 18.8%, and 0.115 for Pt > 0.076, 94%, 16.9%, and 0.087 for Ti|RuO_2. Final carboxylic acids quantified by ion-exclusion HPLC	[131]
Acid Blue 29	Solar flow pre-pilot plant with a two-electrode reactor and a solar CPC [a] photoreactor (DSA/carbon-PTFE GDE) direct sunlight	10 L of 233.5 mg L^{-1} of dye in pure water, 0.050 M Na_2SO_4, 0.50 mM Fe^{2+}, pH 3.0, 35 °C, cathode fed with air, liquid flow rate = 150 L h^{-1}, solar irradiation from 600 to 1240 mW cm^{-2}, j = 25 and 50 mA cm^{-2}, 300 min	Faster discoloration and mineralization at greater solar irradiation and for 50 mA cm^{-2} in the order: EO-H_2O_2 < homo-EF < homo-SPEF. For the latter process at 1240 mW cm^{-2} of solar irradiation and 25 mA cm^{-2}, 100% of color removal, 100% of TOC decay, and EC_{TOC} = 0.057 kWh (g TOC)$^{-1}$. Thirteen aromatic derivatives detected by LC-MS/MS and seven final carboxylic acids quantified by ion-exclusion HPLC	[132]
Acid Orange 7	Two-electrode tank reactor (BDD/$WO_{2.72}$|C GDE) UVC (for homo-PEF) or Xe (for homo-SPEF) lamp	350 mL of 0.260 mM of dye in pure water, 0.10 M K_2SO_4, 0.50 mM Fe^{2+}, pH 3.0, cathode fed with air at 0.2 bar, 20 °C, j = 100–200 mA cm^{-2}, 360 min	CE ≈ 60% for H_2O_2 generation at 100 mA cm^{-2} for EO-H_2O_2. Discoloration, dye content decay, and TOC removal increased with increasing j in the order: EO-H_2O_2 < homo-EF < homo-PEF ≈ homo-SPEF. For the two latter processes at 150 mA cm^{-2}, k_{dis} = 0.041–0.044 min^{-1}, 90% TOC abatement, and MCE = 7.5%. Final carboxylic acids quantified by ion-exclusion HPLC	[133]

(*continued on next page*)

Table 4 (*continued*)

Dye	System (anode/cathode) light irradiation	Experimental remarks	Best results	Ref.
Erythrosine B	Two-electrode tank reactor (BDD/CF) 100 W UVA light or direct sunlight	300 mL of 100 mg L^{-1} of dye in pure water, 0.050 M Na_2SO_4, 0.10 mM Fe^{2+}, pH 3.0, air flow rate = 3 L min^{-1}, j = 2.5–15 mA cm^{-2}, 120 min	Discoloration, COD removal, ACE, and EC (kWh m^{-3}): 100% in 50 min, 90%, 10%, and 21 for homo-EF, 100%, 100% 14%, and 516[b] for homo-PEF, and 100%. 100%, 13%, and 21 for homo-SPEF	[134]
Hetero-PEF				
Sunset Yellow	Two-electrode tank reactor (Pt/GDE) UVA light	350 mL of 100 mg L^{-1} of dye in pure water, 0.10 M Na_2SO_4 or 0.13 M NaCl, 0.25 g of Fe_3O_4 as catalyst, pH 3.0, O_2 gas bubbled at 0.2 bar, 20 °C, I = 100 mA, 90 min	Discoloration in Na_2SO_4: 55% by hetero-EF and 78% by hetero-PEF in 90 min. Total color removal in 15 min for both processes with NaCl. TOC removal, MCE. and EC_{TOC} (kWh (g TOC)$^{-1}$) for hetero-SPEF: 49%, 48%, and 1.90 for Na_2SO_4, and 50%, 57%, and 1.70 with NaCl. Good reusability of catalyst after 8 consecutive cycles by hetero-PEF with Na_2SO_4	[137]
Hetero-SPEF				
Ponceau SS	Two-electrode tank reactor (BDD/carbon-PTFE GDE) 6 W UVA light or direct sunlight	130 mL of 0.075–0.225 mM of dye in pure water, 0.050 M Na_2SO_4, 0.018 mM Fe^{2+} or 0.25–2.0 g L^{-1} sodium vermiculite as catalyst, pH 3.0, cathode fed with 400 mL min^{-1} of air, 25 °C, j = 16.6–66.6 mA cm^{-2}, 360 min	Discoloration and TOC removal increased as EO-H_2O_2 < homo-EF (Fe^{2+}) < hetero-EF (sodium vermiculite) < hetero-PEF < hetero-SPEF. For hetero-PEF, higher percentage of color removal with smaller dye concentration and higher sodium vermiculite content and j. For hetero-SPEF with 0.150 mM dye, 1.0 g L^{-1} sodium vermiculite, and 33.3 mA cm^{-2}: k_{dis} = 0.914 min^{-1}, 84% TOC decay, and MCE = 6.7%. Final carboxylic acids quantified by ion-exclusion HPLC	[139]

[a] CPC: Compound parabolic collector.
[b] Value for $EC_{,total}$ (including the electrical power of the lamp).

light is used, organics can be directly photolyzed and H_2O_2 decomposed to $^{\bullet}OH$ via reaction (41) [7].

$$Fe(OH)^{2+} + h\nu \rightarrow Fe^{2+} + {}^{\bullet}OH \quad (39)$$

$$Fe(OOCR)^{2+} + h\nu \rightarrow Fe^{2+} + CO_2 + R^{\bullet} \quad (40)$$

$$H_2O_2 + h\nu \rightarrow 2{}^{\bullet}OH \quad (41)$$

The homo-PEF results of Table 4 illustrate that the optimum pH was 3.0, as in the case of homo-EF, indicating that the oxidation was governed by the homogeneous $^{\bullet}OH$ formed from Fenton's reaction (1). The discoloration of dye solutions was slightly faster in homo-PEF because of the additional generation of these radicals from the photolytic reaction (39). A similar effect of the kind of anode, electrolyte composition, applied j or E_{cat}, and Fe^{2+} and dye contents on the homo-PEF performance was determined. Raw and modified carbonaceous cathodes, as well as GDE, were used in this method, as can be seen in Table 4.

It is noticeable the work of Zhang et al. [117] using the chelating agent EDTA to stabilize Fe^{2+} in different ratios between 0.5:1 and 4:1. They studied the behavior of many operating variables with 500 mL of 0.02–0.16 mM of Rhodamine B in 0.050 M Na_2SO_4 and 0.10–0.40 mM Fe^{2+} in pure water at pH 3.0–10–0. The system was composed of a flow-through two-electrode reactor with a perforated DSA anode and a carbon-PTFE|GF cathode by applying an I = 20–100 mA, connected with a plane photoreactor illuminated with 5 W UVC light. The solution was recirculated at 7.0–35 mL min^{-1} and H_2O_2 was electrogenerated by pumping an air flow rate = 20–80 mL min^{-1}. Fig. 14a schematizes the diagram of the flow-through cell and highlights the electrochemical, homo-EF, and photolytic reactions involved. The best conditions were obtained at pH = 3.0 for a solution with 0.02 mM dye, 0.20 mM Fe^{2+}, and 0.20 mM EDTA (i.e., [EDTA]:[Fe^{2+}] = 1:1), air flow rate = 20 mL min^{-1}, liquid flow rate = 7.0 mL min^{-1}, and I = 50 mA, where 96% discoloration was achieved with k_{dis} = 0.083 min^{-1} (see Table 4). Nevertheless, good degradation results were found at pH = 7.0 with 87% discoloration and k_{dis} = 0.033 min^{-1}, reaching lower discoloration of 80% with k_{dis} = 0.025 min^{-1} in the absence of EDTA, demonstrating the availability of the PEF system to operate at neutral pH. Fig. 14b and c show the increasing oxidation power obtained in the order: UV/Fe-EDTA (pH = 7.0) < homo-EF-EDTA (pH = 7.0) < homo-PEF (pH = 7.0) < homo-PEF-EDTA (pH = 7.0) < homo-PEF-EDTA (pH = 3.0), according to the increasing generation of homogeneous $^{\bullet}OH$ as the main oxidant. The oxidation of Rhodamine B in these processes competed with that of EDTA, and so, Fig. 14d depicts a raising destruction of the chelating agent in the same sequence, i.e., UV/Fe-EDTA (pH = 7.0) < homo-EF-EDTA (pH = 7.0) < homo-PEF-EDTA (pH = 7.0), The generation of $^{\bullet}OH$ was confirmed by the scavenging effect of isopropanol, as can be seen in Fig. 14e.

The effect of Cl^- in the homo-PEF process has been investigated by Titchou et al. [128] with the same BDD/CF cell and similar experimental conditions to their previous work over homo-EF (see ref. [21] in Table 2), but under irradiation of the solution with a UVA LED lamp at λ = 400 nm. Table 4 shows that the best conditions were obtained with a 75% of 0.050 M Na_2SO_4 + 25% of 0.100 M NaCl mixture by adding 0.10 mM Fe^{2+} at pH 3.0, 20 °C, and j = 20 mA cm^{-2}. The oxidation power of treatments increased in the sequence: EO-H_2O_2 < homo-EF < homo-PEF, with a great enhancement of the latter process due to the additional production of homogeneous $^{\bullet}OH$ by reaction (39), as well as reaction (42) between Fe^{2+} and HClO formed from reactions (23) and (24). Note that Cl^- is a scavenger of $^{\bullet}OH$ to form $Cl^{\bullet}$ that is oxidized again to yield HClO [128].

$$Fe^{2+} + HClO \rightarrow Fe^{3+} + {}^{\bullet}OH + Cl^- \quad (42)$$

Based on this reaction, Murrieta et al. [129] proposed homo-PEF-like and homo-SPEF-like processes in which homogeneous $^{\bullet}OH$ was only produced by reaction between Fe^{2+} and HClO without H_2O_2 generation, i.e., without Fenton process. The assays were carried out with a flow pre-pilot plant composed of an FM01-LC reactor with a DSA anode and a stainless-steel cathode connected with a compound parabolic collector (CPC) photoreactor exposed to a 15 W UVA light or direct sunlight. 6 L of solutions of 0.096–0.385 mM of the azo dye Acid Red 1 (see chemical structure in Fig. 1) with 0.025 M Na_2SO_4 + 0.035 M NaCl and 0–0.50 mM Fe^{2+}in pure water at pH 3.0 and recirculating at liquid flow rate = 3.2 L min^{-1} were electrolyzed at j = 5–20 mA cm^{-2}. Better performance was obtained with higher dye content and j, but up to 0.40 mM Fe^{2+}. Surprisingly, the percent of color removal decreased in the order: homo-EF-like > EO-HClO > homo-PEF-like > homo-SPEF-like (see Table 4). This trend can be observed in Fig. 15a for 0.192 mM dye with 0.40 mM Fe^{2+} at j = 15 mA cm^{-2}. In EO-HClO, M($^{\bullet}OH$) formed from reaction (6)

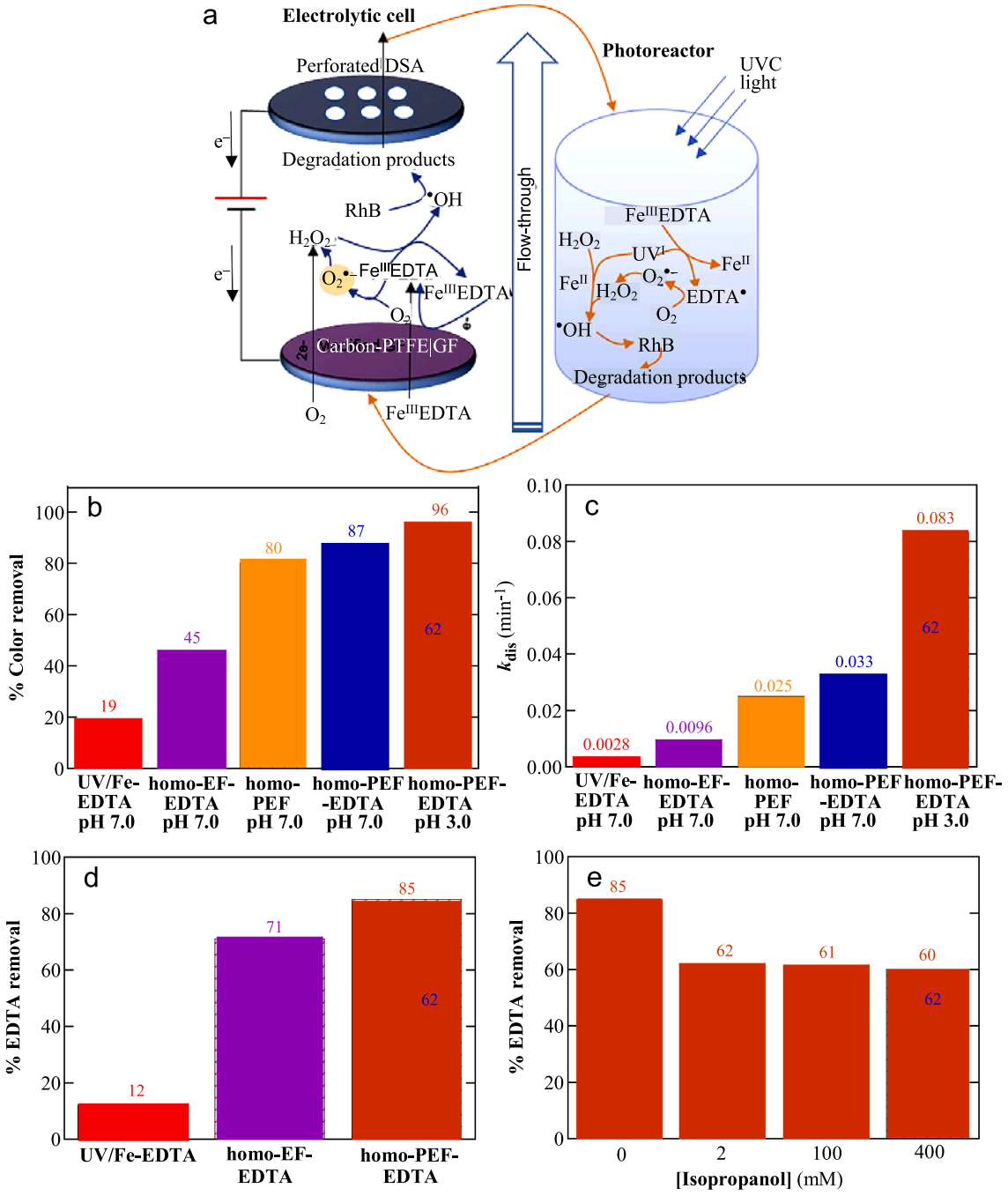

Fig. 14. (a) Schematic diagram of the flow-through two-electrode reactor with a plane photoreactor for the homo-photoelectro-Fenton (PEF)-EDTA treatment of Rhodamine B (RhB) including the electrochemical and photolytic reactions involved. A perforated DSA anode and a carbon-PTFE onto graphite felt cathode were used upon a 5 W UVC light and added EDTA as a chelating agent of Fe(III). (b) Percent of color removal and (c) the rate constant for discoloration after 60 min of different treatments of 500 mL of 0.02 mM dye with 0.050 M Na_2SO_4, 0.20 mM Fe^{2+}, and 0.20 mM EDTA in pure water at air flow rate = 20 mL min^{-1}, liquid flow rate = 7.0 mL min^{-1}, and I = 50 mA. (d) Percentage of EDTA removal in the above trials at pH = 7.0, and (e) effect of isopropanol content on the hetero-EF-EDTA process.
Adapted from [117]

and HClO generated from reactions (23) and (24) were the main oxidants leading to overall discoloration in about 60 min, whereas its oxidation process was slightly upgraded by homo-EF-like due to the extra formation of homogeneous •OH by reaction (42), maintained thanks to the continuous Fe^{2+} regeneration from Fe^{3+} reduction by reaction (7). The negative effect of UVA irradiation in homo-PEF-like can be attributed to the enhancement of Fe^{2+} regeneration from photo-Fenton reaction (39) that accelerates the homogeneous •OH removal by its parasitic reaction with Fe^{2+} via reaction (27). The higher intensity of sunlight irradiation explains the much slower discoloration found by homo-SPEF-like that needed practically 180 min to yield a colorless solution. In contrast, Fig. 15b highlights that faster COD removal was achieved for homo-PEF-like and homo-SPEF-like, achieving 70% and 74% at 480 min, respectively. The homo-SPEF-like treatment then presented a higher ACE = 25% (see Fig. 15c) and a lower EC_{COD} = 0.076 kWh (g COD)$^{-1}$ (see Fig. 15d). This behavior can be related to the quick photolysis of Fe(III) species formed, like complexes with final carboxylic acids that can be photodecarboxylated via reaction (40). This was

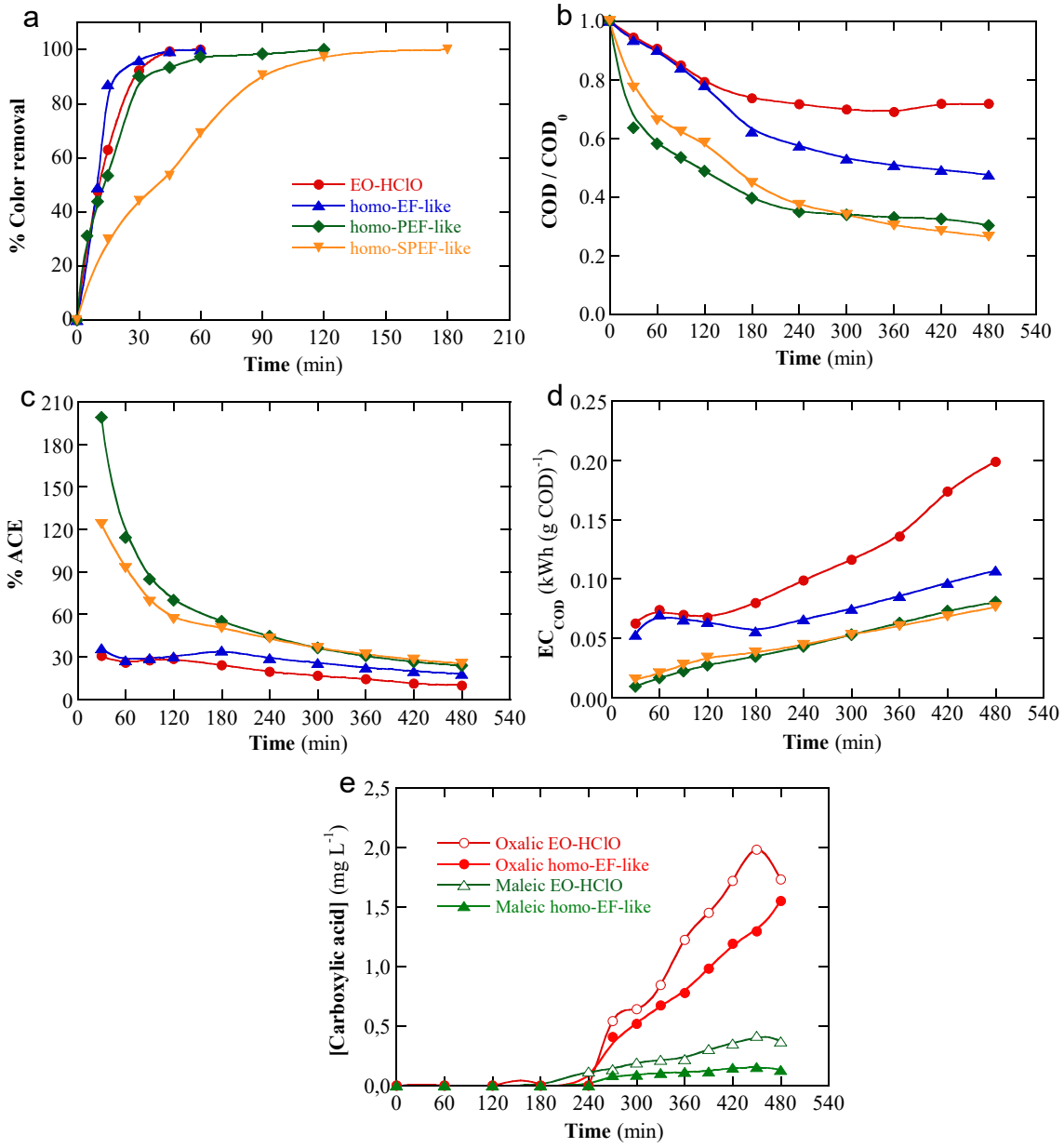

Fig. 15. (a) Percentage of color removal, (b) normalized COD, (c) average current efficiency, and (d) energy consumption per unit COD mass vs. time for the remediation of 6 L of 0.192 mM of the azo dye Acid Red 1 with 0.025 M Na_2SO_4 + 0.035 M NaCl in pure water at pH 3.0 by EO-H_2O_2, homo-EF-like, homo-PEF-like, and homo-SPEF-like using a flow pre-pilot plant with an FM01-LC reactor equipped with a DSA anode and a stainless steel cathode, and a compound parabolic collector (CPC) photoreactor under 15 W UVA light or direct sunlight, at liquid flow rate = 3.2 L min^{-1} and j = 15 mA cm^{-2}. The Fenton-based processes were made with 0.40 mM Fe^{2+}. (e) Time-course of the concentration of carboxylic acids detected in the above runs.
Adapted from [129]

confirmed by the detection of recalcitrant maleic and acetic acids only in the EO-HClO and homo-EF-like processes, as shown in Fig. 15e.

The homo-SPEF treatment has been performed in a synthetic sulfate medium at pH 3.0 with CF [134] and GDE [131,132] cathodes. In all these cases, Table 4 displays that the dyes solutions were more rapidly discolored and mineralized in the sequence: EO-H_2O_2 < homo-EF < homo-SPEF, being more potent with a BDD anode than Pt and a DSA like Ti|RuO_2. As an example, Fig. 16a presents a sketch of the solar flow pre-pilot plant with a DSA/GDE reactor and a solar CPC photoreactor used by Salazar et al. [132] for the treatment of 10 L of 233.5 mg L^{-1} of the azo dye Acid Blue 29 in 0.050 M Na_2SO_4 at pH = 3.0, 35 °C, and liquid flow rate = 150 L h^{-1} upon an average solar irradiation = 1240 mW cm^{-2}. Homo-EF and homo-SPEF ran after adding 0.50 mM Fe^{2+}. The variation of the percent of normalized absorbance and dye concentration with electrolysis time shown in Fig. 16b and 16c, respectively, make evident the superiority of homo-SPEF over homo-EF followed by EO-H_2O_2, with faster abatement at j = 50 mA cm^{-2} as compared with j = 25 mA cm^{-2} by the greater production of M(•OH) and homogeneous •OH, as pointed out above. For the homo-SPEF process, total discoloration and total dye removal were reached at 120 and 180 min for 50 and 25 mA cm^{-2}, respectively. Under these conditions, Fig. 16d depicts that overall mineralization was achieved after 300 min of electrolysis, whereas Fig. 16e illustrates that the smaller EC_{TOC} = 0.057 kWh (g TOC)$^{-1}$ was determined for the lower j = 25 mA cm^{-2} (see also Table 4), The authors detected 13 aromatic derivatives by LC-MS/MS and quantified the evolution of 7 final carboxylic acids by ion-exclusion HPLC. It was thus confirmed that total mineralization achieved by homo-SPEF was feasible by the total removal of all carboxylic

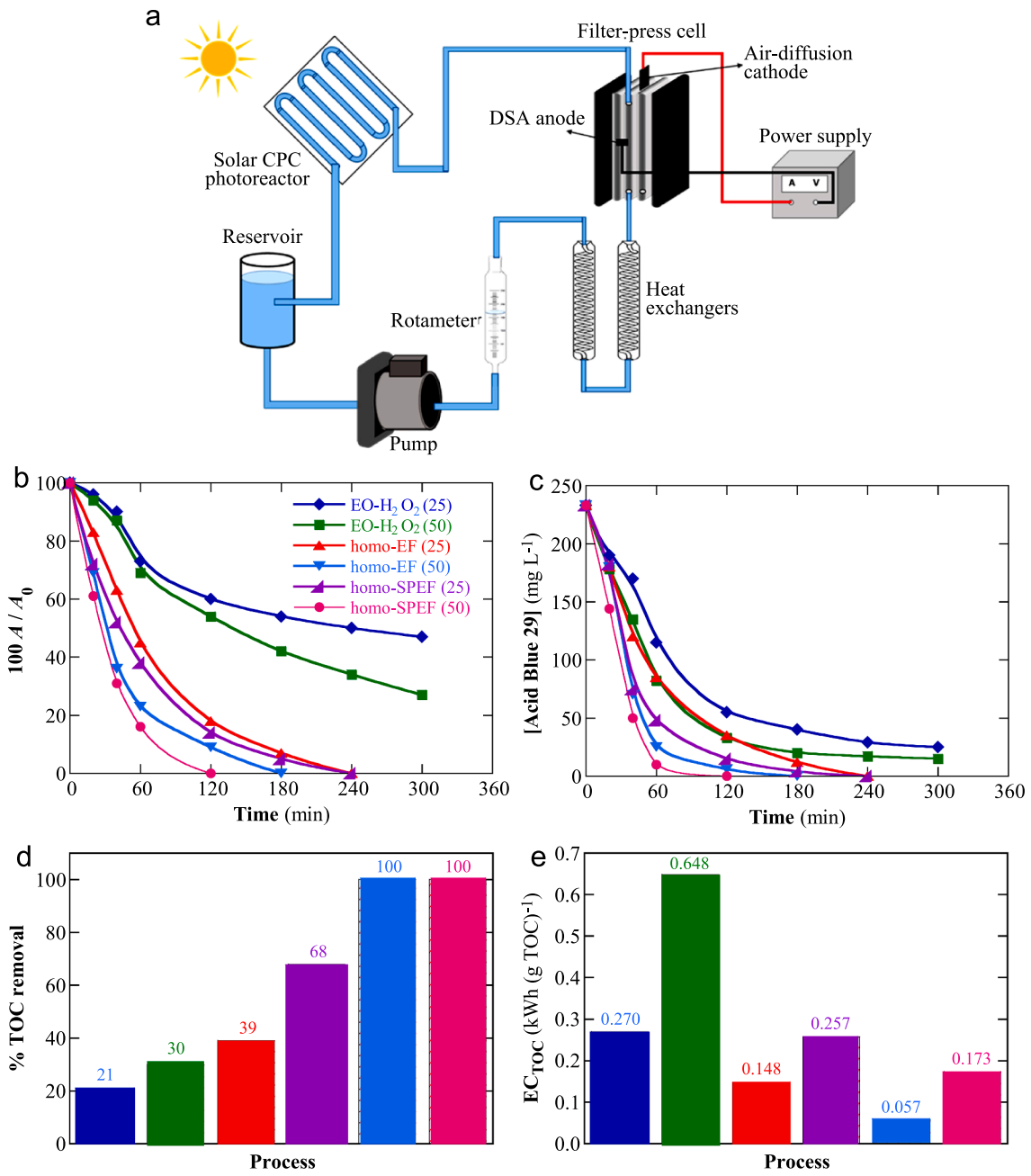

Fig. 16. (a) Sketch of the solar flow pre-pilot plant with a two-electrode reactor and a solar CPC photoreactor used for the homo-solar PEF (SPEF) process of the azo dye Acid Blue 29. The two-electrode reactor was a filter-press cell equipped with a DSA anode and a carbon-PTFE air-diffusion (GDE) cathode. (b) Percentage of normalized absorbance and (c) Acid Blue 29 concentration vs. time for the EO-H_2O_2, homo-EF and homo-SPEF treatments with the above pre-pilot plant at 25 and 50 mA cm^{-2} (stated the numbers in parenthesis) of 10 L of 233.5 mg L^{-1} of dye with 0.050 M Na_2SO_4 in pure water at pH = 3.0, 35 °C, liquid flow rate = 150 L h^{-1}, and solar irradiation = 1240 mW cm^{-2}. 0.50 mM Fe^{2+} were added for homo-EF and homo-SPEF. (d) Percentage of TOC removal and (e) energy cost per unit TOC mass after 300 min of the above assays.
Adapted from [132]

acids due to the fast photolysis of their Fe/III) complexes by reaction (40).

5.2. Heterogeneous process

Few articles have considered the remediation of dyes solutions by hetero-PEF with solid catalysts [136–138]. It is noticeable the work of Pinheiro et al. [137] who used a two-electrode tank reactor like of Fig. 3a with a Pt anode and a GDE cathode under UVA light to treat 350 mL of 100 mg L^{-1} of the azo dye Sunset Yellow in 0.10 M Na_2SO_4 or 0.13 M NaCl with 0.25 g of Fe_3O_4 as the catalyst at pH 3.0 and 20 °C by applying an I = 100 mA lasting 90 min. They found that Fe_3O_4 gave a low quantity of heterogeneous •OH from the heterogeneous Fenton's reaction (28) to destroy the dye in front of the high amount of active chlorine formed from reactions (23) and (24). So, total discoloration was obtained after 15 min of hetero-EF and hetero-SPEF in 0.13 M NaCl, whereas these processes were much slower in 0.10 M Na_2SO_4, with 55% and 78% color removal, respectively (see Table 4). In contrast, similar TOC decay and MCE and EC_{TOC} values were found for the hetero-SPEF in both media at 90 min (see Table 4). This points to an effective formation of heterogeneous •OH from Fe_3O_4 for the simultaneous non-selective removal of the dye and its by-products. This means that the attack of

active chlorine over the dye was much more selective, thus yielding a much quicker discoloration. The authors find a good reusability of the catalyst after 8 consecutive cycles by hetero-PEF with Na_2SO_4, corroborating its practical application.

dos Santos et al. [139] proposed the mineral sodium vermiculite as a solid catalyst for the hetero-SPEF remediation of 130 mL of 0.075–0.225 mM of the diazo dye Ponceau SS (see chemical structure in Fig. 1) in 0.050 M Na_2SO_4, at pH 3.0, and 25 °C. The catalysts used were 0.018 mM Fe^{2+} for homo-EF or 0.25–2.0 g L^{-1} sodium vermiculite for hetero-EF, hetero-PEF, and hetero-SPEF. The electrolytic system was a two-electrode tank reactor like of Fig. 3a with a BDD anode and a carbon-PTFE GDE cathode fed with 400 mL min^{-1} of air by applying a j = 16.6–66.6 mA cm^{-2} upon illumination with a 6 W UVA light or direct sunlight. Fig. 17 shows the best results obtained for 0.150 mM dye, 1.0 g L^{-1} of sodium vermiculite, and j = 33.3 mA cm^{-2}. From Fig. 17a, one can infer an enhancement of the percentage of color removal as: EO-H_2O_2 < homo-EF < hetero-EF < hetero-PEF < hetero-SPEF, indicating a greater oxidation power of the heterogeneous $^{\bullet}OH$ formed at the sodium vermiculite surface than homogeneous $^{\bullet}OH$ proceeding from Fe^{2+}. Total loss of color with k_{dis} = 0.914 min^{-1} was achieved after 300 min of hetero-SPEF (see Table 4). This process also yielded quicker TOC removal, up to 84% at 360 min (see Fig. 17b), with the higher MCE = 6.6% (see Fig. 17c). The partial mineralization attained can be attributed to the incomplete removal of the final carboxylic acids since their complexes with the surface ≡Fe(III) were more slowly photodecarboxylated than those with soluble Fe(III). Fig. 17d illustrates the presence of large amounts of tartronic, malic, oxamic, and oxalic acids in the final solution of hetero-SPEF, preventing their total mineralization.

6. Combined processes

Several combined treatments of EF and PEF have been proposed to upgrade the removal of dyes in waters. They include MFCs, other hybrid processes, and sequential treatments, which will be detailed in this section. The best results obtained from selected works are listed in Table 5.

6.1. Microbial fuel cells

A reduced number of papers have described small MFCs as an electrical energy source and simultaneous EF destruction of dyes such as Methylene Blue (see chemical structure in Fig. 1) [140], Methyl Orange [141,142], Rhodamine B [142], Acid Orange G [143], and Reactive Black 5 [144].

The dual-chamber separated by a proton exchange membrane (PEM) with a carbon fiber anode and a carbon fiber|Fe-Mn-Mg cathode designed by Wang et al. [140] is schematized in Fig. 18a. Carbohydrate active enzymes acted in the anodic biofilms in an anaerobic environment enhancing the biofilm degradation and the electron transfer and yielding an excess of sludge, whereas the hetero-EF took place in the cathodic compartment filled with 30 mg L^{-1} of Methylene Blue in 0.10 M Na_2SO_4 at pH = 2.0–7.0, upon an air flow rate = 200–500 mL min^{-1}. An external resistance between 10 and 1000 Ω was used. The best results were determined at pH 3.0 after 480 min, where 93.5% discoloration and 27.5% COD removal were achieved with an external resistance = 100 Ω and air flow rate = 400 mL min^{-1} (see Table 5). This small MFC operated with an open circuit voltage = 0.96 V and power density =

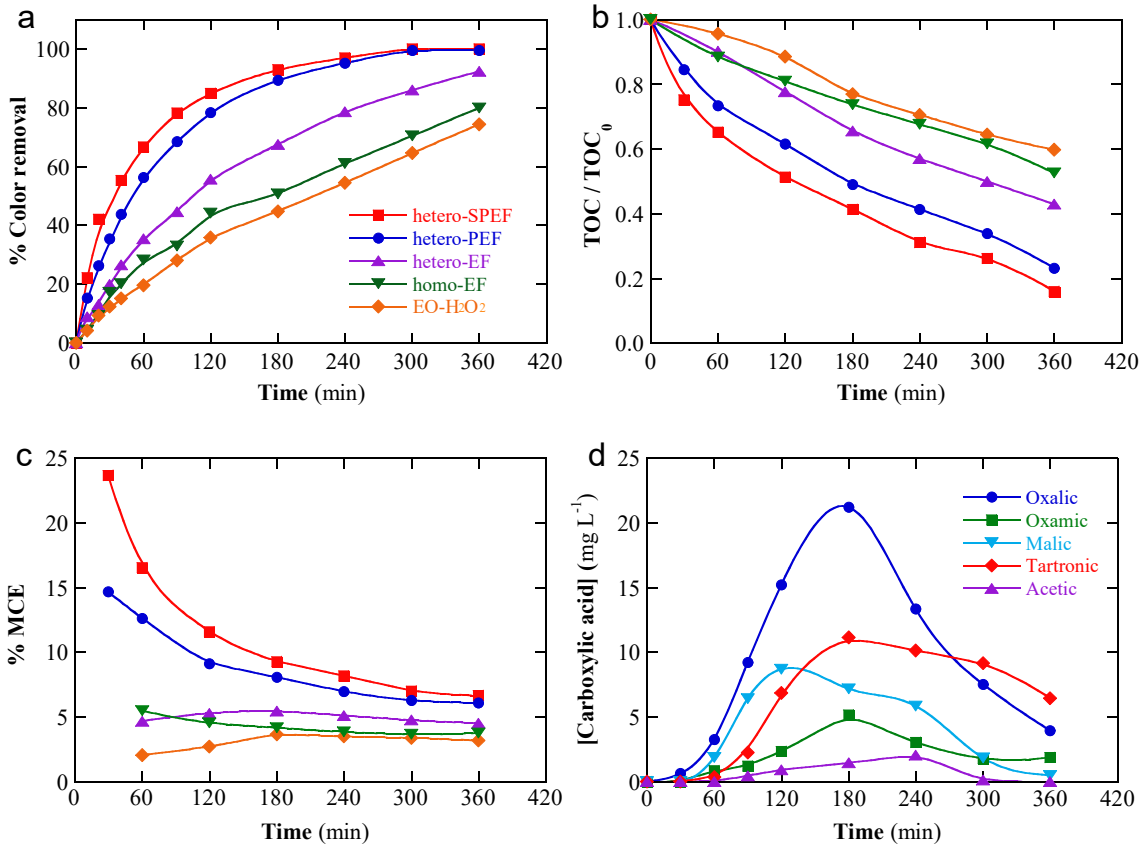

Fig. 17. Time course of the (a) percent of color removal, (b) normalized TOC, and (c) mineralization current efficiency for the EO-H_2O_2, homo-EF, hetero-EF, hetero-PEF, and hetero-SPEF treatments of 130 mL of 0150 mM of the diazo dye Ponceau SS with 0.050 M Na_2SO_4 in pure water at pH 3.0 and 25 °C using a two-electrode tank reactor with a BDD anode and a carbon-PTFE GDE cathode under 6 W UVA light or direct sunlight by applying a j = 33.3 mA cm^{-2}. The homo-EF process was carried out with 0.018 mM Fe^{2+}, whereas the hetero ones were made with 1.0 g L^{-1} sodium vermiculite as the catalyst. (d) Evolution of the concentration of carboxylic acids detected during the hetero-PEF assay.
Adapted from [139]

Table 5
Selected results reported for combined EF-based treatments of synthetic organic dyes from wastewaters.

Dye	System (anode/cathode)	Experimental remarks	Best results	Ref.
Microbial fuel cell (MFC)				
Methylene Blue	Dual-chamber with closed cylinder anodic and rectangular parallelepiped part separated by a PEM [a] (carbon fiber/carbon fiber|Fe-Mn-Mg)	Excess of sludge in the anodic chamber under an anaerobic environment. 30 mg L^{-1} dye in pure water, 0.10 M Na_2SO_4 in the cathodic-chamber, pH = 2.0–7.0, external resistance = 10–1000 Ω, air flow rate = 200–500 mL min^{-1}, 480 min	93.5% discoloration, and 27.5% COD removal for pH 3.0, external resistance = 100 Ω, and air flow rate = 400 mL min^{-1}. Open circuit voltage = 0.96 V and power density = 1.99 W m^{-3}, (Control: 0.81 V and 1.31 W m^{-3}). Thirteen aromatic derivatives identified by LC-MS. Generated oxidants detected by scavengers. Carbohydrate active enzymes on anodic biofilms enhanced biofilm degradation metabolism, reaction rate, and electron transfer	[140]
Rhodamine B Methyl Orange	Dual-chamber MFC powered double-cathode reactor (Pt/air–cathode and CF cathode). Air cathode for H_2O_2 generation and CF for cathodic iron reduction	50 mM of PBS served as anodic substrate containing 1 g L^{-1} $C_2H_3NaO_2$, 12.5 mL L^{-1} minerals, 5 mL L^{-1} vitamins. In cathodic-chamber, 14 mL of 40 or 74 mg L^{-1} of dye in pure water, 0.050 M Na_2SO_4, 0.50 mM Fe^{2+}, pH = 2.80, 25 °C, external resistor = 50–10000 Ω	64.5 mg L^{-1} of accumulated H_2O_2 with AC&G (1:5) [b] air cathode with CE = 49% from − 0.4 to − 1.2 V/Ag|AgCl in 60 min and j = 2.5 mA cm^{-2}. For CF cathode, 95.4% iron reduction in 20 min with rate constant of 0.11 min^{-1} at −0.8 V/Ag|AgCl. After 10 min of MFC-EF of 40 mg L^{-1} Rhodamine B: 97% discoloration and 98.2% TOC decay with MCE = 6.22%. Maximum power densities of 1.51, 1.11, and 0.66 W m^{-2} at − 0.8, − 0.6, and −0.4 V/Ag|AgCl. Six aromatic by-products detected via LC-MS and nine final carboxylic acids were quantified by HPLC	[142]
Acid Orange 7	Three systems: I. Single-chamber reactor for hetero-EF (Graphite/Fe@KSC [c]) II. Two-electrode AMEFS [d] (CB|SSM [e]/Fe@KSC-800) III. Single-electrode AMEFS (Fe@KSC-800/ Fe@KSC-800)	For system I: 28 mL of 13.35 mg L^{-1} dye in pure water, 5 g L^{-1} Na_2SO_4, 30 °C, E_{cat} from −0.5 -to + 0.2 V/Ag|AgCl, 24 h. For system II: 28 mL of anolyte with 50 mM PBS (pH = 7.0) containing vitamin and trace metal (0.31 g L^{-1} NH_4Cl, 0.13 g L^{-1} KCl, 3.04 g L^{-1} $NaH_2PO_4{\cdot}H_2O$, 10.923 g L^{-1} $Na_2HPO_4{\cdot}H_2O$, 12.5 mL L^{-1} mineral, and 12.5 mL L^{-1} vitamin) and 20 mM sodium acetate. E_{cat} = +0.2 V/Ag||AgCl for preselecting electroactive biofilms at CB/SSM. 28 mL of catholyte with 20–50 mg L^{-1} of dye in pure water, 5 g L^{-1} Na_2SO_4, load = 0–1000 Ω, 30 °C For system III: 28 mL of 20–50 mg L^{-1} dye in pure water, 50 mM PBS with vitamin, trace metal, 20 mM sodium acetate, 5 g L^{-1} Na_2SO_4, 30 °C, load = 0–1000 Ω, 24 h	For system I, 90% discoloration with Fe@KSC-800 cathode at −0.3 V and −0.5 V/Ag|AgCl, whereas only 30% discoloration for Fe@KSC-900. For system II, 96% discoloration for 13.5 mg L^{-1} dye in the absence of external resistance. Using the single-electrode AMEFS for system III, 98% discoloration for 13.5 mg L^{-1} dye in the absence of external resistance, quite stable after six cycles. Discoloration was 94–96% for 20–50 mg L^{-1} of dye.No need for extra addition of Fe^{2+} as Fenton catalyst and pH control using AMEFS, especially for the single-electrode one	[143]
Other hybrid processes				
Reactive Black 5	Self-power crossflow two-electrode cell integrated nanofiltration and EF process (Stainless-steel/ graphite paper) and NF270 membrane	20 mg L^{-1} of dye in pure water, 0.050 M Na_2SO_4, 0.20 mM Fe^{2+}, pH = 3.0, air flow rate = 5 mL min^{-1}, 120 min	Energy harvested from hydraulic pressure vibration into electrical energy via PENG [f] ceramic and used for EF. (219.6 V voltage at 20 psi pressure). 8.8% discoloration for rectified negative and positive wires imposed to electrode > 6.8% for alternating piezoelectricity > 4.5% for rectified positive and negative wires imposed to electrodes. The low performance of dye degradation mainly came from low H_2O_2 accumulation (2.65 mg L^{-1} after 120 min)	[146]
Amaranth	Dual-chamber photocatalytic fuel cell (PFC)/EF reactor with two identical chambers (C|ZnO/carbon) under 36 W UVA lamp/(Fe /carbon)	500 mL of 10 mg L^{-1} of dye in pure water, pH = 5.7 in PFC and pH = 3.0 in EF, 25 °C, external load = 1 kΩ, air flow rate = 1 L min^{-1}, 480 min. Four configurations with different number of cathodes and anodes so-called S1, S2, S3, and S4	Discoloration increased both in PFC and homo-EF with decreasing electrode distance. Better discoloration, 94.0% with k_{dis} = 0.3610 h^{-1} for PFC by S1 and 78.1% with k_{dis} = 0.2204 h^{-1} for EF by S2 at 2 cm electrode distance. Maximum power for S1 to S4 configurations; 25.3934 27.8347, 30.9602, and 38.7434 μW	[149]
Acid Orange 7 Real WWTP effluent	Cylindrical reactor for AC adsorption and EF system (porous carbon/porous carbon)	2.0 L of 10 mg L^{-1} dye in pure water or real WWTP effluent, 4 mM K_2SO_4, pH = 7.0, 20 °C, Fe(II) loaded resin = 2 g, liquid flow rate = 50 mL min^{-1}, j = 0–2.27 mA cm^{-2}, 60 min	3.5 and 6.6 mg L^{-1} of H_2O_2 accumulation in 60 min under air and O_2 saturation at 2.27 mA cm^{-2}, without granular AC and Fe(II) loaded resin. •OH concentration increased from 1 to 1.70 μM with 100% packing level of AC using Fe(II) loaded resin at j = 1.36 mA cm^{-2}. Discoloration of 59, 70, 80 and 83% in 90 min for j of 0.45, 0.90, 1.36 and 2.27 mA $cm^{-2,}$ in pure water. Lower (around 10%) for WWTP effluent with 35% AC packing level	[151]
Bright Blue FCP	Three compartments (C_1-C_3) connected in series used for AC adsorption and EF process (graphite cloth/graphite cloth)	100 mg L^{-1} of dye in pure water, 0.050 M Na_2SO_4, pH = 3.0, liquid flow rate = 30 mL min^{-1}, I = 0.5 A (E_{cell} = 8 V), 40 min.	Influence of AC pretreatment, AC source, particle distribution, and amount of iron loaded on resin over discoloration investigated	[152]

(*continued on next page*)

Table 5 (*continued*)

Dye	System (anode/cathode)	Experimental remarks	Best results	Ref.
		Resins in C_1 adjacent to the cathodic side of C_2 loaded with 0.25–2.5 mM Fe(II) and acid, whereas resins in C_3 loaded with Na^+	by response surface methodology. AC source was the most significant factor, followed by interaction of the AC source with other parameters. 98.4% of discoloration in 20 min of AC adsorption and 40 min of hetero-EF with 2.9 mg L^{-1} Fe loaded on resin. Cation exchange resins in C_1 and C_3 for delivering and retaining Fe and acid	
Acid Orange 7 Real wastewater from industry	Two-electrode reactor for electro-peroxone and ultrasound (EP/US) process (Pt/GF)	650 mL of 50 mg L^{-1} of dye in pure water, 0.010 M Na_2SO_4, pH = 3.0–9.0, air flow rate = 0.5 L min^{-1}, O_3 dosage = 15–41 mg L^{-1} (US power = 100 W), 0.50 mM Fe^{2+} for homo-EF comparison, I = 100–400 mA, 60 min	100% discoloration in 20 min with 88% mineralization at 60 min for EP/US at pH = 7.0 with 33 mg L^{-1} O_3 dosage and I = 300 mA > 68.5% for O_3/US > 49.8% for O_3. k_{dis} for EP/US with Na_2SO_4, NaCl, and $NaNO_3$: 0.276, 0.0696, and 0.0644 min^{-1}. 73% and 80 % discoloration for homo-EF and US/EF after 30 min of electrolysis. For the real wastewater, BOD_5/COD grew from 0.18 to 0.36 and 0.32 after 60 min of EP/US and EP	[153]
Orange G	Undivided dual-anode reactor for PEC/PEF process ($TiTiO_2$ anode and stainless steel anode/graphite) under 8 W UVA light	200 mL of 0.10 mM dye in pure water, 0.10 M Na_2SO_4, 0.10 mM $FeSO_4$, pH = 3.0–5.0, O_2 flow rate = 200 mL min^{-1}, 75 and 45 μA cm^{-2} on Ti|TiO_2 and stainless steel, radiation density = 0.33 mW cm^{-2}, 180 min	Discoloration followed the order: PC < PEC < PEC- 0.10 mM $FeSO_4$ < homo-EF < PEC/PEF with 99.8% decolorization at pH 3.0. The carbon oxidation state changed from −0.21 to + 2.03 after 7 h of PEC/PEF. 6 μM Fe^{2+} concentration needed in the PEC/PEF system as compared to 0.1–0.8 mM for the conventional Fenton or homo-EF	[156]
Indigo Carmine	Two-electrode tank reactor (Pt or TiO_2 NTs /air-diffusion cathode or stainless steel (AISI 304) sheet) upon 36-W UV LED	150 mL of 0.260 mM dye in pure water, 0.050 M Na_2SO_4, 0.50 mM Fe^{2+}, pH = 3.0, 25 °C, j = 2–3 mA cm^{-2}, 120 min	2.6 mg L^{-1} of H_2O_2 accumulation with maximum CE = 107% in homo-PEF and 3.2 mg L^{-1} with CE = 101% in PEC/PEF. 46% discoloration by PEC with TiO_2 NTs/air-diffusion at j = 3 mA cm^{-2}. 100% discoloration in 30–35 min in homo-EF with Pt or TiO_2 NTs anode and homo-PEF with Pt anode at such j. k_{dis}: 0.058, 5.1 × 10^{-3}, 4.9 × 10^{-3}, and 2.2 × 10^{-3} min^{-1} for PEC/PEF, PEC, EO with Pt/stainless steel, and EO-H_2O_2. TOC removal: 4.6%, 43.2%, 81.5%, and 84.6% for EO-H_2O_2 with a Pt anode, homo-EF with a Pt anode, homo-PEF with a Pt anode, and PEC/PEF with TiO_2 NTs at j = 3 mA cm^{-2} at 480 min. MCE rose in the sequence: EO-H_2O_2 ≪ homo-EF ≪ homo-PEF < PEC/PEF (131.4%). Isatin-5-sulfonic acid identified as primary derivative by HPLC and final carboxylic acids detected by ion-exclusion HPLC	[157]
Sequential processes				
Acid Blue 29	Continuous EC single-cell reactor - ECO-cell [g] for PEF-like process (1018-steel plates/ 1018-steel plates) - (Ti|Ir-Sn-Sb oxides /316-type stainless-steel) upon 15 W UVA light	EC: 2 L of simulated tannery effluent with 0.71–1.42 mM dye in pure water, COD = 150–300 mg L^{-1}, 2000 mg L^{-1} NaCl, neutral pH = 7.0, j = 12–36 mA cm^{-2}, linear flow rate (u) = 0.69–3.47 cm s^{-1}, linear flow velocity (t_R) = 23, 11.5, 7.7, and 4.6 s, 60 min for flocs sedimentation. PEF-like process: 0–0.4 mM Fe^{2+} added, pH = 3.0, j = 15 mA cm^{-2}, u = 24.2 cm s^{-1}, 480 min	For EC at 150 mg L^{-1} COD, discoloration of 12, 61, 83, 85, and 84% for 12, 18, 24, 30, and 36 mA cm^{-2}, respectively, at the lowest flow velocity of 0.69 cm s^{-1}. 62% COD removal at 0.69 cm s^{-1} and 36 mA cm^{-2} with EC = 1.689 kWh m^{-3}. 131, 197, 258, 324, and 400 mg L^{-1} of Fe obtained at 12, 18, 24, 30, and 36 mA cm^{-2}, respectively. For PEF-like, 100% discoloration and 84% COD removal at j = 36 mA cm^{-2} and 0.69 cm s^{-1} of residual dye by active chlorine-based PEF-like. Detection of the components of iron flocs. Total cost via the hybrid process EC/PEF-like was 0.87 and 0.89 USD m^{-3} for 150 and 300 mg L^{-1} COD, respectively	[158]
Methylene Blue	Three-electrode reactor for hetero-EF - aerobic granular sludge (AGS) (Ti|IrO_2-RuO_2/GF)	Hetero-EF: 0.2 L of 100 mg L^{-1} dye in pure water, 0.050 M Na_2SO_4, Fe-C catalyst = 10 g L^{-1}, pH = 3.0, E_{cat} = -0.75 V/SCE, air flow rate = 0.6 L min^{-1}, 120 min. AGS: 0.2 L of supernatant from hetero-EF, pH = 7.5, air flow rate = 0.6 L min^{-1}, 360 min	94.2 mg L^{-1} of H_2O_2 accumulation with CE = 91.2% for modified GF, 2-fold higher than 46.2 mg L^{-1} for raw GF. For hetero-EF, 90.2% and 97.9% discoloration for PEDOT:NaPSS modified GF [i] and GO/PEDOT:NaPSS modified GF [j] in 30 min > 69.7% for raw GF in 120 min. 68.9%, 73.2% and 47.6% TOC removal for PEDOT:NaPSS, GO/PEDOT:NaPSS. and raw GF. TOC and COD removals for the hetero-EF-AGS: 86.5% and 60.5%	[164]
Real textile wastewater	Two-electrode tank reactors for EC-EF (Fe/ Fe) - (BDD/CF)	EC: 400 mL of real textile wastewater with Methylene Blue as the main dye (COD = 325 mg L^{-1}, TOC = 52 mg L^{-1}, BOD_5 = 35 mg L^{-1}),	97% TOC removal for EC-EF. EC_{TOC} (kWh (g $TOC)^{-1}$): 0.003 for EC at 20 mA cm^{-2} < 0.0182 for EC-EO at 10 mA cm^{-2} < 0.00045 for EC-EF	[160]

(*continued on next page*)

Table 5 (*continued*)

Dye	System (anode/cathode)	Experimental remarks	Best results	Ref.
		pH = 8.75, j = 20 mA cm^{-2}, 60 min EF: pH = 3.0, 25 °C, j = 10 mA cm^{-2}, 60 min	at 10 mA cm^{-2}. BOD_5/COD grew from 0.1 to 0.46 after EC-EF. Removal efficiencies of 74, 89, 75, 84, and 74% for Cu, Mn, Zn, Fe, and Cr after EC treatment alone and 82, 93, 94, 97, and 81% after EC-EF	
Real wastewater from a dye manufacturing industry	Two-electrode tank reactor for EF-US process (Graphite/graphite)	750 mL of real dye wastewater (COD = 15360 mg L^{-1}, TOC = 20040 mg L^{-1}, BOD_5 = 90 mg L^{-1}, NH_4-N = 741.44 mg L^{-1}), 50–200 mg L^{-1} of $FeSO_4$ pH = 0.89–3.5, 25 °C, E_{cell} = 1–4 V, 120 min.Sonication (33 kHz frequency and 100 W power), 38–40 °C, 60 min	59.4% and 79.2% for NH_4-N and COD removals by homo-EF with 100 mg L^{-1} $FeSO_4$ at pH 3.0 and 3 V. Further improvement by subsequent sonication to 63.2% and 81.3%, respectively. In EF-US, EC_{COD} = 0.0837 kWh (g COD)$^{-1}$ and EC for NH_4-N = 2.985 kWh g^{-1}. BOD_5/COD increased from 0.00585 to 0.0265 after 120 min of EF	[162]

[a] PEM: proton exchange membrane.
[b] AC&G(1:5): cathode prepared with 1:5 mass ratio of AC and graphite powder.
[c] Fe@KSC: direct carbonization of Kenaf (*Hibiscus cannabinus*) and then decorated with iron oxides. [d] AMEFS: automatic microbial electro-Fenton systems.
[e] CB|SSM: carbon black modified stainless steel.
[f] PENG: piezoelectric nanogenerator. [g]: ECO-cell: filter-press reactor.
[i] PEDOT: NaPSS modified GF: poly (3,4-ethylenedioxythiophene) (PEDOT) and sodium polystyrenesulfonate (NaPSS) modified graphite fiber (GF).
[j] GO/PEDOT: NaPSS modified GF: graphene oxide with PEDOT|NaPSS modified GF.

1.99 W m^{-3}. The authors identified 13 aromatic derivatives of the dye by LC-MS and generated oxidants were detected by scavengers.

Wang et al. [142] proposed a dual-chamber MFC powered with a double-cathode reactor. Fig. 18b shows the cathodic chamber with a Pt/air–cathode system for H_2O_2 generation from an applied j or E_{cat} and a CF cathode for cathodic iron reduction when connected to a biofilm anode that spontaneously yielded CO_2 from a 50 mM PBS substrate (see composition in Table 5) in the anodic chamber. The EF reactions occurring at the cathodic chamber for dye removal are schematized as well. The air cathode was a 1:5 mass ratio of AC and graphite powder (AC&G) and a PEM separated both solutions. This curious arrangement aimed to minimize the electricity consumption for dye removal, supplied to the Pt/air–cathode system and partially countered by that produced by the coupled MFC. The cathodic chamber contained 40 mg L^{-1} of Rhodamine B or 74 mg L^{-1} of Methyl Orange in 0.050 M Na_2SO_4 with 0.50 mM Fe^{2+} at pH = 2.80 and 25 °C. Table 5 shows the best results obtained, being remarkable the excellent ability of the CF cathode for Fe^{2+} reduction favoring the 97% discoloration and 98.2% TOC decay with MCE = 6.22% achieved by the Rhodamine B solution in only 10 min at a low j = 2.5 mA cm^{-2}, demonstrating the high oxidative effectiveness of the hybrid system. Maximum power densities of 1.51, 1.11, and 0.66 W m^{-2} for the MFC were determined at − 0.8, − 0.6, and −0.4 V/Ag|AgCl applied to the air cathode. 6 aromatic by-products of Rhodamine B were detected by LC-MS, along with 9 final carboxylic acids quantified by HPLC.

Yu et al. [143] considered three systems including two automatic MFC-EF systems for Acid Orange 7 (AO7) removal. The system I corresponded to a two-electrode reactor like of Fig. 3a for the hetero-EF process and Fig. 18c presents the sketch related to a two-electrode configuration with the cathode separated from the bioanode (System II, left) and that of a single-electrode configuration with the microchannel-structured carbon as both anode and EF cathode (system III, right). The different operating variables of these three systems with different Fe@KSC cathodes at several calcination temperatures (800 and 900 °C) are given in Table 5. The intermediate box of Fig. 18c remarks the main EF reactions involved in dye destruction. From the data of Table 5, one can infer that the best performance was reached with System III that yielded 98% discoloration after a long treatment of 24 h for 13.5 mg L^{-1} dye in the absence of external resistance, quite stable after six cycles. The loss of color was slightly decreased to 94–96% for 20–50 mg L^{-1} of dye. Note that the cathodes were well efficient in these systems and non-extra addition of Fe^{2+} as Fenton catalyst and pH control was required.

The above findings highlight the effectiveness of MFC systems with homo-EF and hetero-EF for dyes removal, although much more research is needed for its feasible implementation in practice.

6.2. Other hybrid processes

Other hybrid treatments have been developed for the removal of dyes with persulfate/EF [145], nanofiltration/EF [146], photocatalytic fuel cell (PFC)/EF [147,148,149,150], AC adsorption/EF [151,152], electroperoxone/ultrasound (EP/US) [153], US/PEF [154], US/persulfate/PEF [155], and photoelectrocatalysis (PEC) with EF [156] or PEF [157].

A flow stainless-steel/graphite paper cell connected to a nanofiltration (NF270) membrane was checked to remediate a solution of 20 mg L^{-1} of the diazo dye Reactive Black 5 in 0.050 M Na_2SO_4 with 0.20 mM Fe^{2+} at pH = 3.0 with air flow rate = 5 mL min^{-1} for 120 min [146]. However, this hybrid system only gave a very small discoloration of 8.8% as maximal due to the low H_2O_2 generated (see Table 5) and hence, it was not a valid proposal for dye treatment.

Much better performance has been described by Thor et al. [149] who proposed four hybrid PFC/EF configurations for the parallel treatment of two solutions of 500 mL of 10 mg L^{-1} of the azo dye amaranth in pure water at pH = 5.7 in PFC, pH = 3.0 in EF, and 25 °C. The PFC cell contained a C|ZnO photoanode illuminated with a 36 W UVA light and a carbon cathode, whereas the EF cell contained an iron anode and a carbon cathode under an air flow rate = 1 L min^{-1}. In the PFC cell, the light irradiation caused the separation of charges with an electron in the conduction band (e^-_{CB}) and a hole in the valence band (h^+_{VB}) over the semiconductor photoanode by reaction (43). Spontaneously, the photoexcited e^-_{CB} then circulated to the cathode, and so, the remaining h^+_{VB} reacted either with organic pollutants or more quickly with H_2O to originate $^{\bullet}OH$ from the reaction (44).

$$\text{Semiconductor} + h\nu \rightarrow e^-_{CB} + h^+_{VB} \quad (43)$$

$$H_2O + h^+_{VB} \rightarrow {}^{\bullet}OH + H^+ \quad (44)$$

The EF cell worked by the current supplied by the PFC with an external load = 1 kΩ by dissolving the iron anode to Fe^{2+} to further react with electrogenerated H_2O_2 at the cathode yielding homogeneous $^{\bullet}OH$ from Fenton's reaction (1). This corresponds to a variant of homo-EF so-called peroxi-coagulation [1]. Fig. 19a shows the schemes of the four configurations tested with different number of cathodes and anodes, so-called S1, S2, S3, and S4. It was found that discoloration always increased at a smaller electrode gap, being optimal for 2 cm. Under these conditions, Fig. 19b and c highlight a quite similar percentage of color

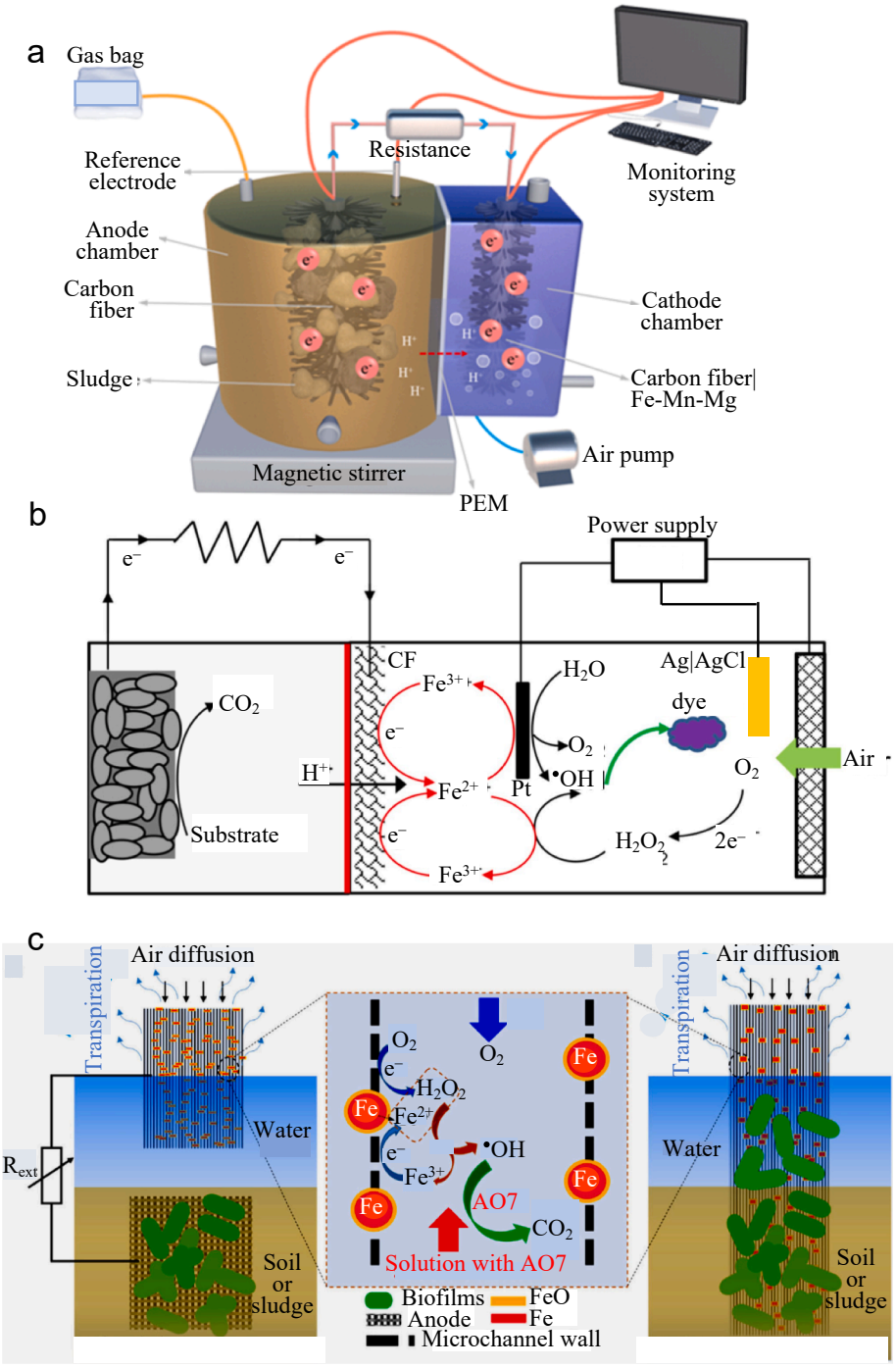

Fig. 18. Schematic diagrams of microbial fuel cells (MFCs) coupled with EF for dyes removal. (a) Dual-chamber separated by a proton exchange membrane (PEM) with a carbon fiber anode and a carbon fiber| Fe-Mn-Mg cathode (adapted from [140]). (b) MFC-powered double-cathode EF system (adapted from [142]). (c) Automatic microbial EF system for Acid Orange 7 (AO7) destruction using (left) a two-electrode configuration with the cathode separated from the bioanode and (right) a single-electrode configuration with the microchannel-structured carbon as both anode and EF cathode (adapted from [143].

removal for all PFC and EF configurations, with maximum values at 480 min of 94.0% with k_{dis} = 0.3610 h^{-1} for PFC by S1 and 78.1% with k_{dis} = 0.2204 h^{-1} for EF by S2. Nevertheless, a greater power of 38.7434 μW was achieved for the S4 configuration. This procedure then allowed efficient dye destruction with electricity production in an analogous way to an MFC. In the next future, more research should check the feasible use of more cost-effective PFC cells under sunlight, avoiding the electric cost of artificial UVA lamps.

Hybrid AC adsorption/EF systems [151,152] led to good discoloration of several synthetic and real wastewater with dyes, as can be seen in Table 5. A more complex and potent hybrid process involving EP/US has been developed by Ghanbari et al. [153]. The scheme of the two-electrode system tested is depicted in Fig. 20a. It contained a Pt anode, a GF cathode, and a sonoctrode of 100 W to generate a low frequency of 25 kHz of US. An air flow rate = 0.5 L min^{-1} and an O_3 dosage = 15–41 mg L^{-1} were maintained in 650 mL of 50 mg L^{-1} of the azo dye Acid Orange 7 with 0.010 M Na_2SO_4 in pure water at pH = 3.0–9.0 by applying an I = 100–400 mA lasting 30 min. In EP, the electrogenerated H_2O_2 at the cathode reacted with injected O_3 to form homogeneous $^{\bullet}OH$ from the peroxone reaction (45). Additionally, O_3 can directly attack organic pollutants as well. The US raised the mass transport of all these species to accelerate their reaction.

$$2H_2O_2 + 2O_3 \rightarrow H_2O + 3O_2 + HO_2^{\bullet} + {}^{\bullet}OH \quad (45)$$

This EP/US system allowed efficient working at neutral pH that is beneficial for the treatment of natural waters and real wastewater.

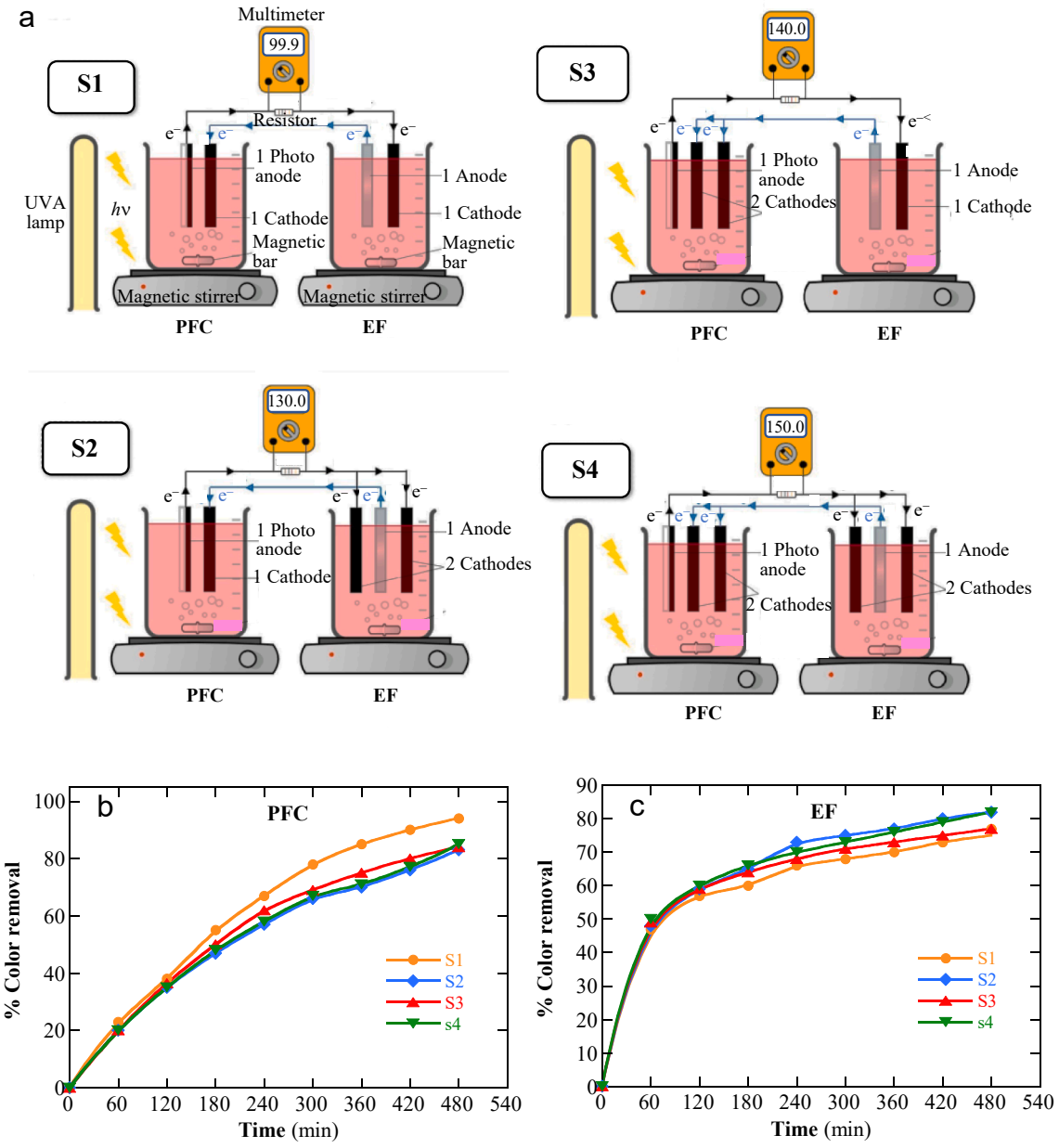

Fig. 19. Schemes of four dual-chamber configurations (S1, S2, S3, and S4) used for the hybrid photocatalytic fuel cell (PFC)/EF treatment of the azo dye amaranth. The PFC process was made with a C|ZnO photoanode under a 36 W UVA lamp and a carbon cathode to provide power to the one EF process with Fe/carbon cells. (b) Percentage of color removal with time for the PFC treatment of 500 mL of 10 mg L^{-1} of dye in pure water at pH 5.7 and 25 °C using an interelectrode gap = 2 cm, external load = 1 kΩ, and air flow rate = 1 L min^{-1} for the different configurations. (c) Discoloration obtained for the corresponding EF systems for the same solution but at pH 3.0.
Adapted from [149]

Fig. 20b shows a faster discoloration of the above solution at pH = 7.0, O_3 dosage = 33 mg L^{-1}, and I = 300 mA in the sequence: O_3 < O_3/US < homo-EF (with 0.50 mM Fe^{2+}) < homo-EF/US < EP < EP/US. The latter process gave rapid overall discoloration in only 20 min with k_{dis} = 0.276 min^{-1}(see Table 5). Fig. 20c illustrates that this k_{dis}-value was strongly reduced with 0.010 M NaCl or $NaNO_3$ due to the scavenging effect of Cl^- and NO_2^- (formed at the cathode from NO_3^-reduction) over O_3. The mineralization ability of EP/US was also superior to the other methods, achieving 88% TOC abatement after 60 min of electrolysis, as shown in Fig. 20d. This treatment was extended to real industrial wastewater contaminated with 50 mg L^{-1} Acid Orange 7 and found a growth of the BOD_5/COD from 0.18 to 0.36 (see Table 5). This suggests that the EP/US process could be applied as a pre-treatment of real wastewater polluted with dyes, followed by a biological treatment for their cheaper and more effective decontamination.

The combination of PEC and EF represents an excellent hybrid treatment of dyes. Liu et al. [156] used this arrangement to remediate solutions of the azo dye Orange G, whose chemical structure is given in Fig. 21a. Fig. 21b shows the schematic diagram of the undivided dual-anode reactor tested by these authors in which the tank reactor with the solution contained a Ti|TiO_2 photoanode exposed to an 8 W UVA light and a stainless-steel anode coupled to each graphite cathode. So, two independent Ti|TiO_2/graphite and stainless-steel/graphite systems for PEC and homo-EF, respectively, were simultaneously electrolyzed by two power supplies. The PEC process involved the photocatalysis (PC) of the semiconductor TiO_2 by UVA light through reaction (43), followed by the extraction of the photoexcited e^-_{CB} by the external current causing a high concentration of oxidant h^+_{VB}. While a small amount of M(•OH)

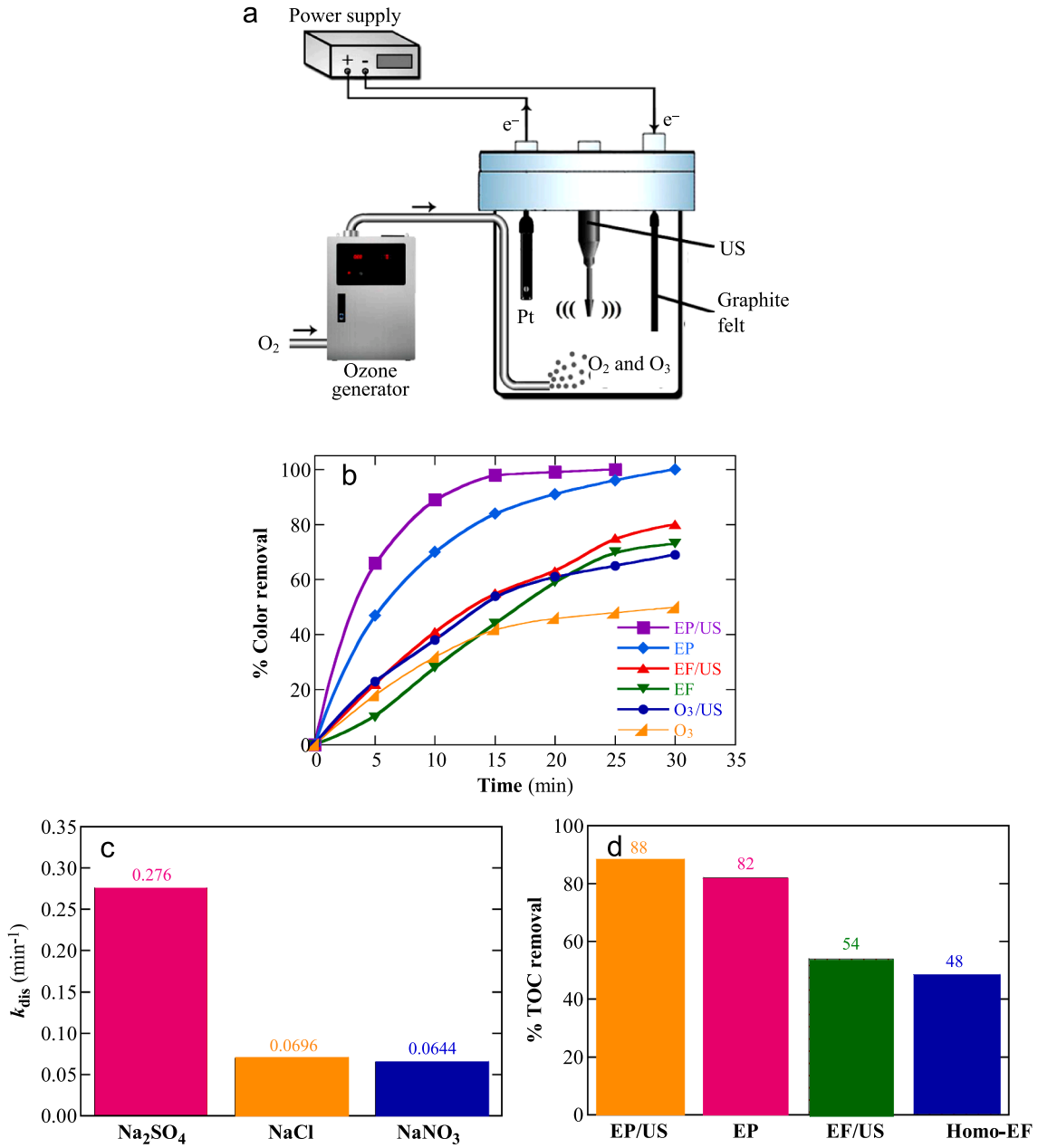

Fig. 20. (a). Scheme of the hybrid electroperoxone (EP)/ultrasound (US) system with a Pt anode and a GF (graphite felt) cathode used for Acid Orange 7 azo dye removal. (b) Percentage of color removal for various processes of 650 mL of a solution with 50 mg L^{-1} of the dye and 0.010 M Na_2SO_4 in pure water at pH = 7.0, air flow rate = 0.5 L min^{-1}, O_3 dosage = 33 mg L^{-1} (US power = 100 W), and 0.50 mM Fe^{2+} for homo-EF comparison using the above cell at I = 300 mA. (c) Comparative rate constant for discoloration of Acid Orange 7 for EP/US upon the above conditions with 0.010 M of several electrolytes. (d) Percentage of TOC removal after 60 min of the treatments of graphic (b).
Adapted from [153]

from reaction (6) was formed at both anodes, a large quantity of $^{\bullet}OH$ was originated from: (i) the oxidation of H_2O with h^{+}_{VB} by reaction (44) at the photoanode surface from PEC and (ii) Fenton's reaction (1) from the electrogenerated H_2O_2 at both graphite cathodes and added Fe^{2+} from homo-EF. Fig. 21c depicts the normalized absorption measured for several treatments of 200 mL of 0.10 mM of dye with 0.10 M Na_2SO_4 and 0.10 mM Fe^{2+} at pH = 3.0 using 75 and 45 μA cm^{-2} on Ti|TiO_2 photoanode and stainless-steel anode, respectively, for 180 min. The discoloration followed the order: PC < PEC < PEC- 0.10 mM $FeSO_4$ < homo-EF < PEC/PE. For the latter most powerful process, the solution became colorless in 150 min. The authors remarked on the very low amount of Fe^{2+} catalyst needed in the hybrid PEC/EF system of only 6 μM, a value much lower than 0.1–0.8 mM necessary for the conventional Fenton or homo-EF (see Table 5).

Another interesting paper has been published by Oriol et al. [157] dealing with the treatment of Indigo Carmine (see the chemical formula in Fig. 1) by a hybrid PEC/PEF process. They used a two-electrode tank reactor with a Pt anode and a stainless-steel cathode for EO, the same anode and an air-diffusion cathode for EO-H_2O_2 (without Fe^{2+}), homo-EF, and homo-PEF, a TiO_2 nanotubes (NTs) photoanode and a stainless-steel cathode for PEC, and the same photoanode and an air-diffusion cathode for PEC/PEF. In the photo-assisted processes, the solution was illuminated with a 36 W UV LED. The runs were carried out with 150 mL of 0.260 mM of the dye in 0.050 M Na_2SO_4 with 0.50 mM Fe^{2+} in pure water at pH = 3.0, 25 °C, and j = 2–3 mA cm^{-2} during 120 min. It was found a similar H_2O_2 accumulation (2.6–3.2 mg L^{-1}) with CE =

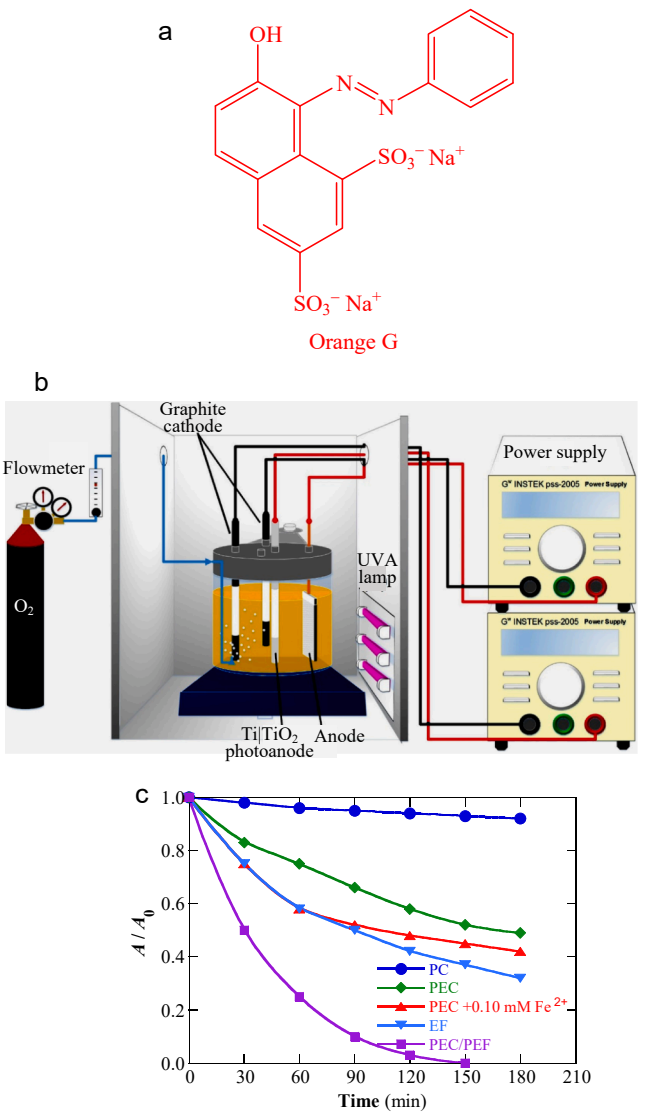

Fig. 21. (a) Chemical structure of the azo dye Orange G. (b) Schematic diagram of a hybrid photoelectrocatalysis (PEC)/homo-PEF process. (c) Normalized absorbance for different treatments with the above cell of 200 mL of 0.10 mM Orange G in pure water with 0.10 M Na_2SO_4 and 0.10 mM Fe^{2+} at pH = 3.0 using 75 and 45 μA cm^{-2} on $Ti|TiO_2$ photoanode and stainless steel anode upon a 6 W (0.33 mW cm^{-2}) UVA light.
Adapted from [156]

101–107% for homo-EF and PEC/PEF at j = 3 mA cm^{-2}, demonstrating the good H_2O_2 generation at the air-diffusion cathode. Larger performance was obtained at j = 3 mA cm^{-2} than j = 2 mA cm^{-2} due to the generation of more $^{\bullet}OH$ from the quicker H_2O_2 generation, $Fe(OH)^{2+}$ photolysis, and e^-_{CB} extraction yielding more water oxidation with h^+_{VB}. Table 5 reveals that the percent of color and TOC removal increased in the order: EO < EO-H_2O_2 < PEC < homo-EF < homo-PEF < PEC/PEF. The latter process was quite powerful because TOC was reduced by 84.6% with a high MCE = 131.4% in 480 min. Isatin-5-sulfonic acid was identified as the primary derivative by HPLC and final carboxylic acids such as oxalic, oxamic, and pre-eminently formic were detected by ion-exclusion HPLC.

More research should be made on the potent PEC/EF and PEC/PEF processes for their implementation at a large scale. The use of sunlight as an energy source seems necessary to be assessed to develop more cost-effective treatments that are more attractive for industrial applications.

6.3. Sequential processes

The remediation of dyeing wastewaters has also been investigated by sequential processes such as EC-PEF [158,159,160,161], EF-US [162], EF-adsorption [163], EF-aerobic granular sludge (AGS) [164], and anaerobic-PEF in photo-assisted MFCs [165].

Márquez et al. [158,159] have developed the EC-PEF treatment of various dyes in NaCl medium. Fig. 22a shows the two-electrode reactor with two Fe electrodes and the sketch of the pre-pilot EC set-up used for the continuous removal of dyes in solution. EC is based on the continuous dissolution of the Fe anode to Fe^{2+}, which precipitates as $Fe(OH)_3$ sludge with coagulation of the organic pollutants on its surface. The supernatant liquid containing the remaining dye and small contents of soluble Fe^{2+} from EC was further treated by a homo-PEF-like process. Fig. 22b schematizes the filter-press two-electrode cell with a Ti|Ir-Sn-Sb oxides anode and a 316-type stainless-steel cathode and the pre-pilot homo-PEF-like set-up for the sequential decontamination of the pre-treated EC effluent. This method was first introduced by Murrieta et al. [129], as pointed in subsection 5.1, and consists of the organic oxidation by generated HClO and homogeneous $^{\bullet}OH$ from the photolytic reaction (35) and the Fenton-like reaction (38) with the Fe^{2+} solubilized in the EC pre-treatment. For the azo dye Acid Blue 29 [158], 2 L of 0.71–1.42 mM dye (150–300 mg L^{-1} COD) with 2000 mg L^{-1} NaCl in pure water at pH = 7.0 by applying j = 36 mA cm^{-2} at a linear flow rate (u) = 0.69 cm s^{-1} during 60 min were treated by EC for 60 min. As expected, Fig. 22c and d highlight a greater percentage of color removal (84% vs. 72%) and lower remaining COD (56 vs. 212 mg L^{-1}) for 0.71 mM dye as compared to 1.42 mM owing to the smaller organic load. The resulting solutions were sequentially treated by homo-PEF like at pH = 3.0, j = 15 mA cm^{-2}, and u = 24.2 cm s^{-1} lasting 480 min, with 400 mg L^{-1} of solubilized Fe^{2+} (see Table 5). Again, the best performance was achieved for the starting 0.71 mM dye with 100% discoloration and 4.6 mg L^{-1} of remaining COD (97% of COD removal), as shown in Fig. 22c and d, with a cost of 0.87 USD m^{-3}. The sequential EC-PEF then possesses good effectiveness for dye remediation, opening the door to its application to real effluents with Cl^- enough to run a homo-PEF-like process. Techno-economic studies should be made to benchmark this sequential process with other conventional methods.

Liu et al. [164] proposed the sequential hetero-EF and aerobic granular sludge (AGS) process schematized in Fig. 23a for the removal of the thiazine dye Methylene Blue with unmodified GF, poly(3,4-ethylenedioxythiophene) (PEDOT): sodium polystyrenesulfonate (NaPSS) GF, or graphene oxide (GO)|PEDOT: NaPSS GF as alternative cathodes. Fig. 23a presents the H_2O_2 concentration accumulated at 120 min and CE at 30 min for 0.2 L of 0.050 M Na_2SO_4 at pH 3.0 under an airflow = 0.6 mL min^{-1} with the 3 cathodes at E_{cat} = -0.75 V/SCE during 120 min. Greater values of 94.2 mg L^{-1} H_2O_2 and CE = 91.2% were found for the GO|PEDOT: NaPSS GF cathode. This modified cathode offered the best performance for the treatment of 100 mg L^{-1} dye with 10 g L^{-1} of C-Fe catalyst (see Table 5), yielding 97.9% discoloration in 30 min and 73.2% of TOC and 60.5% of COD removal in 120 min. Parallel trials with AGS alone at pH 7.5 and air flow = 0.6 mL min^{-1} for 360 min gave smaller values of 63.9% of TOC and 50.3% of COD abatements, as can be seen in Fig. 23a. The sequential hetero-EF-AGS improved the mineralization of the individual methods to obtain 86.5% of TOC and 75.7% of COD decays. Hetero-EF treatments with other cathodes and catalysts should be assessed to enhance their mineralization process and hence, upgrade the above sequential method.

Sequential EC-EF [160] Aganga 2020] and EF-US [162] [Menon 2021] processes have been described for real wastewaters with dyes (see Table 5). The runs of the EC-EF process were performed with separated two-electrode tank reactors by treating 400 mL of real textile wastewater with Methylene Blue as the main dye. EC was carried out with 2 iron electrodes at pH 8.75 by applying a j = 20 mA cm^{-2} for 60 min, and the supernatant liquid (with solubilized Fe^{2+}) was then treated by homo-

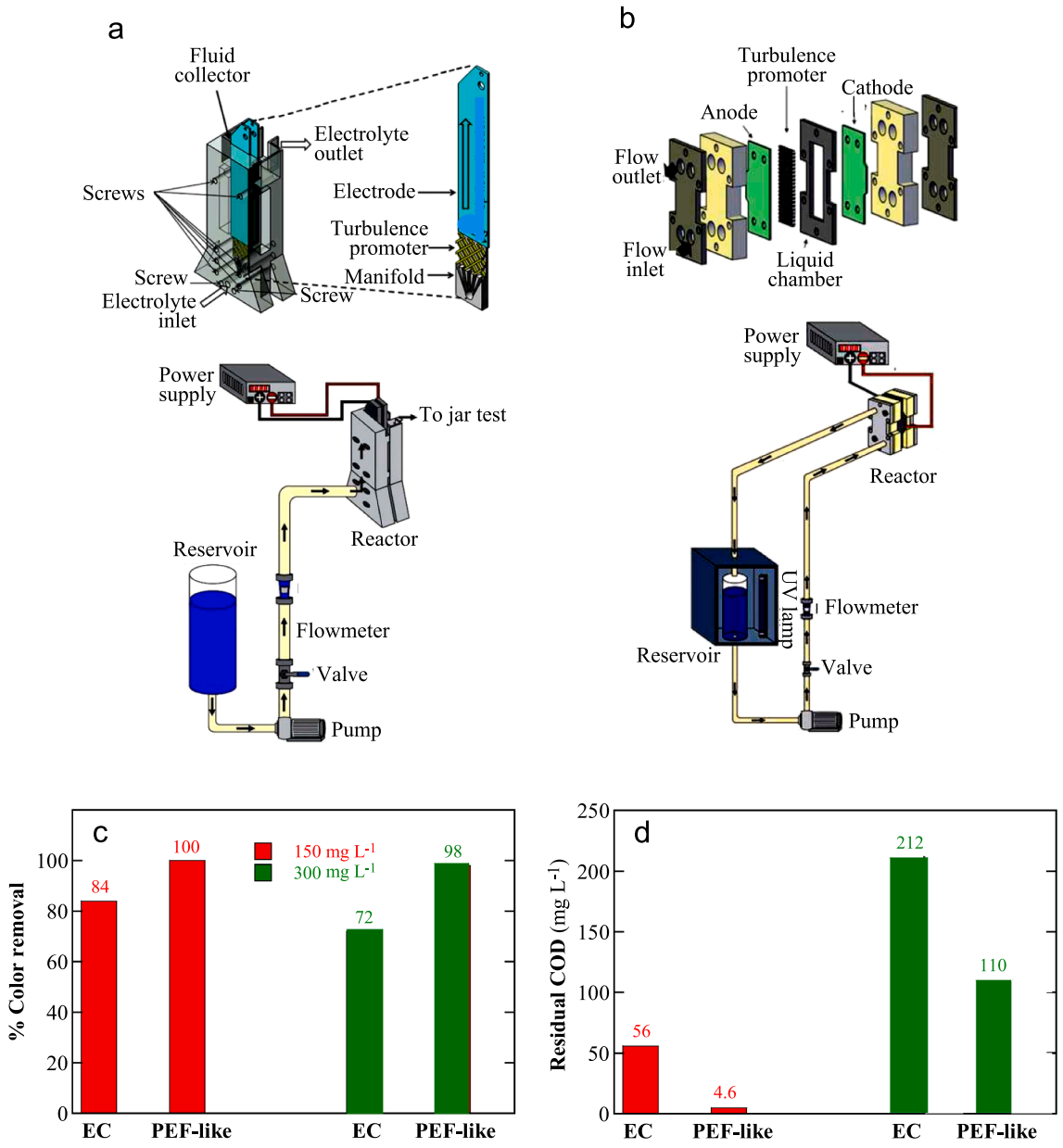

Fig. 22. Sketches of (a) the electrocoagulation (EC) reactor with two Fe electrodes and EC set-up, and (b) the electrochemical reactor with a Ti|Ir-Sn-Sb oxides anode and a 316-type stainless-steel cathode and homo-PEF-like set-up used for the sequential treatment of the azo dye Acid Blue 29. (c) Percentage of color removal and (d) residual COD after 60 min of EC and consecutive 480 min of homo-PEF-like starting from 2 L of 0.71–1.42 mM dye (150–300 mg L^{-1} COD) in pure water with 2000 mg L^{-1} NaCl at pH = 7.0 by applying j = 36 mA cm^{-2} and linear flow rate (u) = 0.69 cm s^{-1}, For the homo-PEF-like process, no Fe^{2+} was added and the pH was adjusted to 3.0 at j = 15 mA cm^{-2} and u = 24.2 cm s^{-1}.
Adapted from [158]

EF with a BDD anode and a CF cathode at pH 3.0 and j = 10 mA cm^{-2} for 60 min as well, Excellent performance of the sequential process was found, analogously to reported above in ref. [158,159], with 97% TOC removal and a very low EC_{TOC} = 0.00045 kwh (g TOC)$^{-1}$ (see Table 5). The BOD_5/COD ratio strongly grew up to a biodegradable value of 0.46, and 81–97% of metals like Cu, Mn, Zn, Fe, and Cr were removed from the solution, yielding a more depurated effluent. The sequential EF-US was carried out with a graphite/graphite tank reactor for homo-EF and a tank reactor equipped with a US of 33 kHz frequency and 100 W power. The homo-EF process was assessed for 750 mL of real dye wastewater by adding 50–200 mg L^{-1} of $FeSO_4$ at pH = 0.89–3.5, 25 °C, and E_{cell} = 1–4 V lasting 120 min. Under the best conditions of 100 mg L^{-1} $FeSO_4$ pH 3.0, and E_{cell} = 3 V, 59.4% of NH_4-N and 79.2% COD removals were found, which slightly raised up to 63.2% and 81.3%, respectively, after 60 min of US (see Table 5). Although low EC_{COD} = 0.0837 kWh (g COD)$^{-1}$ and EC for NH_4-N = 2.985 kWh g^{-1} were calculated for this sequential EC-US process, much better performance has been reported by the above sequential EC-EF because of the very low oxidation power of US that seems rather unappropriated for a sequential process.

7. Conclusions and prospects

This review summarizes the advances in electrochemical Fenton-based processes to remediate synthetic and real wastewaters containing synthetic organic dyes within the period 2018–2022. The works were made at a laboratory scale and provided fundamental information on the potential interest of these processes for wastewater remediation.

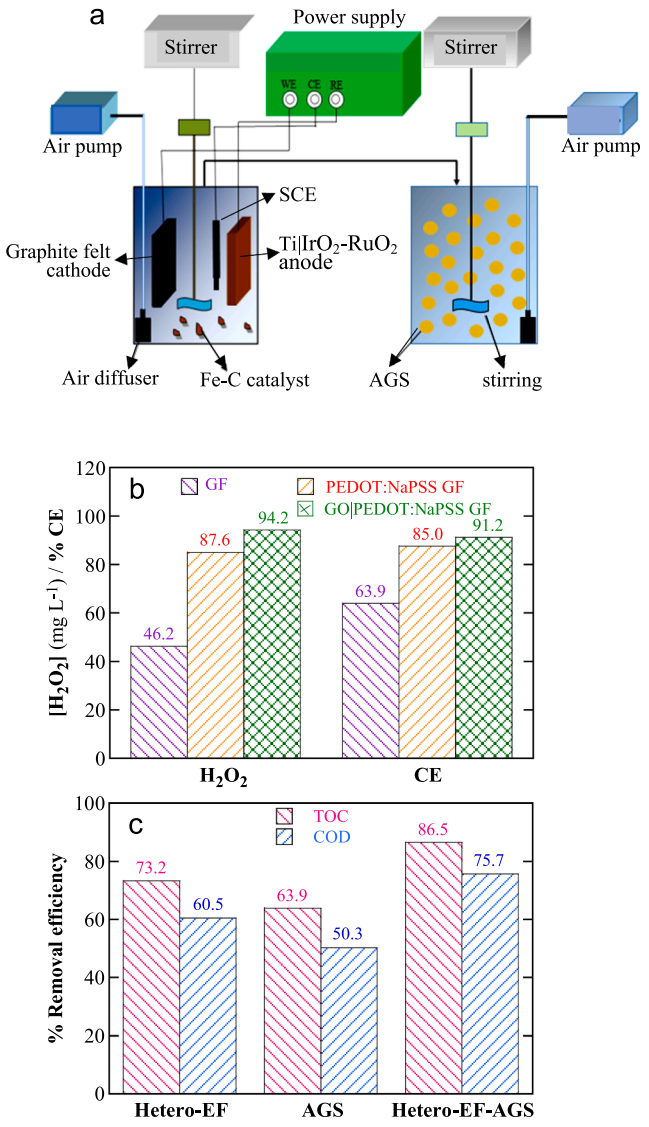

Fig. 23. (a) Schematic diagram of the sequential hetero-EF and aerobic granular sludge (AGS) process proposed for the Methylene Blue thiazine dye treatment. (b) H_2O_2 concentration accumulated at 120 min and CE at 30 min determined for the electrolysis of 0.2 L of 0.050 M Na_2SO_4 at pH 3.0 using three of the above hetero-EF system without catalysts and with unmodified GF, poly (3,4-ethylenedioxythiophene) (PEDOT): sodium polystyrenesulfonate (NaPSS) GF, or graphene oxide (GO)|PEDOT: NaPSS GF cathode under air flow = 0.6 mL min^{-1} and at E_{cat} = -0.75 V/SCE. (c) Percentage of TOC and COD removals determined for the above solution with 100 mg L^{-1} dye after 120 min of hetero-EF upon the above conditions with a GO|PEDOT: NaPSS GF cathode and 10 g L^{-1} of C-Fe catalyst, after 360 min of AGS at pH 7.5 and air flow = 0.6 mL min^{-1}, and after the sequential hetero-EF-AGS process.
Adapted from [164]

However, much more research efforts are required to show their actual interest in industrial applications. In this way, the treatment of dyeing effluents at a pilot scale should be largely developed to clearly establish the advantages and drawbacks of such processes. Electrochemical engineering studies should be made to design appropriate and efficient electrolytic reactors with the characterization of optimum operating variables to achieve the best performance of treatments. The current development of these technologies at a small scale allows the selection of good cathodes to electrogenerated H_2O_2 and provides a vast knowledge of the oxidation ability of the oxidizing agents produced in many aqueous matrices. The building-up of electrolytic systems at the industrial level should take into account all these advantages for their rapid development. Techno-economic studies should also be carried out in the next future to show the feasible viability of selected electrochemical Fenton-based processes in front of other conventional oxidation methods to discolorize and mineralize dyeing effluents.

The works on the homo-EF process have been centered on the use of different cathodes such as raw and modified carbonaceous materials and GDE with excellent reusability. Graphite and CF have been widely tested as raw carbonaceous cathodes, whereas a large variety of modified cathodes have been prepared with higher H_2O_2 production, thus enhancing the $^{\bullet}OH$ production from Fenton's reaction and the ability to destroy the synthetic organic dyes. The GDE possessed a large efficiency to electrogenerate H_2O_2 as well. The best discoloration and mineralization of dye solutions in all homo-EF treatments were then achieved at the optimum pH = 3.0 of Fenton's reaction. This limits their application to acidic media since iron ions precipitate as $Fe(OH)_3$ at pH > 4. The physisorbed M($^{\bullet}OH$) radical formed at the anode surface also played an important oxidative role, and so, the quicker degradations of the synthetic organic dyes and their by-products were obtained with a BDD anode, much more powerful than other conventional ones like Pt and DSA. The discoloration always obeyed pseudo-first-order kinetics, whereas the process efficiency increased with decreasing the dye concentration and increasing *j*, although with lower MCE and higher energy consumption. Similar behavior has been found for the other electrochemical Fenton-based treatments. An enhancement of homo-EF performance has been found in chloride media as compared to sulfate ones due to the competitive removal with generated active chlorine. The action of this species along with that of hydroxyl radical has then to be considered in the treatment of real wastewaters containing Cl^-. The organic components of these wastewaters are also oxidized, decelerating the destruction of dyes. Other metallic ions like Co^{2+}, Ce^{3+}, Ni^{2+}, and Mn^{2+} have shown a good ability for $^{\bullet}OH$ production as catalysts from the corresponding Fenton-like reactions, but their toxicity excludes their application in homo-EF, where the key catalyst Fe^{2+} is compatible with all living beings.

The hetero-EF processes with solid catalysts and functionalized cathodes have been developed to destroy the synthetic organic dyes near neutral pH with very low precipitation of iron ions. This is feasible because heterogeneous $^{\bullet}OH$ was produced at the material surface by the $\equiv Fe^{3+}/\equiv Fe^{2+}$ cycle through the heterogeneous Fenton's reaction. Natural minerals such as pyrite and chalcopyrite regulated the solution pH close to 3.0, but they possessed lower power to destroy dyes than iron materials like sponge iron and iron-carbon composite at pH = 6.0. Other iron solid hetero-catalysts such as nano-stick $FeSe_2$ and $Fe_{83}Si_5B_8P_4$ also yielded a good performance for dyes removal with excellent reusability. The same behavior has been described for $LaCu_{0.5}Mn_{0.5}O_3$ perovskite to destroy Methylene Blue in the pH range 6.5–8.5. Many solid hetero-catalysts composed of iron-bearing materials deposited on supports such as magnetic hybrid Hb200 and HbLN, and ZSM-5 with Cu at pH = 3.0, as well as Mn^{2+} chelated on resins, have shown excellent results. Another approach of hetero-EF considered functionalized cathodes that simultaneously originated in situ H_2O_2 and heterogeneous $^{\bullet}OH$. Several iron-containing functionalized cathodes like Fe-NCCC, Fe_3O_4|ACF, ferrocene-graphite|CNTs, graphene|(AlCrCuFeNi)O, and $CoFe_2O_4$|CF have shown good effectiveness on dye discoloration and mineralization. Other excellent cathodes tested were a non-iron cathode such as N-CNF-Co|CoO_x and a metal-free material like N,S-EEGr-CF, which need more attention to understand the role of their oxidizing agents generated and how these species evolved. Hence, in-situ measurements could help to uncover more fundamental mechanisms under these conditions. The current absence of comparative results between the different solid catalysts or functionalized cathodes proposed for the destruction of a large variety of synthetic organic dyes makes it impossible to establish the best system for hetero-EF. In this manner, some potential unified key indicators are suggested to be used as a benchmark between diverse solid catalysts and functionalized cathodes. The synthetic organic dyes underwent a faster degradation and mineralization by homo-PEF or

homo-SPEF than homo-EF due to the additional •OH production in the bulk by photo-Fenton reaction and the photolysis of final Fe(III)-carboxylate complexes. The use of the chelating agent EDTA to stabilize Fe^{2+} allowed a good degradation of Rhodamine B by homo-EF at pH = 7.0. The homo-SPEF process was more powerful than the homo-EF one and the study of Acid Blue 29 removal with a solar flow pre-pilot plant yielded acceptable and low $EC_{TOC} < 0.06$ kWh (g TOC)$^{-1}$. Alternative processes with homogeneous •OH generation from added Fe^{2+} and electrogenerated HClO have been checked for Acid Red 1 in chloride medium, showing a greater discoloration in the order homo-EF-like > EO-HClO > homo-PEF-like > homo-SPEF-like. Hetero-PEF and hetero-SPEF treatments have been developed with magnetic Fe_3O_4 and sodium vermiculite, respectively. The SPEF processes are the best option for the remediation of dyeing effluents.

Few MFCs at bench scale have been constructed to simultaneously obtain electricity and remediate dyes wastewaters, which need much development in the next future. Other hybrid processes have been proposed aiming to improve the destructive power of homo-EF and homo-PEF. PFC/EF, AC adsorption/EF, and PEC with EF or PEF seem the more promising methods for future research. The removal power of synthetic organic dyes at bench scale was also upgraded with sequential processes like EC-PEF, EF-US, EF-adsorption, and EF-AGS, which should be further scaled to search the best conditions for practical application.

CRediT authorship contribution statement

Fengxia Deng: Conceptualization, Investigation, Methodology, Formal analysis, Writing – original draft, Writing – review & editing. **Enric Brillas:** Conceptualization, Investigation, Methodology, Formal analysis, Writing – original draft, Writing – review & editing.

Declaration of Competing Interest

The authors declare that they have no known competing financial interests or personal relationships that could have appeared to influence the work reported in this paper.

Data availability

Data will be made available on request.

Acknowledgements

This work was supported by National Natural Science Foundation of China (No. 52000052) and State Key Laboratory of Urban Water Resource and Environment (Harbin Institute of Technology, No. 2021TS26). The postdoctoral scholarship awarded to Fengxia. Deng. (State Scholarship Fund, CSC, China) is acknowledged.

References

[1] C.A. Martínez-Huitle, E. Brillas, Decontamination of wastewaters containing synthetic organic dyes by electrochemical methods: a general review, Appl. Catal. B: Environ. 87 (2009) 105–145, https://doi.org/10.1016/j.apcatb.2008.09.017.
[2] T. Shindhal, P. Rakholiya, S. Varjani, A. Pandey, H.H. Ngo, W. Guo, H.Y. Ng, M. J. Taherzadeh, A critical review on advances in the practices and perspectives for the treatment of dye industry wastewater, Bioengineered 12 (2021) 70–87, https://doi.org/10.1080/21655979.2020.1863034.
[3] R. Al-Tohamy, S.S. Ali, F. Li, K.M. Okasha, Y.-A.-G. Mahmoud, T. Elsamahy, H. Jiao, Y. Fu, J. Sun, A critical review on the treatment of dye-containing wastewater: ecotoxicological and health concerns of textile dyes and possible remediation approaches for environmental safety, Ecotox. Environ. Saf. 231 (2022) 113160, https://doi.org/10.1016/j.ecoenv.2021.113160.
[4] B. Jain, A.K. Singh, H. Kim, E. Lichtfouse, V.K. Sharma, Treatment of organic pollutants by homogeneous and heterogeneous Fenton reaction processes, Environ. Chem. Lett. 16 (2018) 947–967, https://doi.org/10.1007/s10311-018-0738-3.
[5] M.D.N. Ramos, C.S. Santana, C.C.V. Velloso, A.H.M. da Silva, F. Magalhães, A. Aguiar, A review on the treatment of textile industry effluents through Fenton processes, Process Saf. Environ. Prot. 155 (2021) 366–386, https://doi.org/10.1016/j.psep.2021.09.029.
[6] E. Brillas, C.A. Martinez-Huitle, Decontamination of wastewaters containing synthetic organic dyes by electrochemical methods. An updated review, Appl. Catal. B: Environ. 166–167 (2015) 603–643, https://doi.org/10.1016/j.apcatb.2014.11.016. /.
[7] E. Brillas, A review on the photoelectro-Fenton process as efficient electrochemical advanced oxidation for wastewater remediation. Treatment with UV light, sunlight, and coupling with conventional and other photo-assisted advanced technologies, Chemosphere 250 (2020) 126198, https://doi.org/10.1016/j.chemosphere.2020.126198.
[8] P.V. Nidheesh, M. Zhou, M.A. Oturan, An overview on the removal of synthetic dyes from water by electrochemical advanced oxidation processes, Chemosphere 197 (2018) 210–227, https://doi.org/10.1016/j.chemosphere.2017.12.195.
[9] C. Martínez-Sánchez, I. Robles, L.A. Godínez, Review of recent developments in electrochemical advanced oxidation processes: application to remove dyes, pharmaceuticals, and pesticides, Int. J. Environ. Sci. Technol. (2022), https://doi.org/10.1007/s13762-021-03762-9.
[10] S. Li, T. Hua, F. Li, Q. Zhou, Bio-electro-Fenton systems for sustainable wastewater treatment: mechanisms, novel configurations, recent advances, LCA and challenges. An updated review, J. Chem. Technol. Biotechnol. 95 (2020) 2083–2097, https://doi.org/10.1002/jctb.6332.
[11] P.V. Nidheesh, G. Divyapriya, N. Oturan, C. Trellu, M.A. Oturan, Environmental applications of boron-doped diamond electrodes: 1. Applications in water and wastewater treatment, ChemElectroChem 6 (2019) 2124–2142, https://doi.org/10.1002/celc.201801876.
[12] T. Hu, I. Tang, H. Feng, J. Zhang, X. Li, Y. Zuo, Z. Lu, W. Tang, Metal-organic frameworks (MOFs) and their derivatives as emerging catalysts for electro-Fenton process in water purification, Coord. Chem. Rev. 451 (2022) 214227, https://doi.org/10.1016/j.ccr.2021.214277.
[13] T. Yu, C.B. Breslin, Graphene-modified composites and electrodes and their potential applications in the electro-Fenton process, Materials 13 (2020), https://doi.org/10.3390/ma13102254.
[14] S. Rafaqat, N. Ali, C. Torres, B. Rittmann, Recent progress in treatment of dyes wastewater using microbial-electro-Fenton Technology, RSC Adv. 12 (2022) 17104–17137, https://doi.org/10.1039/d2ra01831d.
[15] S.M. Sathe, I. Chakraborty, B.K. Dubey, M.M. Ghangrekar, Microbial fuel cell coupled Fenton oxidation for the cathodic degradation of emerging contaminants from wastewater: applications and challenges, Environ. Res. 204 (2022) 112135, https://doi.org/10.1016/j.envres.2021.112135.
[16] E. Brillas, Progress of homogeneous and heterogeneous electro-Fenton treatments of antibiotics in synthetic and real wastewaters. A critical review on the period 2017-2021, Sci. Total Environ. 819 (2022) 153102, https://doi.org/10.1016/j.scitotenv.2022.153102.
[17] E. Brillas, Fenton, photo-Fenton, electro-Fenton, and their combined treatments for the removal of insecticides from waters and soils. A review, Sep. Purif. Technol. 284 (2022) 120290. Doi:10.1016/j.seppur.2021.120290.
[18] E. Brillas, Recent development of electrochemical advanced oxidation of herbicides. A review on its application to wastewater treatment and soil remediation, J. Clean. Prod. 290 (2021) 125841, https://doi.org/10.1016/j.jclepro.2021.125841.
[19] E. Brillas, A critical review on ibuprofen removal from synthetic waters, natural waters, and real wastewaters by advanced oxidation processes, Chemosphere 286 (2022) 131849, https://doi.org/10.1016/j.chemosphere.2021.131849.
[20] B.T. Ergan, E. Gengec, Dye degradation and kinetics of online Electro-Fenton system with thermally activated carbon fiber cathodes, J. Environ. Chem. Eng. 8 (2020) 104217, https://doi.org/10.1016/j.jece.2020.104217.
[21] F.E. Titchou, H. Zazou, H. Afanga, J. El Gaayda, R. Ait Akbour, M. Hamdani, M. A. Oturan, Electro-Fenton process for the removal of Direct Red 23 using BDD anode in chloride and sulfate media, J. Electroanal. Chem. 897 (2021) 115560, https://doi.org/10.1016/j.jelechem.2021.115560.
[22] D. Villaseñor-Basulto, A. Picos-Benítez, N. Bravo-Yumi, T. Perez-Segura, E. R. Bandala, J.M. Peralta-Hernández, Electro-Fenton mineralization of diazo dye Black NT2 using a pre-pilot flow plant, J. Electroanal. Chem. 895 (2021) 115492, https://doi.org/10.1016/j.jelechem.2021.115492.
[23] E. Rosales, D. Anasie, M. Pazos, I. Lazar, M.A. Sanromán, Kaolinite adsorption-regeneration system for dyestuff treatment by Fenton based processes, Sci. Total Environ. 622–623 (2018) 556–562, https://doi.org/10.1016/j.scitotenv.2017.11.301.
[24] A. Sennaoui, S. Alahiane, F. Sakr, A. Assabbane, E.H.A. Addi, M. Hamdani, Advanced oxidation of Reactive Yellow 17 dye: a comparison between Fenton, photo-Fenton, electro-Fenton, anodic oxidation and heterogeneous photocatalysis processes, Port. Electrochim. Acta 36 (2018) 163–178, https://doi.org/10.4152/pea.201803163.
[25] C. Yang, X. Kong, L. Zhu, D. Wang, Application of electro-Fenton internal circulation batch reactor for Methylene Blue removal with a focus on optimization by response surface method, Desal, Water Treat. 132 (2018) 307–316, https://doi.org/10.5004/dwt.2018.23057.
[26] G. Matyszczak, A. Fidler, E. Polesiak, M. Sobieska, K. Morawiec, W. Zajkowska, K. Lawniczak-Jablonska, P. Kuzmiuk, Application of sonochemically synthesized SnS and SnS_2 in the electro-Fenton process: kinetics and enhanced decolorization, Ultrason. Sonochem. 68 (2020) 105186, https://doi.org/10.1016/j.ultsonch.2020.105186.
[27] G. Matyszczak, A. Sedkowska, S. Kus, Comparative degradation of Metanil Yellow in the electro-Fenton process with different catalysts: a simplified kinetic model

study, Dyes Pigments 174 (2020) 108076, https://doi.org/10.1016/j.dyepig.2019.108076.
[28] G. Matyszczak, K. Krzyczkowska, A. Fidler, A novel, two-electron catalysts for the electro-Fenton process, J. Water Process Eng. 36 (2020) 101242, https://doi.org/10.1016/j.jwpe.2020.101242.
[29] G. Matyszczak, K. Krzyczkowska, K. Krawczyk, Removal of Bromocresol Green from aqueous solution by electro-Fenton and electro-Fenton-like processes with different catalysts: Laboratory and kinetic model investigation, Water Sci. Technol. 84 (2021) 3227-3236. https:/doi.org/10.2166/wst.2021.407.
[30] M. Ebratkhahan, S. Naghash Hamed, M. Zarei, A. Jafarizad, M. Rostamizadeh, Removal of Neutral Red dye via electro-Fenton process: a response surface methodology modeling, Electrocatalysis 12 (2021) 579–594, https://doi.org/10.1007/s12678-021-00640-3.
[31] A.A. Elbatea, S.A. Nosier, A.A. Zatout, I. Hassan, G.H. Sedahmed, M.H. Abdel-Aziz, M.A. El-Naggar, Removal of Reactive red 195 from dyeing wastewater using electro-Fenton process in a cell with oxygen sparged fixed bed electrodes, J. Water Process Eng. 41 (2021) 102042, https://doi.org/10.1016/j.jwpe.2021.102042.
[32] A. Adachi, F. El Ouadrhiri, M. Kara, I. El Manssouri, A. Assouguem, M. H. Almutairi, R. Bayram, H.R.H. Mohamed, I. Peluso, N. Eloutassi, A. Lahkimi, Decolorization and degradation of Methyl Orange azo dye in aqueous solution by the electro Fenton process: application of optimization, Catalysts 12 (2022), https://doi.org/10.3390/catal12060665.
[33] A. Wakrim, Z. Zaroual, S.E. Ghachtouli, J.J. Eddine, M. Azzi, Treatment and degradation of azo dye waste industry by electro-Fenton process, Phys. Chem. Res. 10 (2022) 495–504, https://doi.org/10.22036/PCR.2022.315931.1991.
[34] B. Bouzayani, E. Bocos, S.C. Elaoud, M. Pazos, M.Á. Sanromán, E. González-Romero, An effective electroanalytical approach for the monitoring of electroactive dyes and intermediate products formed in electro-Fenton treatment, J. Electroanal. Chem. 808 (2018) 403–411, https://doi.org/10.1016/j.jelechem.2017.06.035.
[35] A.A. Özcan, A. Özcan, Investigation of applicability of electro-Fenton method for the mineralization of naphthol blue black in water, Chemosphere 202 (2018) 618–625, https://doi.org/10.1016/j.chemosphere.2018.03.125.
[36] S.Z.J. Zaidi, F.C. Walsh, C. Harito, Mass transport control of oxygen reduction at graphite felt with subsequent decolourisation of RB-5 dye in a parallel plate flow reactor, J. Taiwan Inst. Chem. Eng. 104 (2019) 123–129, https://doi.org/10.1016/j.jtice.2019.08.020.
[37] H. Afanga, H. Zazou, F.E. Titchou, J.E. Gaayda, F. Sopaj, R.A. Akbour, M. Hamdani, Electrochemical oxidation of Naphthol Blue Black with different supporting electrolytes using a BDD/carbon felt cell, J. Environ. Chem. Eng. 9 (2021) 104498, https://doi.org/10.1016/j.jece.2020.104498.
[38] Z. Benredjem, K. Barbari, I. Chaabna, S. Saaidia, A. Djemel, R. Delimi, S. Douas, K. Bakhouche, Comparative investigation on the removal of Methyl Orange from aqueous solution using three different advanced oxidation processes, Int. J. Chem. React. Eng. 19 (2021) 597–604, https://doi.org/10.1515/ijcre-2020-0243.
[39] S.A. Hien, C. Trellu, N. Oturan, A.S. Assémian, B.G.H. Briton, P. Drogui, K. Adouby, M.A. Oturan, Comparison of homogeneous and heterogeneous electrochemical advanced oxidation processes for treatment of textile industry wastewater, J. Hazard. Mater. 437 (2022) 129326, https://doi.org/10.1016/j.jhazmat.2022.129326.
[40] B. Ramírez-Pereda, A. Álvarez-Gallegos, J.G. Rangel-Peraza, Y.A. Bustos-Terrones, Kinetics of Acid Orange 7 oxidation by using carbon fiber and reticulated vitreous carbon in an electro-Fenton process, J. Environ. Manage. 213 (2018) 279–287, https://doi.org/10.1016/j.jenvman.2018.01.022.
[41] Y.A. Bustos-Terrones, J.J. Hermosillo-Nevárez, B. Ramírez-Pereda, M. Vaca, J. G. Rangel-Peraza, V. Bustos-Terrones, M.N. Rojas-Valencia, Removal of BB9 textile dye by biological, physical, chemical, and electrochemical treatments, J. Taiwan Inst. Chem. Eng. 121 (2021) 29–37, https://doi.org/10.1016/j.jtice.2021.03.041.
[42] E. Lacasa, P. Cañizares, F.C. Walsh, M.A. Rodrigo, C. Ponce-de-León, Removal of Methylene Blue from aqueous solutions using an Fe^{2+} catalyst and in-situ H_2O_2 generated at gas diffusion cathodes, Electrochim. Acta 308 (2019) 45–53, https://doi.org/10.1016/j.electacta.2019.03.218.
[43] P.C. Soto, C.A.R. Salamanca-Neto, J.T. Moraes, E.R. Sartori, G.G. Bessegato, F. Lopes, L.C. Almeida, A novel sensing platform based on self-doped TiO_2 nanotubes for Methylene Blue dye electrochemical monitoring during its electro-Fenton degradation, J. Solid State Electrochem. 24 (2020) 1951–1959, https://doi.org/10.1007/s10008-020-04509-1.
[44] H. Huang, C. Han, G. Wang, C. Feng, Lignin combined with polypyrrole as a renewable cathode material for H_2O_2 generation and its application in the electro-Fenton process for azo dye removal, Electrochim. Acta 259 (2018) 637–646, https://doi.org/10.1016/j.electacta.2017.11.014.
[45] H. Xu, H. Guo, C. Chai, N. Li, X. Lin, W. Xu, Anodized graphite felt as an efficient cathode for in-situ hydrogen peroxide production and electro-Fenton degradation of Rhodamine B, Chemosphere 286 (2022), 131936, https://doi.org/10.1016/j.chemosphere.2021.131936.
[46] W. Zhou, X. Meng, J. Gao, F. Sun, G. Zhao, Janus graphite felt cathode dramatically enhance the H_2O_2 yield from O_2 electroreduction by the hydrophilicity-hydrophobicity regulation, Chemosphere 278 (2021) 130382, https://doi.org/10.1016/j.chemosphere.2021.130382.
[47] T.X. Huong Le, B. Alemán, J.J. Vilatela, M. Bechelany, M. Cretin, Enhanced electro-Fenton mineralization of Acid Orange 7 using a carbon nanotube fiber-based cathode, Front. Mater. 5 (2018), https://doi.org/10.3389/fmats.2018.00009.
[48] S. Tu, Z. Ning, X. Duan, X. Zhao, L. Chang, Efficient electrochemical hydrogen peroxide generation using TiO_2/rGO catalyst and its application in electro-Fenton degradation of Methyl Orange, Colloids Surf. A: Physicochem. Eng. Asp. 651 (2022) 129657, https://doi.org/10.1016/j.colsurfa.2022.129657.
[49] Y.-J. Ko, H.-G. Kim, M.G. Seid, K. Cho, J.-W. Choi, W.-S. Lee, S.W. Hong, Ionic-liquid-derived nitrogen-doped carbon electrocatalyst for peroxide generation and divalent iron regeneration: its application for removal of aqueous organic compounds, ACS Sustain. Chem. Eng. 6 (2018) 14857–14865, https://doi.org/10.1021/acssuschemeng.8b03383.
[50] C. Chen, Y. Zhu, M. Tian, Y. Chen, Y. Yang, K. Jiang, S. Gao, Sustainable self-powered electro-Fenton degradation using N, S co-doped porous carbon catalyst fabricated with adsorption-pyrolysis-doping strategy, Nano Energy 81 (2021) 105623, https://doi.org/10.1016/j.nanoen.2020.105623.
[51] C. Chen, M. Tian, H. Han, D. Wu, Y. Chen, Z. Gao, S. Gao, K. Jiang, N, P-dual doped carbonaceous catalysts derived from bifunctional-salt activation for effective electro-Fenton degradation on waterborne organic pollutions, Electrochim. Acta 389 (2021) 138732, https://doi.org/10.1016/j.electacta.2021.138732.
[52] C. Chen, H. Han, X. Liu, Y. Chen, D. Wu, Z. Gao, S. Gao, K. Jiang, Nitrogen, phosphorus, sulfur tri-doped porous carbon derived from covalent polymer with versatile performances in supercapacitor, oxygen reduction reaction and electro-Fenton degradation, Micropor. Mesopor. Mater. 325 (2021) 111335, https://doi.org/10.1016/j.micromeso.2021.111335.
[53] J.L. Colades, C.-P. Huang, J.D. Retumban, S. Garcia-Segura, M.D.G. de Luna, Electrochemically-driven dosing of iron (II) for autonomous electro-Fenton processes with in situ generation of H_2O_2, J. Electroanal. Chem. 856 (2020) 113639, https://doi.org/10.1016/j.jelechem.2019.113639.
[54] B. Temur Ergan, M. Soybelli, E. Gengec, E., Impact of thermal modification of carbon felt on the performance of oxygen reduction reaction and mineralisation of dye in on-line electro Fenton system, Int. J. Environ. Anal. Chem. (2021), https://doi.org/10.1080/03067319.2021.2015341.
[55] Y. Jiao, L. Ma, Y. Tian, M. Zhou, A flow-through electro-Fenton process using modified activated carbon fiber cathode for Orange II removal, Chemosphere 252 (2020) 126483, https://doi.org/10.1016/j.chemosphere.2020.126483.
[56] X. Zhao, H. Yang, J. Xu, T. Cheng, Y. Li, Bimetallic PdAu nanoframes for electrochemical H_2O_2 production in acids, ACS Mater. Lett. 3 (2021) 996–1002, https://doi.org/10.1021/acsmaterialslett.1c00263.
[57] Y.-T. Wang, C.-H. Tu, Y.-S. Lin, Application of graphene and carbon nanotubes on carbon felt electrodes for the electro-Fenton system, Materials 12 (2019), https://doi.org/10.3390/MA12101698.
[58] L. Zhang, J. Liang, L. Yue, Z. Xu, K. Dong, Q. Liu, Y. Luo, T. Li, X. Cheng, G. Cui, B. Tang, A.A. Alshehri, K.A. Alzahrani, X. Guo, X. Sun, N-doped carbon nanotubes supported $CoSe_2$ nanoparticles: a highly efficient and stable catalyst for H_2O_2 electrosynthesis in acidic media, Nano Res. 15 (2022) 304-309. https:/doi.org/10.1007/s12274-021-3474-0.
[59] H. Zhang, Y. Li, Y. Zhao, G. Li, F. Zhang, Carbon black oxidized by air calcination for enhanced H_2O_2 generation and effective organics degradation, ACS Appl. Mater. Interfaces 11 (2019) 27846–27853, https://doi.org/10.1021/acsami.9b07765.
[60] S. Qiu, L. Yu, D. Tang, W. Ren, K. Chen, J. Sun, Rapidly enhanced electro-Fenton efficiency by in situ electrochemistry-activated graphite cathode, Ind. Eng. Chem. Res. 57 (2018) 4907–4915, https://doi.org/10.1021/acs.iecr.7b05380.
[61] A.K. Ortiz-Martínez, L.A. Godínez, C. Martínez-Sánchez, J.D. García-Espinoza, I. Robles, Preparation of modified carbon paste electrodes from orange peel and used coffee ground. New materials for the treatment of dye-contaminated solutions using electro-Fenton processes, Electrochim. Acta 390 (2021) 138861, https://doi.org/10.1016/j.electacta.2021.138861.
[62] Y. Wang, B. Lin, Enhancement of performance for graphite felt modified with carbon nanotubes activated by KOH as cathode in electro-Fenton systems, J. Appl. Biomater. Funct. Mater. 19 (2021), https://doi.org/10.1177/22808000211005386.
[63] M.A.N. Mohd Nohan, C.H. Chia, A.S. Hashimi, S.X. Chin, P.S. Khiew, S. Zakaria, A. Azmi, K.S. Lau, N.F. Razali, Highly stable binder free CNTs/rGO aerogel electrode for decolouration of Methylene Blue & palm oil mill effluent via electro-Fenton oxidation process, RSC Adv. 9 (2019) 16472–16478, https://doi.org/10.1039/c9ra02364j.
[64] M. Liu, Y. Yu, S. Xiong, P. Lin, L. Hu, S. Chen, H. Wang, L. Wang, A flexible and efficient electro-Fenton cathode film with aeration function based on polyphenylene sulfide ultra-fine fiber, React. Funct. Polym. 139 (2019) 42–49, https://doi.org/10.1016/j.eactfunctpolym.2019.03.009.
[65] H. Su, Y. Chu, B. Miao, Degreasing cotton used as pore-creating agent to prepare hydrophobic and porous carbon cathode for the electro-Fenton system: enhanced H_2O_2 generation and RhB degradation, Environ. Sci. Pollut. Res. 28 (2021) 33570–33582, https://doi.org/10.1007/s11356-021-12965-z.
[66] J. Liu, J. Jia, H. Yu, J. Zhang, J. Li, H. Ge, Y. Zhao, Graphite felt modified by nanoporous carbon as a novel cathode material for the EF process, New J. Chem. 46 (2022) 12696–12702, https://doi.org/10.1039/d2nj01679f.
[67] F. Deng, J. Jiang, I. Sirés, State-of-the-art review and bibliometric analysis on electro-Fenton process, Carbon Lett. (2022), https://doi.org/10.1007/s42823-022-00420-z.
[68] Y. Yao, Q. Chen, Z. Huang, J. Zhou, Catalytic activity comparison of typical iron-bearing particle electrodes in heterogeneous electro-Fenton oxidation processes, Environ. Technol. Innov. 21 (2021) 101321, https://doi.org/10.1016/j.eti.2020.101321.
[69] W. Sun, N. Yu, J. Chen, Z. Gu, J. Wei, Y. Yao, Heterogeneous Ti/PbO_2-electro-Fenton degradation of aromatic methane dyes using industrial pyrite waste slag

as catalyst, Environ. Sci. Pollut. Res. 29 (2022) 50218–50236, https://doi.org/10.1007/s11356-022-19372-y.
[70] N. Ben Hafaiedh, F. Fourcade, N. Bellakhal, A. Amrane, Iron oxide nanoparticles as heterogeneous electro-Fenton catalysts for the removal of AR18 azo dye, Environ. Technol. (United Kingdom) 41 (2020) 2146–2153, https://doi.org/10.1080/09593330.2018.1557258.
[71] S.O. Ganiyu, E.C.T. de Araújo Costa, C.A. Martínez-Huitle, E.V. dos Santos, Electro-Fenton catalyzed by Fe-rich lateritic soil for the treatment of food colorant Bordeaux Red (E123): catalyst characterization, optimization of operating conditions and mechanism of oxidation, Sep. Purif. Technol. 242 (2020) 116776. Doi:10.1016/j.seppur.2020.116776.
[72] A. Cruz del Álamo, R. Zou, M.I. Pariente, R. Molina, F. Martínez, Y. Zhang, Catalytic activity of $LaCu_{0.5}Mn_{0.5}O_3$ perovskite at circumneutral/basic pH conditions in electro-Fenton processes, Catal. Today 361 (2021) 159–164, https://doi.org/10.1016/j.cattod.2020.03.027.
[73] H. Mohammadi, A. Alinejad, M. Khajeh, M. Darvishmotevalli, M. Moradnia, A. M. Tehrani, G. Hosseindost, M.R. Zare, N. Mengelizadeh, Optimization of the 3D electro-Fenton process in removal of Acid Orange 10 from aqueous solutions by response surface methodology, J. Chem. Technol. Biotechnol. 94 (2019) 3158–3171, https://doi.org/10.1002/jctb.6122.
[74] K. Karuppasamy, P. Santhoshkumar, T. Hussain, D. Vikraman, C.-J. Yim, S. Hussain, P. Shanmugam, A. Alfantazi, S. Manickam, H.-S. Kim, Influence of selenium precursors on the formation of iron selenide nanostructures ($FeSe_2$): efficient electro-Fenton catalysts for detoxification of harmful organic dyestuffs, Chemosphere 272 (2021) 129639, https://doi.org/10.1016/j.chemosphere.2021.129639.
[75] M. Zuo, S. Yi, J. Choi, Excellent dye degradation performance of FeSiBP amorphous alloys by Fenton-like process, J. Environ. Sci. (China) 105 (2021) 116–127, https://doi.org/10.1016/j.jes.2020.12.032.
[76] P. Nazari, S.R. Setayesh, Effective degradation of Reactive Red 195 via heterogeneous electro-Fenton treatment: theoretical study and optimization, Int. J. Environ. Sci. Technol. 16 (2019) 6329–6346, https://doi.org/10.1007/s13762-018-2048-5.
[77] M. Rostamizadeh, A. Jafarizad, S. Gharibian, High efficient decolorization of Reactive Red 120 azo dye over reusable Fe-ZSM-5 nanocatalyst in electro-Fenton reaction, Sep. Purif. Technol. 192 (2018) 340–347, https://doi.org/10.1016/j.seppur.2017.10.041.
[78] A.A. Zahrani, B. Ayati, Improving Fe-based heterogeneous electro-Fenton nano catalyst using transition metals in a novel orbiting electrodes reactor, Chemosphere 256 (2020) 127049, https://doi.org/10.1016/j.chemosphere.2020.127049.
[79] A.A. Zahrani, B. Ayati, Using heterogeneous Fe-ZSM-5 nanocatalyst to improve the electro Fenton process for Acid Blue 25 removal in a novel reactor with orbiting electrodes, J. Electroanal. Chem. 873 (2020) 114456, https://doi.org/10.1016/j.jelechem.2020.114456.
[80] D.R.S. Cruz, G.K. de Jesus, C.A. Santos, W.R. Silva, A. Wisniewski Jr., G.C. Cunha, L.P.C. Romão, Magnetic nanostructured material as heterogeneous catalyst for degradation of AB210 dye in tannery wastewater by electro-Fenton process, Chemosphere 280 (2021) 130675, https://doi.org/10.1016/j.chemosphere.2021.130675.
[81] A.J. dos Santos, G. da Costa Cunha, D.R.S. Cruz, L.P.C. Romeo, C.A. Martínez-Huitle, Iron mining wastes collected from Mariana disaster: reuse and application as catalyst in a heterogeneous electro-Fenton process, J. Electroanal. Chem. 848 (2019) 113330, https://doi.org/10.1016/j.jelechem.2019.113330.
[82] R. Jinisha, R. Gandhimathi, S.T. Ramesh, P.V. Nidheesh, S. Velmathi, Removal of Rhodamine B dye from aqueous solution by electro-Fenton process using iron-doped mesoporous silica as a heterogeneous catalyst, Chemosphere 200 (2018) 446–454, https://doi.org/10.1016/j.chemosphere.2018.02.117.
[83] Q. Wang, S. Zhou, S. Xiao, F. Wei, X. Zhao, J. Qu, H. Wang, Novel perovskite-based composites, $La_{1-x}Nd_xFeO_3$@activated carbon, as efficient catalysts for the degradation of organic pollutants by heterogeneous electro-Fenton reactions, RSC Adv. 8 (2018) 14775–14786, https://doi.org/10.1039/c8ra00244d.
[84] P. Nazari, P. Tootoonchian, S.R. Setayesh, Efficient degradation of AO7 by ceria-delafossite nanocomposite with non-inert support as a synergistic catalyst in electro-Fenton process, Environ. Pollut. 252 (2019) 749–757, https://doi.org/10.1016/j.envpol.2019.06.011.
[85] C. Zhang, G. Ren, W. Wang, X. Yu, F. Yu, Q. Zhang, M. Zhou, A new type of continuous-flow heterogeneous electro-Fenton reactor for Tartrazine degradation, Sep. Purif. Technol. 208 (2019) 76–82, https://doi.org/10.1016/j.seppur.2018.05.016.
[86] M. Fayazi, M. Ghanei-Motlagh, Electrochemical mineralization of Methylene Blue dye using electro-Fenton oxidation catalyzed by a novel sepiolite/pyrite nanocomposite, Int. J. Environ. Sci. Technol. 17 (2020) 4541–4548, https://doi.org/10.1007/s13762-020-02749-2.
[87] S.R. Setayesh, P. Nazari, R. Maghbool, Engineered $FeVO_4/CeO_2$ nanocomposite as a two-way superior electro-Fenton catalyst for model and real wastewater treatment, J. Environ. Sci. (China) 97 (2020) 110–119, https://doi.org/10.1016/j.jes.2020.04.035.
[88] Y. Yang, Y. Liu, X. Fang, W. Miao, X. Chen, J. Sun, B.-J. Ni, S. Mao, Heterogeneous electro-Fenton catalysis with HKUST-1-derived Cu@C decorated in 3D graphene network, Chemosphere 243 (2020) 125423, https://doi.org/10.1016/j.chemosphere.2019.125423.
[89] N. Taheri Ashtiani, B. Ayati, Using chitosan-based heterogeneous catalyst for degradation of Acid Blue 25 in the effective electro-Fenton process with rotating cathodes, J. Electroanal. Chem. 905 (2022) 115983, https://doi.org/10.1016/j.jelechem.2021.115983.
[90] N. Barhoumi, N. Oturan, H. Olvera-Vargas, E. Brillas, A. Gadri, S. Ammar, M. A. Oturan, Pyrite as a sustainable catalyst in electro-Fenton process for improving oxidation of sulfamethazine. Kinetics, mechanism and toxicity assessment, Water Res. 94 (2016) 52–61, https://doi.org/10.1016/j.watres.2016.02.042.
[91] G. da Costa Cunha, L.P.C. Romao, Z.S. Macedo, Production of alpha-alumina nanoparticles using aquatic humic substances, Powder Technol. 254 (2014) 344–351. Doi:10.1016/j.powtec.2014.01.008.
[92] E. Rosales, G. Buftia, M. Pazos, G. Lazar, M.A. Sanromán, Highly active based iron-carbonaceous cathodes for heterogeneous electro-Fenton process: application to degradation of parabens, Process Saf. Environ. Prot. 117 (2018) 363–371, https://doi.org/10.1016/j.psep.2018.05.014.
[93] Z. Xu, L. Qin, Y. Zhang, X. Li, J. Nan, X. Guo, G. Zhang, In-situ green assembly of spherical Mn-based metal-organic composites by ion exchange for efficient electrochemical oxidation of organic pollutant, J. Hazard. Mater. 369 (2019) 299–308, https://doi.org/10.1016/j.jhazmat.2019.02.050.
[94] Y. Huang, C. Han, Y. Liu, M.N. Nadagouda, L. Machala, K.E. O'Shea, V.K. Sharma, D.D. Dionysiou, Degradation of atrazine by $Zn_xCu_{1-x}Fe_2O_4$ nanomaterial-catalyzed sulfite under UV–vis light irradiation: green strategy to generate $SO_4^{\bullet-}$, Appl. Catal. B: Environ. 221 (2018) 380-392. https://doi.org/10.1016/j.apcatb.2017.09.001.
[95] C. Chi, X. Zhou, Y. Wang, H. Zhang, G. Meng, Y. Hu, Z. Bai, Preparation of needle coke composite cathode and its treatment of RhB wastewater, J. Electroanal. Chem. 920 (2022) 116612, https://doi.org/10.1016/j.jelechem.2022.116612.
[96] W. Peng, W. Niu, S. Paerhati, W. Guo, J. Ma, J. Hou, Facile synthesis of n-Fe_3O_4/ACF functional cathode for efficient dye degradation through heterogeneous E-Fenton process, Catalysts 12 (2022), https://doi.org/10.3390/catal12080879.
[97] S. Zghal, I. Jedidi, M. Cretin, S. Cerneaux, D. Cot, S. Lagerge, S. Deabate, M. Abdelmouleh, Electroactive adsorbent composites of porous graphite carbon/carbon nanotube for highly efficient organic dye removal, Kor. J. Chem. Eng. 39 (2022) 2239–2251, https://doi.org/10.1007/s11814-022-1119-y.
[98] Z. Bencheqroun, N.E. Sahin, O.S.G.P. Soares, M.F.R. Pereira, H. Zaitan, M. Nawdali, E. Rombi, A.M. Fonseca, P. Parpot, I.C. Neves, Fe(III)-exchanged zeolites as efficient electrocatalysts for Fenton-like oxidation of dyes in aqueous phase, J. Environ. Chem. Eng. 10 (2022) 107891. https://doi.org 10.1016/j.jece.2022.107891.
[99] Y. Li, R. Lin, F. Lv, X. Zhao, T. Yong, X. Zuo, Tannic acid-Fe complex derivative-modified electrode with pH regulating function for environmental remediation by electro-Fenton process, Environ. Res. 204 (2022) 111994, https://doi.org/10.1016/j.envres.2021.111994.
[100] Y. Liu, C. Gao, L. Liu, T. Yu, Y. Li, Improved degradation of tetracycline, norfloxacin and Methyl Orange wastewater treatment with dual catalytic electrode assisted self-sustained Fe^{2+} electro-Fenton system: regulatory factors, mechanisms and pathways, Sep. Purif. Technol. 284 (2022) 120232, https://doi.org/10.1016/j.seppur.2021.120232.
[101] C.-T. Chiu, Y.-J. Teng, B.-H.Dai, B.-H. Tsao, W.-C. Lin, K.-W. Wang, L.-C. Hsu, Y.-C. Chang, C.-T. Li, H.T. Thai Nguyen, C.-Y. Chiang, W.-H. Hung, Novel high-entropy ceramic/carbon composite materials for the decomposition of organic pollutants, Mater. Chem. Phys. 275 (2022) 125274. https:/doi.org/10.1016/j.matchemphys.2021.125274.
[102] N.T. Dung, L.T. Duong, N.T. Hoa, V.D. Thao, L.V. Ngan, N.N. Huy, A comprehensive study on the heterogeneous electro-Fenton degradation of Tartrazine in water using $CoFe_2O_4$/carbon felt cathode, Chemosphere 287 (2022) 132141. https:/doi.org/10.1016/j.chemosphere.2021.132141.
[103] S.Z.J. Zaidi, Y. Luan, C. Harito, L. Utari, B. Yuliarto, F.C. Walsh, Synthesis and application of gas diffusion cathodes in an advanced type of undivided electrochemical cell, Sci. Rep. 10 (2020), https://doi.org/10.1038/s41598-020-74199-2.
[104] W. Yang, M. Zhou, L. Mai, H. Ou, N. Oturan, M.A. Oturan, E.Y. Zeng, Generation of hydroxyl radicals by metal-free bifunctional electrocatalysts for enhanced organics removal, Sci. Total Environ. 791 (2021) 148107, https://doi.org/10.1016/j.scitotenv.2021.148107.
[105] A. Barhoum, T. Favre, S. Sayegh, F. Tanos, E. Coy, I. Iatsunskyi, A. Razzouk, M. Cretin, M. Bechelany, 3d Self-supported nitrogen-doped carbon nanofiber electrodes incorporated Co/CoO_x nanoparticles: application to dyes degradation by electro-Fenton-based process, Nanomaterials 11 (2021), https://doi.org/10.3390/nano11102686.
[106] Y. Wang, Y. Lin, Study on the performance of nano-titanium nitride-coated stainless steel electrodes in electro-Fenton systems, Nanomaterials 8 (2018), https://doi.org/10.3390/nano8070494.
[107] L.-Z. Huang, M. Zhu, Z. Liu, Z. Wang, H.C.B. Hansen, Single sheet iron oxide: an efficient heterogeneous electro-Fenton catalyst at neutral pH, J. Hazard. Mater. 364 (2019) 39–47, https://doi.org/10.1016/j.jhazmat.2018.10.026.
[108] T.X. Huong Le, M. Drobek, M. Bechelany, J. Motuzas, A. Julbe, M. Cretin, Application of Fe-MFI zeolite catalyst in heterogeneous electro-Fenton process for water pollutants abatiment, Micropor. Mesopor. Mater. 278 (2019) 64–69, https://doi.org/10.1016/j.micromeso.2018.11.021.
[109] T.X.H. Le, M.G. Cowan, M. Drobek, M. Bechelany, A. Julbe, M. Cretin, Fe-nanoporous carbon derived from MIL-53(Fe): a heterogeneous catalyst for mineralization of organic pollutants, Nanomaterials 9 (2019), https://doi.org/10.3390/nano9040641.
[110] S.Z.J. Zaidi, E. Hurter, F.C. Walsh, C. Ponce de León, Fe(II)-Based GDE electrodes for the demineralization of Methylene Blue dye, Arab. J. Sci. Eng. 44 (2019) 5527–5533, https://doi.org/10.1007/s13369-019-03813-x.
[111] L. Zhou, Y. Xiao, J. Liang, D. Tang, J. Sun, Application of self-supplying iron cathode prepared by gas sludge in electro-Fenton, Emerg. Contam. 5 (2019) 61–69, https://doi.org/10.1016/j.emcon.2019.02.006.

[112] L. Cui, H. Huang, P. Ding, S. Zhu, W. Jing, X. Gu, Cogeneration of H_2O_2 and $^{\bullet}OH$ via a novel Fe_3O_4/MWCNTs composite cathode in a dual-compartment electro-Fenton membrane reactor, Sep. Purif. Technol. 237 (2020) 116380. Doi:10.1016/j.seppur.2019.116380.
[113] M. Ferreira, N.E. Sahin, A.M. Fonseca, P. Parpot, I.C. Neves, Oxidation of pollutantsviaan electro-Fenton-like process in aqueous media using iron-zeolite modified electrodes, New J. Chem. 45 (2021) 12750–12757, https://doi.org/10.1039/d1nj01077h.
[114] S. Biton Seror, D. Shamir, Y. Albo, H. Kornweitz, A. Burg, Elucidation of a mechanism for the heterogeneous electro-Fenton process and its application in the green treatment of azo dyes, Chemosphere 286 (2022) 131832. https:/doi.org/10.1016/j.chemosphere.2021.131832.
[115] Q. Wu, H. Zhang, L. Zhou, C. Bao, H. Zhu, Yi. Zhang , Synthesis and application of rGO/$CoFe_2O_4$ composite for catalytic degradation of methylene blue on heterogeneous Fenton-like oxidation, J. Taiwan Inst. Chem. Eng. 67 (2016) 484–494. Doi:10.1016/j.jtice.2016.08.004.
[116] P. Hong, Y. Li, J. He, A. Saeed, K. Zhang, C. Wang, L. Kong, J. Liu, Rapid degradation of aqueous doxycycline by surface $CoFe_2O_4/H_2O_2$ system: behaviors, mechanisms, pathways and DFT calculation, Appl. Surf. Sci 526 (2020) 146557, https://doi.org/10.1016/j.apsusc.2020.146557.
[117] Y. Zhang, G. Luo, Q. Wang, Y. Zhang, M. Zhou, Kinetic study of the degradation of Rhodamine B using a flow-through UV/electro-Fenton process with the presence of ethylenediaminetetraacetic acid, Chemosphere 240 (2020) 124929, https://doi.org/10.1016/j.chemosphere.2019.124929.
[118] S. Alcocer, A. Picos, A.R. Uribe, T. Pérez, J.M. Peralta-Hernández, Comparative study for degradation of industrial dyes by electrochemical advanced oxidation processes with BDD anode in a laboratory stirred tank reactor, Chemosphere 205 (2018) 682–689, https://doi.org/10.1016/j.chemosphere.2018.04.155.
[119] A.J. dos Santos, C.A. Martínez-Huitle, I. Sirés, E. Brillas, Use of Pt and boron-doped diamond anodes in the electrochemical advanced oxidation of Ponceau SS diazo dye in acidic sulfate medium, ChemElectroChem 5 (2018) 685–693, https://doi.org/10.1002/celc.201701238.
[120] E.C. Paz, L.R. Aveiro, V.S. Pinheiro, F.M. Souza, V.B. Lima, F.L. Silva, P. Hammer, M.R.V. Lanza, M.C. Santos, Evaluation of H_2O_2 electrogeneration and decolorization of Orange II azo dye using tungsten oxide nanoparticle-modified carbon, Appl. Catal. B: Environ. 232 (2018) 436–445, https://doi.org/10.1016/j.apcatb.2018.03.082.
[121] K.C. Nakamura, L.S. Guimaraes, A.G. Magdalena, A.C.D. Angelo, A.R. De Andrade, S. Garcia-Segura, A.R.F. Pipi, Electrochemically-driven mineralization of Reactive Blue 4 cotton dye: on the role of in situ generated oxidants, J. Electroanal. Chem. 840 (2019) 415–422, https://doi.org/10.1016/j.jelechem.2019.04.016.
[122] M.O.A. Pacheco-Álvarez, A. Picos, T. Pérez-Segura, J.M. Peralta-Hernández, Proposal for highly efficient electrochemical discoloration and degradation of azo dyes with parallel arrangement electrodes, J. Electroanal. Chem. 838 (2019) 195–203, https://doi.org/10.1016/j.jelechem.2019.03.004.
[123] L.R. Aveiro, A.G.M. da Silva, E.G. Candido, E.C. Paz, V.S. Pinheiro, L.S. Parreira, F.M. Souza, V.S. Antonin, P.H.C. Camargo, M.C. dos Santos, MnO_2/Vulcan-based gas diffusion electrode for mineralization of diazo dye in simulated effluent, Electrocatalysis 11 (2020) 268–274, https://doi.org/10.1007/s12678-020-00583-1.
[124] J. Kong, W. Huang, S. Yang, H. He, C. Sun, Q. Xian, D. Jiang, Photoelectro-Fenton system including electromagnetic induction electrodeless lamp and black carbon poly tetra fluoro ethylene air-diffusion cathode: degradation kinetics, intermediates and pathway for azo dye, Chemosphere 253 (2020) 126708, https://doi.org/10.1016/j.chemosphere.2020.126708.
[125] A.A. Márquez, I. Sirés, E. Brillas, J.L. Nava, Mineralization of Methyl Orange azo dye by processes based on H_2O_2 electrogeneration at a 3D-like air-diffusion cathode, Chemosphere 259 (2020) 127466, https://doi.org/10.1016/j.chemosphere.2020.127466.
[126] F. Medrano-Rodríguez, A. Picos-Benítez, E. Brillas, E.R. Bandala, T. Pérez, J. M. Peralta-Hernández, Electrochemical advanced oxidation discoloration and removal of three brown diazo dyes used in the tannery industry, J. Electroanal. Chem. 873 (2020) 114360, https://doi.org/10.1016/j.jelechem.2020.114360.
[127] M. Corona-Bautista, A. Picos-Benítez, D. Villaseñor-Basulto, E. Bandala, J. M. Peralta-Hernández, Discoloration of azo dye Brown HT using different advanced oxidation processes, Chemosphere 267 (2021) 129234, https://doi.org/10.1016/j.chemosphere.2020.129234.
[128] F.E. Titchou, H. Zazou, H. Afanga, E.G. Jamila, R. Ait Akbour, M. Hamdani, M. A. Oturan, Comparative study of the removal of Direct Red 23 by anodic oxidation, electro-Fenton, photo-anodic oxidation and photoelectro-Fenton in chloride and sulfate media, Environ. Res. 204 (2022) 112353, https://doi.org/10.1016/j.envres.2021.112353.
[129] M.F. Murrieta, I. Sirés, E. Brillas, J.L. Nava, Mineralization of Acid Red 1 azo dye by solar photoelectro-Fenton-like process using electrogenerated HClO and photoregenerated Fe(II), Chemosphere 246 (2020) 125697, https://doi.org/10.1016/j.chemosphere.2019.125697.
[130] A.J. dos Santos, I. Sirés, C.A. Martínez-Huitle, E. Brillas, Total mineralization of mixtures of Tartrazine, Ponceau SS and Direct Blue 71 azo dyes by solar photoelectro-Fenton in pre-pilot plant, Chemosphere 210 (2018) 1137–1144, https://doi.org/10.1016/j.chemosphere.2018.07.116.
[131] A.S. Fajardo, A.J. dos Santos, E.C.T. de Araújo Costa, D.R. da Silva, C.A. Martínez-Huitle, Effect of anodic materials on solar photoelectro-Fenton process using a diazo dye as a model contaminant, Chemosphere 225 (2019) 880–889, https://doi.org/10.1016/j.chemosphere.2019.03.071.
[132] R. Salazar, J. Gallardo-Arriaza, J. Vidal, C. Rivera-Vera, C. Toledo-Neira, M. A. Sandoval, L. Cornejo-Ponce, A. Thiam, Treatment of industrial textile wastewater by the solar photoelectro-Fenton process: influence of solar radiation and applied current, Solar Energy 190 (2019) 82–91, https://doi.org/10.1016/j.solener.2019.07.072.
[133] E.C. Paz, V.S. Pinheiro, J.F.S. Joca, R.A.S. de Souza, T.C. Gentil, M.R.V. Lanza, H. P.M. de Oliveira, A.M.P. Neto, I. Gaubeur, M.C. Santos, Removal of Orange II (OII) dye by simulated solar photoelectro-Fenton and stability of $WO_{2.72}$/Vulcan XC72 gas diffusion electrode, Chemosphere 239 (2020) 124670, https://doi.org/10.1016/j.chemosphere.2019.124670.
[134] D. Clematis, P. Panizza, Electro-Fenton, solar photoelectro-Fenton and UVA photoelectro-Fenton: degradation of Erythrosine B dye solution, Chemosphere 270 (2021) 129480, https://doi.org/10.1016/j.chemosphere.2020.129480.
[135] A.J. dos Santos, E.C.T.A. Costa, D.R. da Silva, S. Garcia-Segura, C.A. Martínez-Huitle, Electrochemical advanced oxidation processes as decentralized water treatment technologies to remediate domestic washing machine efluents, Environ. Sci. Pollut. Res. 25 (2018) 7002–7011, https://doi.org/10.1007/s11356-017-1039-2.
[136] L.R. Aveiro, A.G.M. da Silva, E.G. Candido, V.S. Antonin, L.S. Parreira, R. Papai, I. Gaubeur, F.L. Silva, M.R.V. Lanza, P.H.C. Camargo, M.C. Santos, Application and stability of cathodes with manganese dioxide nanoflowers supported on Vulcan by Fenton systems for the degradation of RB5 azo dye, Chemosphere 208 (2018) 131–138, https://doi.org/10.1016/j.chemosphere.2018.05.107.
[137] A.C.N. Pinheiro, T.S. Bernardino, F.E.B. Junior, M.R.V. Lanza, W.R.P. Barros, Enhanced electrodegradation of the Sunset Yellow dye in acid media by heterogeneous photoelectro-Fenton process using Fe_3O_4 nanoparticles as a catalyst, J. Environ. Chem. Eng. 8 (2020) 103621, https://doi.org/10.1016/j.jece.2019.103621.
[138] S. Aflaki, M. Farhadian, A.R. Solaimany Nazar, S. Tangestaninejad, N. Davari, Investigation of copper plates as anode and TiO_2/glycine/$ZnFe_2O_4$ stabilized on graphite as cathode for textile dyes degradation from aqueous solution under visible light, J. Appl. Electrochem. 51 (2021) 1387–1405, https://doi.org/10.1007/s10800-021-01580-y.
[139] A.J. dos Santos, I. Sirés, A.P.M. Alves, C.A. Martínez-Huitle, E. Brillas, Vermiculite as heterogeneous catalyst in electrochemical Fenton-based processes: application to the oxidation of Ponceau SS dye, Chemosphere 240 (2020) 124838, https://doi.org/10.1016/j.chemosphere.2019.124838.
[140] W. Wang, J. Jiang, C. Zhang, Q. Zhao, K. Wang, J. Lv, Micro-electricity utilization performance and microbial mechanism in microbial fuel cell powered electro-Fenton system for azo dye treatment, Biochem. Eng. J. 186 (2022) 108583, https://doi.org/10.1016/j.bej.2022.108583.
[141] T. Huang, L. Liu, J. Tao, L. Zhou, S. Zhang, Microbial fuel cells coupling with the three-dimensional electro-Fenton technique enhances the degradation of Methyl Orange in the wastewater, Environ. Sci. Pollut. Res. 25 (2018) 17989–18000, https://doi.org/10.1007/s11356-018-1976-4.
[142] D. Wang, J. Hu, B. Liu, H. Hou, J. Yang, Y. Li, Y. Zhu, S. Liang, K. Xiao, Degradation of refractory organics in dual-cathode electro-Fenton using air-cathode for H_2O_2 electrogeneration and microbial fuel cell cathode for Fe^{2+} regeneration, J. Hazard. Mater. 412 (2021) 125269, https://doi.org/10.1016/j.jhazmat.2021.125269.
[143] X. Yu, W. Fu, M. Jiang, G. Liu, Y. Zou, S. Chen, Automatic microbial electro-Fenton system driven by transpiration for degradation of Acid Orange 7, Sci. Total Environ. 725 (2020) 138508, https://doi.org/10.1016/j.scitotenv.2020.138508.
[144] K. Joksimovic, I. Kodranoc, D. Randjelovic, L. Slavkovic Beskoski, J. Radulovic, M. Ljesevic, D. Manojlovic, V.P. Beskoski, Microbial fuel cells as an electrical energy source for degradation followed by decolorization of Reactive Black 5 azo dye, Bioelectrochemistry 145 (2022) 108088, https://doi.org/10.1016/j.bioelechem.2022.108088.
[145] B. Gozmen, O. Sonmez, A. Sozutek, Comparative mineralization of Basic Red 18 with electrochemical advanced oxidation processes, J. Serb. Chem. Soc. 83 (2018) 93–105, https://doi.org/10.2298/JSC170227095G.
[146] M. Rastgar, J. Fleck, R. Graessner, A. Taghipour, M. Sadrzadeh, Smart harvesting and in-situ application of piezoelectricity in membrane filtration systems, J. Membr. Sci. 660 (2022) 120819, https://doi.org/10.1016/j.memsci.2022.120819.
[147] S.-H. Thor, L.-N. Ho, S.-A. Ong, N. Nordin, Y.-P. Ong, K.-L. Yap, Explicating the importance of aeration and pH for Amaranth degradation and electricity generation in a viable hybrid system of photocatalytic fuel cell and electro-Fenton process, Sep. Purif. Technol. 239 (2020) 116535, https://doi.org/10.1016/j.seppur.2020.116535.
[148] S.-H. Thor, L.-N. Ho, S.-A. Ong, C.Z.A. Abidin, C.-Y. Heah, N. Nordin, Y.P. Ong, K.-L. Yap, Advanced oxidation treatment of amaranth dye synchronized with electricity generation using carbon-based cathodes in a sustainable photocatalytic fuel cell integrated electro-Fenton system, J. Environ. Chem. Eng. 9 (2021) 106439, https://doi.org/10.1016/j.jece.2021.106439.
[149] S.-H. Thor, L.-N. Ho, S.-A. Ong, C.Z.A. Abidin, C.-Y. Heah, N. Nordin, Y.-P. Ong, K.-L. Yap, Discovering the roles of electrode distance and configuration in dye degradation and electricity generation in photocatalytic fuel cell integrated electro-Fenton process, Sep. Purif. Technol. 278 (2022) 119652. https:/doi.org/10.1016/j.seppur.2021.119652.
[150] A.S. Naje, I.S. Samaka, H.M. Zwain, M.A. Ajeel, Photovoltaic cell electro-Fenton oxidation process for treatment of organic content in Methyl Orange wastewater, J. Sustain. Sci. Manage. 16 (2021), https://doi.org/10.46754/JSSM.2021.06.005.
[151] J.D. García-Espinoza, I. Robles, A. Durán-Moreno, L.A. Godínez, Study of simultaneous electro-Fenton and adsorption processes in a reactor containing

porous carbon electrodes and particulate activated carbon, J. Electroanal. Chem. 895 (2021) 115476, https://doi.org/10.1016/j.jelechem.2021.115476.
[152] I. Robles, G. Moreno-Rubio, J.D. Garcia-Espinoza, C. Martínez-Sánchez, A. Rodríguez, Y. Meas-Vong, F.J. Rodríguez-Valadez, L.A. Godínez, Study of polarized activated carbon filters as simultaneous adsorbent and 3D-type electrode materials for electro-Fenton reactors, J. Environ. Chem. Eng. 8 (2020) 104414, https://doi.org/10.1016/j.jece.2020.104414.
[153] F. Ghanbari, F. Zirrahi, K.-Y.-A. Lin, B. Kakavandi, A. Hassani, Enhanced electro-peroxone using ultrasound irradiation for the degradation of organic compounds: a comparative study, J. Environ Chem. Eng. 8 (2020) 194167, https://doi.org/10.1016/j.jece.2020.104167.
[154] N. Mahmoudi, M. Farhadian, A.R. Solaimany Nazar, P. Eskandari, K.N. Esfahani, Investigation and optimization of the performance of sono-photo-electro-Fenton process for removal of Acid Black 172 and Disperse Blue 56 from polluted water: comparison of the degradation activity with electro-Fenton-based processes, Int. J. Environ. Sci. Technol. 19 (2022) 1671–1682, https://doi.org/10.1007/s13762-021-03296-0.
[155] S. Meddah, M. El Hadi Samar, M. Bououdina, L. Khezami, Outstanding performance of electro-Fenton/ultra-violet/ultra-sound assisted-persulfate process for the complete degradation of hazardous pollutants in contaminated water, Process Saf. Environ. Prot. 165 (2022) 739–753, https://doi.org/10.1016/j.psep.2022.08.002.
[156] C.-F. Liu, C.P. Huang, C.-C. Hu, C. Huang, A dual TiO_2/Ti-stainless steel anode for the degradation of Orange G in a coupling photoelectrochemical and photo-electro-Fenton system, Sci. Total Environ. 659 (2019) 221–229, https://doi.org/10.1016/j.scitotenv.2018.12.224.
[157] R. Oriol, I. Sirés, E. Brillas, A.R. De Andrade, A hybrid photoelectrocatalytic/photoelectro-Fenton treatment of Indigo Carmine in acidic aqueous solution using TiO_2 nanotube arrays as photoanode, J. Electroanal. Chem. 847 (2019) 113088, https://doi.org/10.1016/j.jelechem.2019.04.048.
[158] A.A. Márquez, O. Coreño, J.L. Nava, A hybrid process combining electrocoagulation and active chlorine-based photoelectro-Fenton-like methods during the removal of Acid Blue 29 dye, J. Electroanal. Chem. 922 (2022) 116732, https://doi.org/10.1016/j.jelechem.2022.116732.
[159] A.A. Márquez, O. Coreño, J.L. Nava, An innovative process combining electrocoagulation and photoelectro-Fenton-like methods during the abatement of Acid Blue 113 dye, Process Saf. Environ. Protect. 163 (2022) 475–486, https://doi.org/10.1016/j.psep.2022.05.061.
[160] H. Afanga, H. Zazou, F.E. Titchou, Y. Rakhila, R.A. Akbour, A. Elmchaouri, J. Ghanbaja, M. Hamdani, Integrated electrochemical processes for textile industry wastewater treatment: system performances and sludge settling characteristics, Sustain. Environ. Res. 30 (2020), https://doi.org/10.1186/s42834-019-0043-2.
[161] H. Zazou, H. Afanga, S. Akhouairi, H. Ouchtak, A.A. Addi, R.A. Akbour, A. Assabbane, J. Douch, A. Elmchaouri, J. Duplay, A. Jada, M. Hamdani, Treatment of textile industry wastewater by electrocoagulation coupled with electrochemical advanced oxidation process, J. Water Process Eng. 28 (2019) 214–221, https://doi.org/10.1016/j.jwpe.2019.02.006.
[162] P. Menon, T.S. Anantha Singh, N. Pani, P,V. Nidheesh, Electro-Fenton assisted sonication for removal of ammoniacal nitrogen and organic matter from dye intermediate industrial wastewater, Chemosphere 269 (2021) 128739. Doi: 10.1016/j.chemosphere.2020.128739.
[163] T.S. Machado, B.C. Ludwig, I.M. Rodegheri, K. Zambonin, J.R. de Mello, M. Hemkemeier, G.L. Dotto, J.S. Piccin, Sequential process of electro-Fenton and adsorption for the treatment of gemstones dyeing wastewater, Desal Water Treat. 194 (2020) 235–247, https://doi.org/10.5004/dwt.2020.25841.
[164] Y. Liu, K. Li, W. Xu, B. Du, Q. Wei, B. Liu, D. Wei, GO/PEDOT:NaPSS modified cathode as heterogeneous electro-Fenton pretreatment and subsequently aerobic granular sludge biological degradation for dye wastewater treatment, Sci. Total Environ. 700 (2020) 134536, https://doi.org/10.1016/j.scitotenv.2019.134536.
[165] Q. Wang, L. Huang, X. Quan, G. Li Puma, Sequential anaerobic and electro-Fenton processes mediated by W and Mo oxides for degradation/mineralization of azo dye Methyl Orange in photo assisted microbial fuel cells, Appl. Catal. B: Environ. 245 (2019) 672–680, https://doi.org/10.1016/j.apcatb.2019.01.026.